SYMPOSIUM ON SURFACE SCIENCE 2016

St. Christoph am Arlberg, Austria
February 21 - 27, 2016

CONTRIBUTIONS

EDITORS
Friedrich Aumayr, Ulrike Diebold, Christoph Lemell and Peter Varga
TU Wien

Tailored Solutions

from an unparalleled
spectrum of technologies.

Most Advanced Solutions

With the merger of VG Scienta and Omicron, the most advanced capabilities in Photoelectron Spectroscopy (PES), Scanning Probe Microscopy (SPM), Thin-Films and System Solutions comes together under one roof.

MULTI-TECHNIQUE Systems

Omicron has a long history of delivering systems combining different analytical techniques as well as deposition and other modules. These capabilities are now even stronger with the in-house availability of the complete Scienta range of analysers. An example of an ARPES and low temperature STM combination system is shown above.

ARPES Systems

With the combination of state-of-the-art analytical tools from Scienta and the long-standing design and integration expertise of Omicron, we can now offer a full range of ARPES systems, ranging from very affordable modules based on the Scienta R3000 analyser (example shown above) all the way up to systems featuring the revolutionizing Scienta DA30 analyser.

Please visit our website for more information: www.scientaomicon.com

scientaomicron
www.scientaomicron.com

Excellence in Low Temperature UHV SPM

USM1200 classic LT STM

USM1400 UHV STM and TERS

JT-STM NEW Joule-Thompson STM

USM1500 affordable magnets

USM1300 400mK high fields

USM1600 ultimate Low T

UNISOKU
TII Group
MUTUAL SATISFACTION

Ultra Low Drift

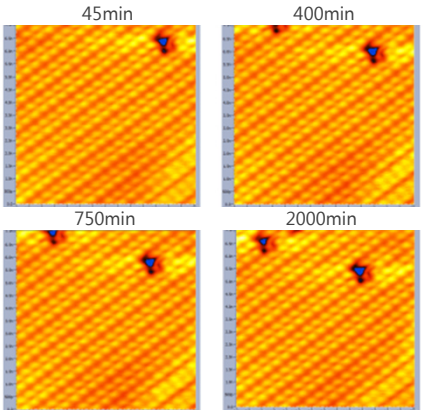

Si(100)2x1 at 360mK

Ultra High Resolution

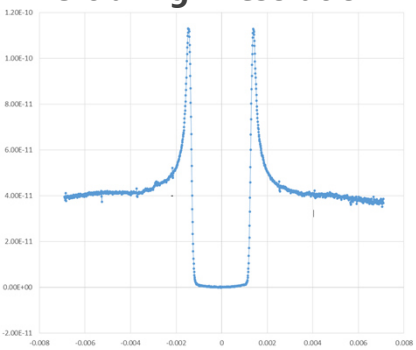

SC gap at 90mK of bulk Pb

USM1600

UHV STM System at 30mK

www.nanoscore.de

SYMPOSIUM ON SURFACE SCIENCE 2016

St. Christoph am Arlberg, Austria
February 21 - 27, 2016

CONTRIBUTIONS

EDITORS
Friedrich Aumayr, Ulrike Diebold, Christoph Lemell and Peter Varga
TU Wien

This symposium is organized by

Friedrich Aumayr, Ulrike Diebold and Peter Varga
Institute of Applied Physics (IAP)
TU Wien
Wiedner Hauptstr. 8-10/E134
1040 Vienna, Austria

Medieninhaber: F. Aumayr, U. Diebold und P. Varga, Institut für Angewandte Physik, Technische Universität Wien, Adresse: Wiedner Hauptstr. 8-10/E134, A-1040 Wien
Druck: R. & W. Smutny OEG, A-1110 Wien

PREFACE

We welcome all participants and accompanying persons to the 29th Symposium on Surface Science (3S). The 3S was founded as a winter school by members of the Institute of Applied Physics of the Vienna University of Technology (TU Wien) in 1983. The conference seeks to promote the growth of scientific knowledge and its effective exchange among scientists in the field of surface physics and chemistry and related areas, including applied topics. Its format is similar to that of Gordon Conferences, with ample time for discussions and joint outdoor activities. The number of participants is kept below 100 in order to guarantee active communication between all attendees.

Initially the 3S was held exclusively in Austria and took place every other year. It became an annual event in 1990, and the site started to alternate between locations in France and Austria. In 1998 the 3S evolved into a truly global conference, with venues in the US, Canada, Bulgaria, Japan, Switzerland, Spain, France and Sweden, always returning to Austria in alternate years. This year we are again happy to host the 3S in Austria; for the 8th time in the Arlberg area.

We hope that all participants will experience a lively and successful meeting while enjoying the surroundings in this beautiful mountain region.

Fritz Aumayr Ulrike Diebold Peter Varga

Dates and locations of 3S conferences:

1983	(31.01.-04.02.)	Obertraun	AT
1985	(27.01.-02.02.)	Obertraun	AT
1988	(22.05.-28.05.)	Kaprun	AT
1990	(11.03.-17.03.)	La Plagne	FR
1991	(10.02.-16.02.)	Obertraun	AT
1992	(15.03.-21.03.)	La Plagne	FR
1993	(09.05.-15.05.)	Kaprun	AT
1994	(06.03.-12.03.)	Les Arcs	FR
1995	(23.04.-29.04.)	Kaprun	AT
1997	(26.01.-31.01.)	Aussois	FR
1998	(29.03.-04.04.)	Park City	US
1999	(21.02.-27.02)	Pamporova	BG
2000	(15.02.-18.02.)	Kananaskis	CA
2001	(07.01.-13.01.)	Furano	JP
2002	(03.03.-09.03.)	St.Christoph/Arlberg	AT
2003	(30.03.-05.04.)	La Plagne	FR
2004	(29.02.-06.03.)	St.Christoph/Arlberg	AT
2005	(13.03.-19.03.)	Les Arcs 1800	FR
2006	(05.03.-11.03.)	St. Christoph/Arlberg	AT
2007	(11.03.-17.03.)	Les Arcs 2000	FR
2008	(02.03.-08.03.)	St. Christoph/Arlberg	AT
2009	(08.03.-14.03.)	St. Moritz	CH
2010	(07.03.-13.03.)	St. Christoph/Arlberg	AT
2011	(06.03.-12.03.)	Baqueira Beret	ES
2012	(11.03.-17.03.)	St. Christoph/Arlberg	AT
2013	(03.03.-09.03.)	Åre	SE
2014	(09.03.-15.03.)	St. Christoph/Arlberg	AT
2015	(22.03.-28.03.)	Les Arcs 1800	FR
2016	(21.02.-27.02.)	St. Christoph/Arlberg	AT

SYMPOSIUM ON SURFACE SCIENCE 2016

St. Christoph am Arlberg, Austria
February 21 - 26, 2016

Time Schedule

Sunday, 21 February 2016

16:00 – 18:30	**Registration**
20:00 – 20:20	**Opening**
	Chair: P. Varga
20:25 – 20:45	**H. Brune** *Realizing the Smallest Surface Adsorbed Quantum Magnets*
20:45 – 21:05	**H. J. Hug** *Magnetic Force Microscopy of Skyrmions in thin Multilayers with interfacially-induced Dzyaloshinski-Moriya Interaction*
21:05 – 21:25	**H. Ibach** *Step-Induced Damping of Exchange-Dominated Spin Waves in Ultra-Thin Films - A Road Block for the Miniaturization of Magnon-Based Devices?*

Monday, 22 February 2016

Chair: P. Varga

08:00 – 08:20 **C. Wöll**
Epitaxially-grown Molecular Frameworks: A new class of Designer Solids?

08:20 – 08:40 **P. Jelínek**
Metamorphoses of Molecular Chirality in Chemical Reactions on an Achiral Surface at Nanoscale

Chair: E. Taglauer

16:40 – 17:00 **T. Koshikawa**
Magnetic Property of Ferromagnetic Material Multi-layer with Spin-polarized LEEM and XMCD

17:00 – 17:20 **M. Maier**
Recent technology advancements in SPM based electrical probing at low temperatures

17:20 – 17:40 **T. U. Kampen**
Spin-resolved time-of-flight momentum microscopy

17:40 – 18:00 **R. Hu**
Friction without dissipation

18:00 – 18:20 **H. Takei**
HIM characterization of noble metal nanostructures for surface-enhanced Raman spectroscopy

Chair: C. Lemell

19:30 – 19:50 **U. Heinzmann**
Attosecond Delays in the Photoemission from the Layered Crystals Bi_2Te_3 and Non-Centrosymmetric BiTeCl

19:50 – 20:10 **W. Eberhardt**
Angle resolved Photoemission from Cu single crystals; New insights into the Photoemission Process

20:10 – 20:30 **J. H. Dil**
Determination of the photoelectron interaction time by spin-resolved ARPES

20:30 – 20:50 **F. Cheynis**
Spatial in-homogeneity and temporal dynamics of a 2D electron gas in interaction with a 2D adatom gas

Tuesday, 23 February 2016

Chair: A. Seitsonen

08:00 – 08:20 **G. Rupprechter**
Model catalysts for reforming and oxidation reactions: ultrathin films of zirconium oxide and cobalt oxide

08:20 – 08:40 **G. Thornton**
Non-Band-gap Photoexcitation of Hydroxylated TiO_2

Chair: U. Diebold

16:40 – 17:00 **W.-D. Schneider**
Molecular adsorption influences the quantum structure of oxide-supported gold nanoparticles: Chemisorption versus physisorption

17:00 – 17:20 **J. E. Ortega**
Interplay between steps and oxygen vacancies on curved TiO_2(110)

17:20 – 17:40 **J. Seifert**
Water Interaction with Oxide Surfaces studied with Single-Crystal Adsorption Calorimetry

17:40 – 18:00 **J. Libuda**
Counting the Electrons: Metal Support Interactions in Catalysis and Nanoscience

18:00 – 18:20 **Y. Suchorski**
Spatio-temporal pattern evolution in oscillating H_2 oxidation on Rh

Chair: M. Setvin

19:30 – 19:50 **J. Åhlund**
Ambient pressure x-ray photoelectron spectroscopy

19:50 – 20:10 **H. E. Hoster**
Lithium-oxygen cells – how a surface science view helps to explain a next- generation battery system

20:10 – 20:30 **P. Ferstl**
Transition metal/oxide hybrid chain structures on Ir(100) -is there a general trend?

20:30 – 20:50 **T. Šikola**
Localized Surfaces Plasmons: Does an ultrathin oxide film matter?

Wednesday, 24 February 2016

Chair: W. Widdra

08:00 – 08:20 **C. Draxl**
Surface energies and equilibrium crystal shapes of wurtzite crystals

08:20 – 08:40 **K. Reuter**
Electronic Friction for Surface Dynamical Processes: Beyond the Independent Atom Approximation

Chair: F. Aumayr

16:40 – 17:00 **Ch. Linsmeier**
Angular distribution of ^{13}C atoms reflected from W surfaces

17:00 – 17:20 **P. Bauer**
Electronic stopping of slow hydrogen ions in oxides

Chair: Ch. Linsmeier

17:25 – 18:20 **Posterintroduction**

A. Arnau
Breaking time-reversal symmetry at the topological insulator surface by metal- organic coordination networks

T. Berghaus
Recent Results in Ultra Low Temperature STM

S. N. Filimonov
Strain induced conversion of adsorption states of small benzene derivatives on Pt (111)

D. Halwidl
Adsorption of Water and Oxygen on $Ca_3Ru_2O_7(001)$

L. Hammer
Reliability of LEED analyses for complex systems

J. Hulva
Temperature programmed desorption studies of metal oxide surfaces

R. Kalousek
Near Field Interference Patterns of Surface Plasmon Polaritons

H. Marbach
Focused electron beam induced processing on surface-anchored metal-organic frameworks

M. Muntwiler
PEARL – The Photo-Emission and Atomic Resolution Laboratory at the Swiss Light Source

J. Schwestka
Electron emission from single layer graphene induced by impact of highly charged ions

M. Setvin
Charging Single O_2 Molecules on Anatase TiO_2 (101)

M. Shipilin
Structure and adsorption properties FeO(111) on Ag(100) and Ag(111)

V. M. Silkin
Description of many-body effects in quasiparticle interference on noble-metal surfaces

R. Stadlmayr
Erosion of iron and iron-tungsten films under deuterium ion impact

P. Varga
Transformation of paramagnetic fcc Fe into ferromagnetic bcc Fe by Focused Ion Beams

Post deadline posters

19:30 – 21:30 **Postersession**

Thursday, 25 February 2016

Chair: T. Berghaus

08:00 – 08:20 **F. J. Giessibl**
Combined STM, IETS, and AFM on CO/Cu(111) reveals that single atom tips maximize the intensity of IETS signal

08:20 – 08:40 **J. Kunze-Liebhäuser**
High-Resolution Imaging with "Scanning Electrochemical Potential Microscopy (SECPM)"

Chair: L. Hammer

16:40 – 17:00 **R. Fasel**
Recent progress in the bottom-up fabrication of graphene nanoribbons: From armchair to zigzag and beyond

17:00 – 17:20 **J. V. Barth**
Fusing tetrapyrroles to graphene edges by surface-assisted covalent coupling

17:20 – 17:40 **M. S. Altman**
Defects, Strain and Polymorphism in Graphene on Metals

17:40 – 18:00 **A. Gölzhäuser**
Tailoring the Mechanics of Carbon Nanomembranes for Molecular Separation

18:00 – 18:20 **U. Starke**
Extreme doping levels and many-body interaction in epitaxial graphene on SiC (0001): Can we access superconductivity and plasmonic?

Chair: A. Arnau

19:30 – 19:50 **M. E. Messing**
Generation of Stainless Steel Nanoparticles with Carefully Tuned Composition

19:50 – 20:10 **J. Yuhara**
Composition and local atomic arrangement of decagonal Al-Co-Ni and Al-Co-Cu quasicrystal surfaces

20:10 – 20:30 **A. P. Protogenov**
Topologically-ordered states on the surface of 3D Dirac materials

20:30 – 20:50 **E. V.Chulkov**
Electronic and spin structure of Sn-based ternary topological insulators

Friday, 26 February 2016

Chair: U. Heinzmann

08:00 – 08:20 **K. Morgenstern**
Local investigation of laser induced damage below the melting threshold

08:20 – 08:40 **M. Riva**
In-situ atomic-scale control of the growth of a polar perovskite oxide: $SrTiO_3$ (110) homoepitaxy by pulsed laser deposition

Chair: H. Marbach

16:30 – 16:50 **M. Penedo**
The Role of Entropic Forces in the Dynamics of a molecular Rotor

16:50 – 17:10 **R. Pétuya**
Bipolar conductance switching of single anthradithiophene molecules

17:10 – 17:30 **M. A. Schneider**
Comparing adsorption and reactivity of pentacene and biphenyl-dicarboxylic acid on thin CoO(111) films

17:30 – 17:50 **G. Zamborlini**
A multi-technique approach in studies of Ni-TPP self-assembly on the Cu (100) surface

17:50 – 18:10 **D. Sánchez-Portal**
Role of Structural and Charge-State Fluctuations on the Tunneling Spectroscopy and Imaging of Dangling-Bond Pairs and Dimers on Si(001):H and Ge(001):H

Chair: R. Fasel

18:30 – 18:50 **M. Buck**
Sterical and conformational aspects of metal-organic coordination in self- assembled monolayers

18:50 – 19:10 **S. Maier**
Self-assembled bridged-triphenylamines on bulk insulator surfaces: The role of functional groups

19:10 – 19:35 **Giant Slalom Race Award Ceremony**

20:00 **Conference Dinner**

TECHNISCHE UNIVERSITÄT WIEN
Vienna University of Technology

Announcement of an open position at the
Institute of Applied Physics, Faculty of Physics,
TU Wien (Vienna University of Technology)

Professorship in Applied Interface Physics

according to § 98 of the Universities Act 2002 (Universitätsgesetz 2002).

The applicant is expected to have outstanding academic credentials and a track record of high international visibility in the field of experimental interface physics. Areas of interest include, but are not limited to, development of novel experimental techniques or devices in the field of surface and interface physics, (bio)nanostructuring of surfaces, bio- or biocompatible interfaces, multilayer structures, nano-sized metamaterials, self assembly, solid-liquid interfaces, or nano-tribology. Synergies with and strengthening of the research portfolio of the institute (see http://www.iap.tuwien.ac.at/) are highly desired. We are looking for candidates who will establish close ties with university-wide and inter-university research efforts, see http://www.iap.tuwien.ac.at/links. Interest in vigorously developing future research networks and the ability to lead large coordination projects in the field of interface physics is desired. A solid track record in attracting external research funding on the national or international level is expected. The successful candidate will carry an appropriate teaching load of mandatory as well as of elective courses of the physics curriculum and will have to teach in German after a reasonable time period.

The applicant must meet the following requirements:

* A doctoral degree in the field under consideration
* An outstanding academic track record in research and teaching
* Pedagogic and didactic skills
* Leadership abilities
* International work experience in the field of research

The appointment will be made either on the tenured or tenure-track level according to previous experience.

University professors belong to grade A1 of the Austrian Collective Agreement for University Staff and receive a minimum salary of EUR 66953.60 per year. A higher salary agreement commensurate with qualifications and relevant experience can be negotiated.

TU Wien is committed to increase the percentage of women in leading scientist positions. Qualified female applicants are explicitly encouraged to apply and will be given preference when equally qualified. We explicitly encourage handicapped persons with appropriate qualifications to apply.

Applications including a detailed curriculum vitae, list of publications, invited lectures, extramural funding, teaching records, copies of the five most outstanding publications, and a research plan should be sent to the Dean of the Faculty of Physics, TU Wien, Prof. Dr. J. Burgdörfer, Wiedner Hauptstraße 8-10/E-130, 1040 Vienna, Austria. For easy access to bibliometric information we request a unique identifier for each applicant, for example a researcherID (www.researcherid.com). Hardcopy applications must include a CD-ROM or an USB-stick containing the entire application in a single pdf-file. Online applications should be sent in a single pdf-file to dekphys@tuwien.ac.at.

Applications received prior to **April 30, 2016** will receive full consideration.

CONTRIBUTIONS

Content

Sunday

Realizing the Smallest Surface Adsorbed Quantum Magnets

Harald Brune

Institute of Physics, Ecole Polytechnique Fédérale de Lausanne (EPFL),

Station 3, CH-1015 Lausanne, Switzerland

E-mail: harald.brune@epfl.ch

The magnetic states of nanostructures are of high interest for information storage and quantum information processing. This has triggered the search for the smallest possible magnets. In devices, electrodes have to be attached to them for readout and manipulation of the magnetic quantum states. This corresponds to their adsorption onto conducting surfaces.

Possible candidates for the smallest surface adsorbed magnets are molecules and small metal clusters down to the ultimate size limit of single metal adatoms. The benchmarks for quantum magnets are their magnetic relaxation and coherence times, T_1 and T_2. The first determines how long information can be stored in a magnetic quantum state, and the second defines the time one has to take out a quantum computation step.

Many molecular magnets that exhibit promising properties in bulk samples loose them entirely when they are surface adsorbed, and all single metal adatoms reported so far are perfect paramagnets, despite their high magnetic anisotropies [1]. This is predominantly due to scattering with metal conduction electrons. In the case of molecules, conformational changes induced by surface adsorption may add to it. Finally, for higher temperature, phonon-induced magnetization reversal starts to override electron scattering.

We show that these problems can largely be overcome by using oxide, graphene, and hexagonal boron-nitride spacer layers that significantly enhance the magnetic lifetimes of the surface adsorbed species as compared to direct adsorption onto a metal substrate. Pc_2Tb double-decker molecules adsorbed on MgO(100) thin films grown on Ag(100) have much longer spin-relaxation time and wider hysteresis than in bulk samples [2]. Ho atoms on the same surface are the first single atom magnets [3]. They exhibit spin-relaxation times of ½ an hour at 2 K and display hysteresis up to 30 K, see Fig. 1 for their magnetization curves measured with X-ray magnetic circular dichroism (XMCD). The Ho atoms on MgO therefore realize Richard Feynmans dream of storing information in a single atom. By the way, they

also outperform best molecular magnets. We note that former reports of magnetic bi-stability in Ho atoms on Pt(111) [4] are incompatible with the magnetic ground state determined with XMCD [5] and could not be reproduced with low-temperature STM [6].

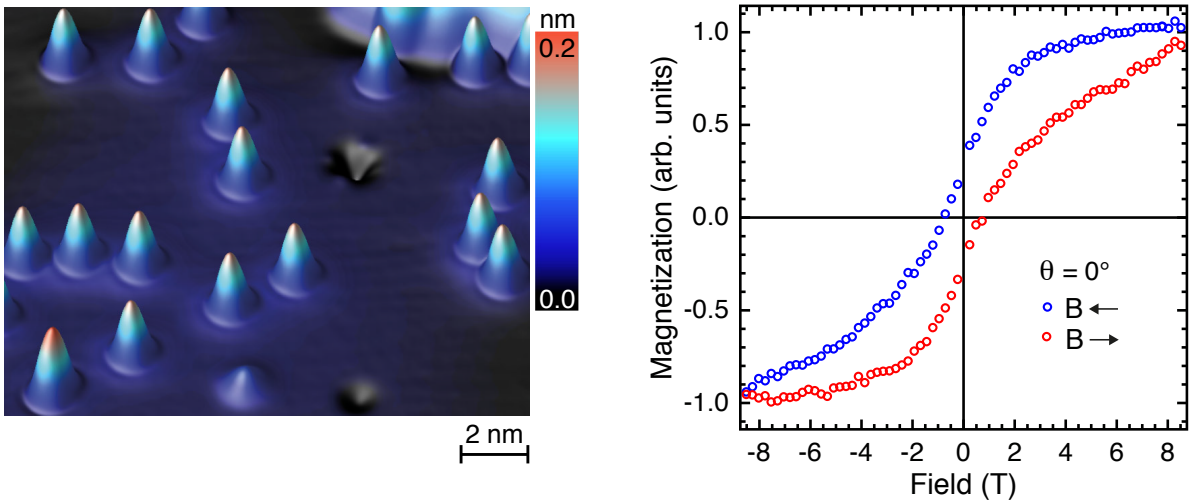

Fig. 1*: left 4 K STM image showing single Ho atoms on MgO on Ag(100); right XMCD magnetization curve for an ensemble of non-interacting individual Ho atoms on MgO/Ag(100) (10 K) [3].*

[1] I. G. Rau *et al.*, Science **344**, 988 (2014).

[2] C. Wäckerlin *et al.*, ACS Nano submitted.

[3] F. Donati *et al.*, Science submitted.

[4] T. Miyamachi *et al.*, Nature **503**, 243 (2013).

[5] F. Donati *et al.*, Phys. Rev. Lett. **113**, 237201 (2014).

[6] M. Steinbrecher *et al.*, Nat. Communic., in press (2016).

Magnetic Force Microscopy of Skyrmions in thin Multilayers with interfacially-induced Dzyaloshinski-Moriya Interaction

Hans J. Hug[1,2], J. Schwenk[1,2], M. Bacani[1], S. Romer[1], A. Guiller[1], X. Zhao[1,2], and M.A. Marioni[1]

[1] *Nanoscale Materials Science, Empa, Swiss Federal Laboratories for Materials Science and Technology, Duebendorf, Switzerland;*
[2] *Department of Physics, University of Basel, Basel, Switzerland*
(corresponding author: Hans J. Hug, e-mail: hans-josef.hug@empa.ch)

Dzyaloshinski-Moriya interaction (DMI), that is a favorable exchange coupling of two spins at 90 degrees, can lead to negative domain wall energy in ferromagnetic systems and consequently to a stabilization of magnetic spin-spiral structures, and skyrmions [1]. The latter are small magnetic vortices comprised of a "core" of upward pointing magnetic moments, downward-pointing magnetic moments far away from the core, and a transitional region in which the magnetic moments turn from core to peripheral orientation progressively with radius and in a plane that is perpendicular to the radial direction. Magnetic skyrmions are small magnetic structures whose particular topology gives rise to effects that suggest application potential e.g. in spintronics and data storage [2].

DMI occurs in non-centrosymmetric magnets [2][3][4] or at the interface between 3d ferromagnetic materials and heavy metal films with strong spin-orbit coupling [5][6].

An important milestone on the way to exploiting the properties of skyrmions in applications is to observe skyrmions in thin film materials fabricated by magnetron sputtering, in particular with an experimental method operating ex-situ at room temperature and allowing for protective capping layers. Here we utilize MFM to identify and characterize the field dependence of the magnetic microstructures in $Pt_{3nm}/[Pt_{1nm}/Co_{0.6nm}/Ir_{1nm}]_{x5}/Pt_{1nm}/Co_{0.6nm}/Pt_{10nm}$ and $Pt_{3nm}/[Pt_{1nm}/Co_{0.6nm}]_{x5}/Pt_{10nm}$ multilayer systems sputtered on Si with a native oxide layer. In the latter system the Co/Pt interfaces provide a strong perpendicular magnetic anisotropy, and the interfacial DMI of the bottom Co/Pt and top Pt/Co interfaces compensates. MFM reveals domains with a size of several microns compatible with the large positive domain wall energy, as expected for a system with large perpendicular magnetic anisotropy and no DMI. At the coercive field domains with a magnetization opposite to the applied field collapse and the film becomes saturated. A small granular MFM contrast remains visible. Using quantitative magnetic force microscopy techniques [7], this contrast can be traced back to spatial variations of the thickness of the ferromagnetic layers of ± 1 Monolayer.

The sample with asymmetric interfaces showed a considerably smaller domain size of

(246±40)nm, independent from the demagnetization process used. We attribute this reduction of the domain size to the existence of a DM anisotropy, which can be obtained from the domain size, the film's uniaxial anisotropy and magnetization determined by vibrating sample magnetometry, and an exchange stiffness taken from literature [8]. This DM anisotropy is too small to support a skyrmion phase, but isolated skyrmions can still exist [9]. MFM experiments revealed a small number of skyrmions with a diameter below 50nm, when the field was reduced from positive saturation. In negative fields these skyrmions were either annihilated by proceeding reversal domains or spontaneously expanded into larger domains. Local D-values estimated from these bursting fields agreed well with the average D. We also observe a magnetic background inhomogeneity, similar to the one observed in the system the symmetric interfaces.

Given the strong dependence of the Dzyaloshinski-Moriya interaction (DMI) on the number of monolayers of Co [10], and in turn the dependence of the skyrmion characteristics on the DMI strength, these observations are consistent with local variations of the DMI. Clearly thin film growth methods with an atomic scale thickness control are needed to improve the films magnetic properties. This may become possible through a better understanding of atomic scale growth processes.

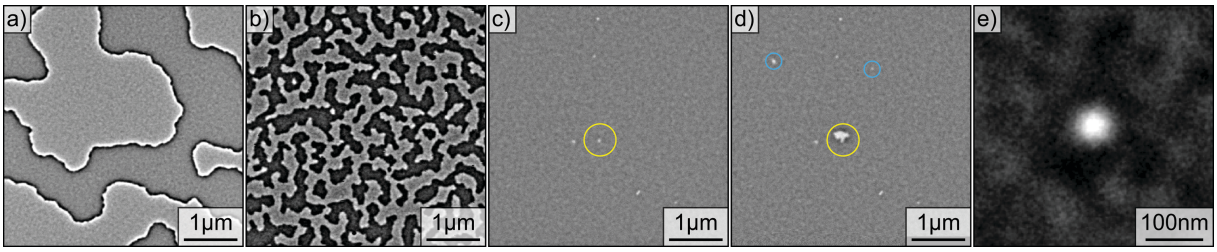

a) Sample with symmetric interfaces: the domains of the as-grown state are several microns in size. b)-d) Micromagnetic states of the sample with asymmetric interfaces: b) the domain size is independent of the demagnetization process used (shown domains of the as-grown state). c) Skyrmions occuring at 1.19mT after saturating in 128mT. d) Data acquired at - 4.04mT. The skyrmion highlighted by the yellow circle in panel b) has expanded into a larger domain. More skyrmions have appeared (blue circles). e) Skyrmion imaged with higher spatial resolution.

References

[1] A. N. Bogdanov, and D. A. Yablonskii, Zh. Eksp. Teor. Fiz 95, 182 (1989).
[2] N. Nagaosa, J. Sinova, S. Onoda, A. H. MacDonald, and N. P. Ong, Rev. Mod. Phys. 82, 1539 (2010).
[3] A. B. Butenko, A.A. Leonov, U. K. Rößler, and A. N. Bogdanov, Phys. Rev. B 82, 052403 (2010).
[4] U. K. Rößler, A. N. Bogdanov, and C. Pfleiderer, Nature 442, 797 (2006).
[5] S. Heinze et al., Nat. Phys. 7, 713 (2011).
[6] M. Bode et al. Nature 447, 190 (2007).
[7] P. J. A. van Schendel, H.J. Hug, B. Stiefel, S. Martin, and H.-J. Güntherodt, J. Appl. Phys. 88, 435 (2000).
[8] C.Moreau-Luchaire et al., arXiv:1502.07853 [cond-mat.mtrl-sci].
[9] N.S. Kiselev, A. N. Bogdanov, R. Schäfer, U.K. Rößler, Journal Physics. D 44, 392001 (2011).
[10] H. Yang, A.,Thiaville, S. Rohart, A. Fert, and M. Chshiev, arXiv:1501.05511 [cond-mat] (2015).

Step-Induced Damping of Exchange-Dominated Spin Waves in Ultra-Thin Films - A Road Block for the Miniaturization of Magnon-Based Devices?

E. Michel[1,3], H. Ibach[2,3*], C. M. Schneider[1,3], D. L. R. Santos[4], A. T. Costa[5]
[1]*Peter Grünberg Institut* (PGI-6), *Forschungszentrum Jülich, 52425 Jülich, Germany*
[2]*Peter Grünberg Institut* (PGI-3), *Forschungszentrum Jülich, 52425 Jülich, Germany*
[3]*Jülich Aachen Research Alliance, Germany*
[4]*Laboratoire Louis Néel, CNRS, Boite Postale 166, 38042 Grenoble Cedex 09, France*[**]
[5]*Instituto de Física, Universidade Federal Fluminense, 24210-346 Niterói, R. J., Brazil*

The miniaturization of magnon-based devices into the nanometer range requires the utilization of exchange-dominated spin waves. We show in experiment and theory that the intrinsic lifetimes of the homogeneous acoustic spin waves in ultra-thin cobalt films are sufficiently long for such applications provided that the films are atomically flat. The presence of surface steps, however, dramatically shortens the lifetime if the steps cross the propagation path of the spin waves.

A high resolution sample spectrum of an 8ML cobalt film is shown in Fig. 1. The wave vector $q_{\parallel}$ is oriented along the [110] ($\bar{\Gamma}\bar{X}$) direction. The film is grown at room temperature and annealed afterwards to about 450K for 30 minutes. The energy losses on the right and left side of the elastic peak are energy loss and gain due to the acoustic mode at ~15meV and the first standing mode of the film at ~28meV.

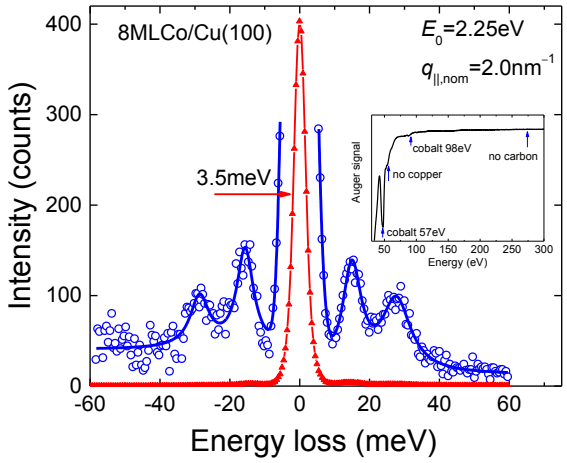

Fig. 1 (color online). Spin wave spectrum of an annealed 8ML fcc cobalt film deposited on Cu(100).

Without annealing the FWHM of the spin waves are considerably larger. Fig 2 shows the FWHM vs. $q_{\parallel}$ of the room temperature grown film as blue circles. The red squares mark the FWHM for the annealed film. Theoretical results are shown as green triangles. Comparison of the elastic diffuse scattering to simulations proves that the broadening of the FWHM is due to steps.

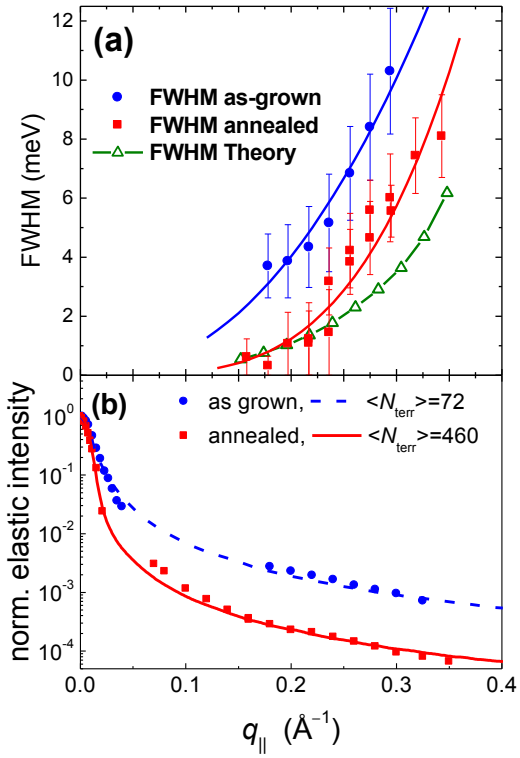

Fig. 2. (a) FWHM of acoustic spin waves in 8ML fcc cobalt film deposited on Cu(100). (b) elastic diffuse scattering.

Direct evidence for the role of steps comes from spin waves observed on stepped surfaces. Fig. 3a shows the LEED pattern of the surface at 122eV electron energy. The pattern displays the characteristic spot splitting due to destructive interference of electrons scattered from different terraces. The splitting into two spots rather than into streaks proves a narrow terrace-width distribution, which is in agreement with STM images [1]. Fig.3b shows a kinematic simulation of the pattern of an ideal (1 1 23) surface.

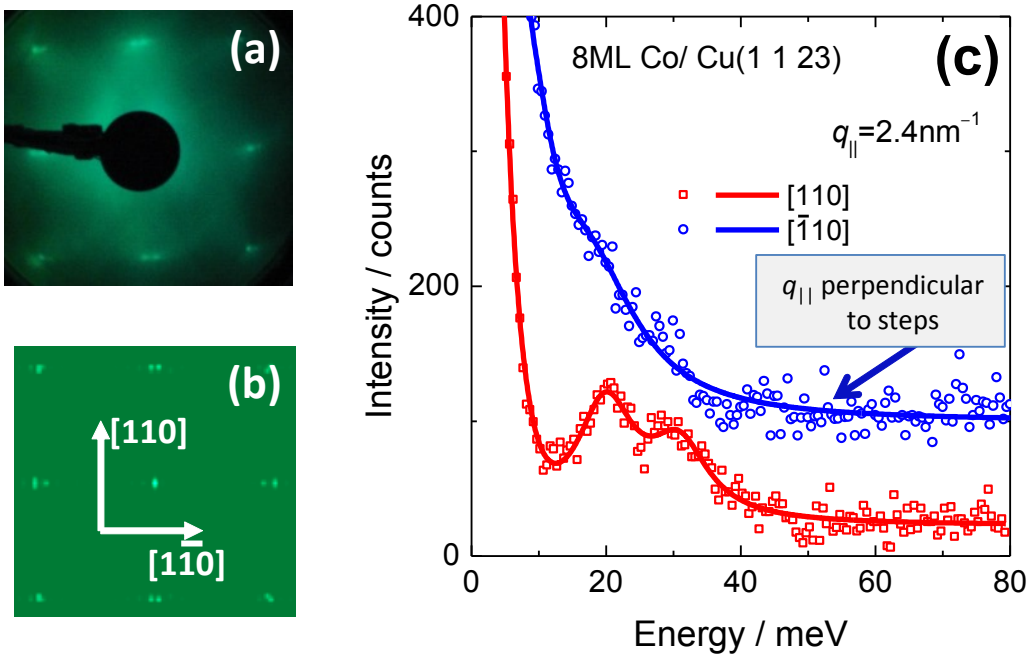

Fig. 3. LEED pattern of the Cu(1 1 23) surface and the simulated LEED pattern ((a) and (b), respectively). (c) Blue circles and squares denote spectra of spin waves travelling parallel to the nominal step orientation for $q_{||}$=2.0nm^{-1} and 2.4nm^{-1}, respectively. Red triangles mark the spectrum for a wave vector perpendicular to the steps ($q_{||}$=2.4nm^{-1}).

For $q_{||}$ oriented along the nominal step direction the spectra are similar to spectra obtained on as-grown films on Cu(100). The measured FWHM (without unfolding) are even slightly smaller on the stepped surface . For wave-vectors oriented perpendicular to the steps, however, spectra display merely a shoulder (Fig.3b). Hence, the high step density crossing the spin wave's propagation path causes a complete damping of the spin waves to the point that they cease to exist as defined excitations.

While a quantitative theory of the effect of steps is still lacking we argue that the creation of evanescent waves at steps [2] causes the damping: The real part of the (complex) wave vector of the evanescent wave perpendicular to the film has a value which is close to the wave vector at the boundary of the Brillouin zone. By analogy to high-momentum acoustic thin-film modes (or to high-momentum bulk spin waves) we argue that the step-generated evanescent waves must couple effectively to Stoner excitations and thereby cause a damping of the acoustic waves from which they originate.

[1] M. Giesen, F. Schmitz, and H. Ibach, Surf. Sci. **336**, 269 (1995).
[2] R. L. Stamps, R. E. Camley, B. Hillebrands *et al.*, Phys. Rev. B **46**, 10836 (1992).

Monday

Epitaxially-grown Molecular Frameworks: A new class of Designer Solids?

Christof Wöll

Institute of Functional Interfaces (IFG)
Karlsruhe Institute of Technology (KIT), FRG
christof.woell@kit.edu, www.ifg.kit.edu

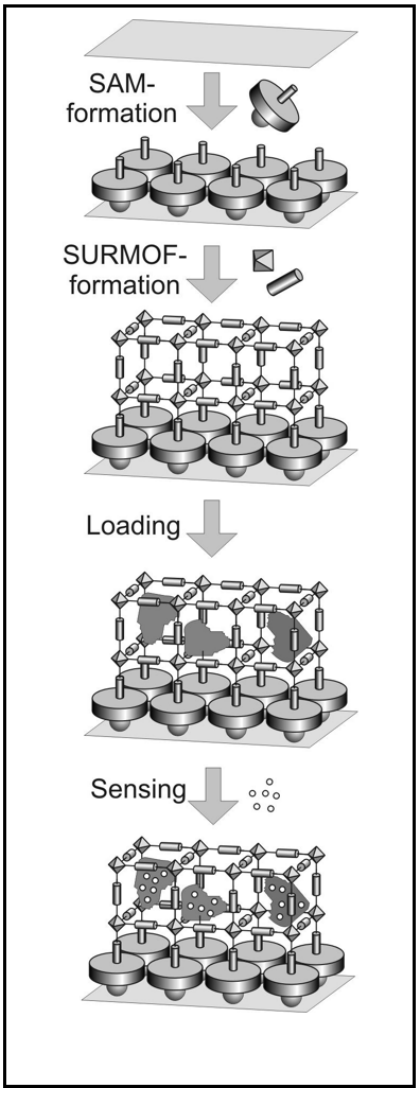

The demand for advanced materials with novel combinations of different functionalities requires the development of new types of solids. In this context supramolecular chemistry holds unique prospects. Self-assembly of one or different types of functional units can be employed to fabricate crystalline arrangements, yielding complex but at the same time structurally well defined, highly ordered "Designer Solids", which exhibit functionalities going well beyond that provided by the individual building blocks.

In this presentation it will be made evident that a recently introduced class of supramolecular materials, metal-organic frameworks, or MOFs, carry an enormous potential with regard to the fabrication of solids with unusual physical properties [1]. This potential has also been recognized by the German Research Council (DFG), which has established a Priority Program (SPP 1928) on *Coordination Networks: Building Blocks for Functional Systems*.

MOFs, a particular, porous form of crystalline coordination networks (CCNs) are stable materials, with decomposition temperatures well above 200°C, and in some cases exceeding 500°C. With selected examples we will demonstrate the interesting, and often surprising (e.g. negative thermal expansion coefficient), mechanical, electronic, magnetic and optical properties of these molecular, crystalline materials.

This fairly recent class of porous solids, introduced in the 1990s, is very large in number, already more than 20.000 different structures have been reported. In order to exploit the properties of these materials for applications in solid state physics, we have developed a liquid phase epitaxy (LPE) process, which allows growing MOFs on modified substrates using a layer-by-layer procedure [1]. The availability of cm-sized, highly oriented MOF thin films, or SUFMOFs, with thickness in the μm-regime allows to determine the basic physical properties (mechanical [2], optical [3], electronic [4], magnetic [5]) of these porous, molecular solids using standard methods. A unique feature of the LPE-process is the ability to use heteroepitaxy [6] to add further functionality to these

materials by creating multilayer systems [7] – allowing to study e.g. diffusion of molecules inside MOFs in considerable detail [8].
In this presentation will discuss electrical and photophysical properties of MOFs, and highlight a recent realization of a single-component, SURMOF-based photovoltaic device [9]. Using the LPE-approach offers unique opportunities for preparing organic solids with well-defined crystallinity, e.g. allowing to explore the potential of indirect band gaps for organic electronics. This will be demonstrated for the case of porphyrin-based SURMOFs.

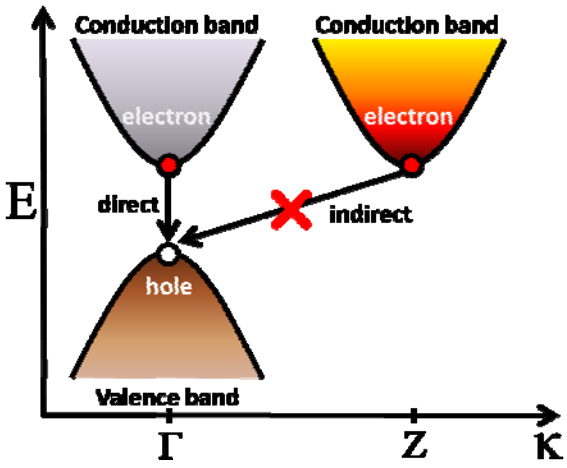

References

[1] H. Gliemann und Ch. Wöll, Materials Today **15**, 110 (2012)

[2] S. Bundschuh, O. Kraft, H. Arslan, H. Gliemann, P. Weidler, C. Wöll, Appl. Phys. Lett. **101**, 101910 (2012)

[3] E. Redel, Z. Wang, S. Walheim, J. Liu, H. Gliemann, Ch. Wöll, Appl. Phys. Lett., **103**, 091903 (2013)

[4] J.Liu, W.Zhou, J.Liu, I.Howard, G.Kilibarda, S.Schlabach, D.Coupry, M.Addicoat, S.Yoneda, Y.Tsutsui, T. Sakurai, S.Seki, Z.Wang, P.Lindemann, E.Redel, T.Heine, C.Wöll, Angew. Chemie, **54**, 7441 (2015)

[5] M.E. Silvestre, M. Franzreb, P.G. Weidler, O.Shekhah, Ch. Wöll, Adv. Funct. Materials, **23**, 1093 (2013)

[6] Z.Wang, J. Liu, B. Lukose, Z. Gu, P.Weidler, H.Gliemann, T. Heine, C. Wöll, Nano Letters, **14**, 1526 (2014)

[7]. J.P. Best, J. Michler, J. Liu, Zh. Wang, M. Tsotsalas, X. Maeder, S. Röse, V. Oberst, J. Liu, S. Walheim, H. Gliemann, P.G. Weidler, E. Redel, Ch. Wöll, Appl. Phys. Lett., **107**, 101902 (2015)

[8] L. Heinke, Z. Gu, Ch. Wöll, Nature Comm., **5**, 4562 (2014)

[9] J. Liu, W. Zhou, J. Liu, I. Howard, G. Kilibarda, S. Schlabach, D. Coupry, M. Addicoat, S. Yoneda, Y. Tsutsui, T. Sakurai, S. Seki, Zh. Wang, P. Lindemann, E. Redel, Th. Heine, Ch. Wöll, Angew. Chemie Intl. Ed., 54, 7441-7445 (2015)

Metamorphoses of Molecular Chirality in Chemical Reactions on an Achiral Surface at Nanoscale

S. Stetsovych, M. Švec, J. Vacek[1], J. Vacek Chocholoušová[1], I.G. Stará[1], A. Jancarík[1], J. Rybácek[1], P. Jelínek, I. Starý[1]

Institute of Physics of the AS CR, Prague, 162 00, Czech Republic;
(corresponding author: P. Jelinek, e-mail: pavel.jelinek@fzu.cz)

[1] *Institute of Organic Chemistry and Biochemistry AS CR, Prague, 166 10, Czech Republic*

We present a novel way how to achieve global chiral control of prochiral molecules on metal surfaces using on-surface chemistry. More precisely, we succeeded transferring chirality from a homochiral helical precursor to enantiofacially adsorbed prochiral products through a cascade of stereoconservative on-surface reactions (schematically depicted on Fig.). What is more, detailed molecular structure of intermediates and final products of the chemical reactions, including their chirality, are identified by means of high-resolution SPM images supported by extensive theoretical DFT-based analysis.

Chirality of molecular structures is paramount in many phenomena including parity violation of weak forces, polarization of light or electron spin, asymmetric reactions or molecular self-assembly. It is also inherent in nature as manifested by the existence of homochiral proteins, nucleic acids and polysaccharides expressing stereospecific interactions in various molecular events. An efficient control over relative or absolute stereochemistry in organic reactions belongs to the greatest achievements of in-solution chemistry within the last half-century. On the other hand, on achiral surfaces recent research on chiral and prochiral molecules has resulted in a considerable control over their local order (see e.g. [1-3]). Nevertheless, spontaneous global mirror-symmetry breaking upon adsorption of prochiral molecules on surfaces is naturally disfavoured (see pathway B on Fig). However the induction and transformation of chirality in on-surface reactions have remained almost unexplored area. Here we show its potential to open a new direction of research, which allows better control of chirality on surfaces.

This is for the first time up to our knowledge, when enantiopure system of prochiral molecules on an achiral substrate is prepared under the chemical control. Notably, a new type of homochiral organic-inorganic surfaces was formed with high configurational stability preventing racemisation process. We believe that the possibility to form globally enantiopure assemblies of prochiral molecules through on-surface synthesis opens a new way of expressing 2D chirality in so far unexplored types of organic-inorganic chiral surfaces.

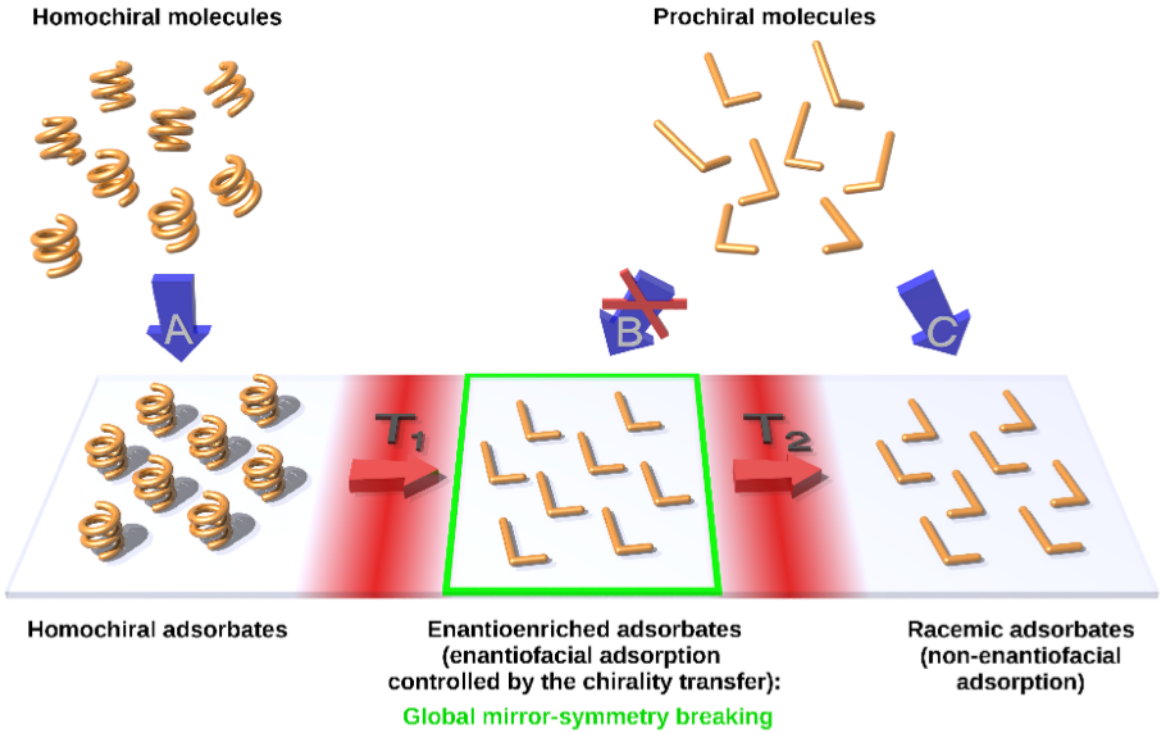

Fig. 1. The proposed concept of global mirror-symmetry breaking in the system of prochiral molecules on an achiral substrate through controlled on-surface chemistry reaction.

This work was financially supported by a Czech Science Foundation grant (14-29667S, 14-16963J) and by the Institute of Organic Chemistry and Biochemistry, Czech Academy of Sciences (RVO: 61388963). The authors declare no conflicts of interest.

[1] Chirality at the Nanoscale, D. B. Amabilino, Ed. (Wiley-VCH, Weinheim, 2009).
[2] S. M. Barlow, R. Raval, Surf. Sci. Rep. **50**, 201–341 (2003).
[3] K.-H. Ernst, Phys. Status Solidi B **249**, 2057–2088 (2012).

Magnetic Property of Ferromagnetic Material Multi-layer with Spin-polarized LEEM and XMCD

T. Koshikawa[1], M. Suzuki[1], T. Yasue[1], E. Bauer[2], T. Nakagawa[3], Y. Takagi[4] and T. Yokoyama[4]

1) Osaka Electro-Communication University Osaka, Japan,
2) Arizona State University, Tempe, USA,
3) Kyushu Univ., Fukuoka, Japan
4) Institute of Molecular Science, Okazaki, Japan

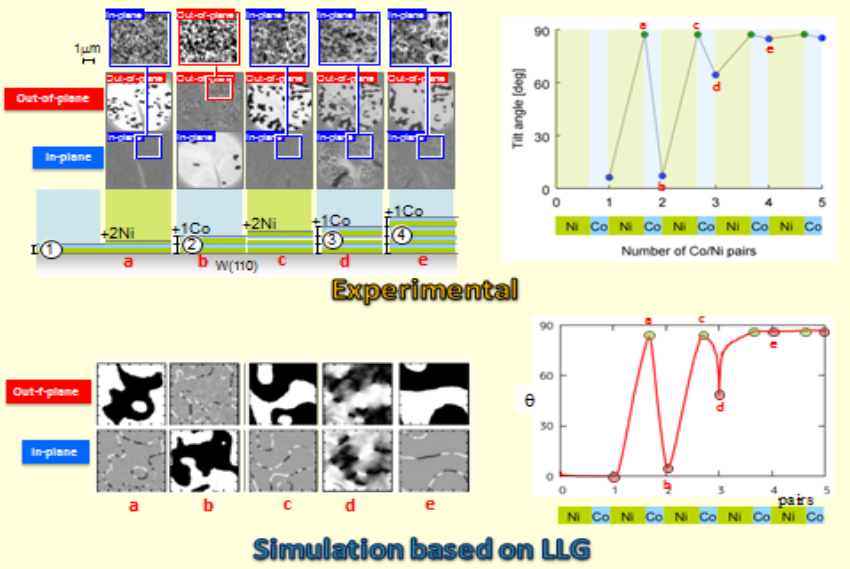

Fig.1 Magnetic domains of Co/Ni multi-layers with experiments and simulations

We have already developed a novel very high brightness and high spin-polarized low energy electron microscope (SPLEEM) [1-4]. [CoNix] multi-layer is known to exhibit perpendicular magnetic anisotropy and is expected as a material for the devices with low operation current. We investigated magnetic property during growth of the [CoNix]y multi-layer with our SPLEEM [1-4] and. Numerical simulations based on the Landau-Lifshitz-Gilbert (LLG) equation was also carried out for [$CoNi_2$] on W(110) as shown in Fig.1 [5.6]..

Detailed experimental results will be shown on the magnetic property for different pairs of Co/Ni systems, i.e., Co/Ni_2, Co/Ni_3 and Ni_2/Co on W(110) in Fig.2. Fig.2 shows that the changing angle between the in-plain and the out-of-plain for the same kinds of materials. Three systems show the similar property and the contribution of Ni layer is not large. The main contribution to the perpendicular magnetization would cause with the un-isotropy of the interface of Co and Ni layer.

The experiments have been carried out also with the XMCD which can separate the contribution of Ni and Co, which showed the Ni contribution is dominant which would contradict each other. These results would be discussed.

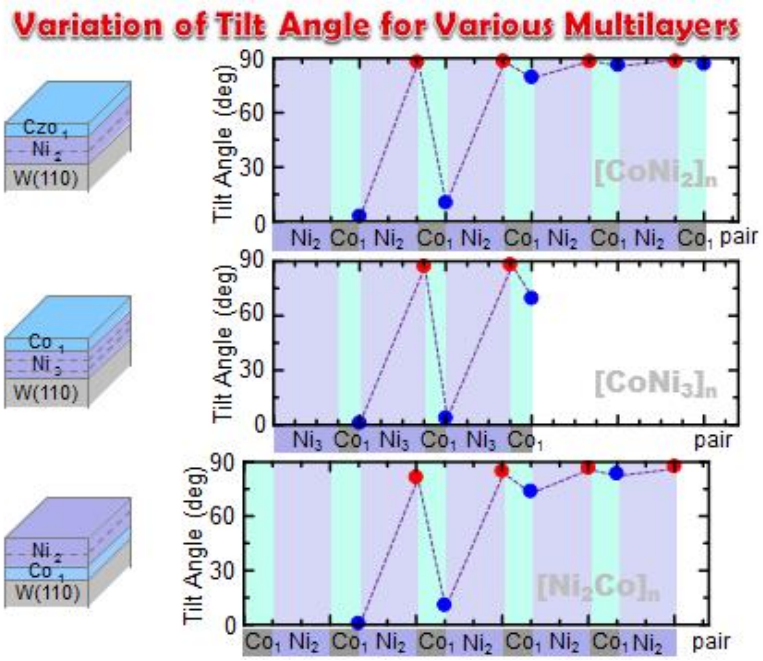

Fig.2 Magnetic direction of Co/Ni2, CoNi3 and Ni2/Co multi-layers on W(110)

Reference;

[1] N.Yamamoto *et al.*, J. Appl. Phys. **103**, 064905 (2008).
[2] X.G. Jin *et al.*, Appl. Phys. Express **1**, 045602 (2008).
[3] M.Suzuki *et al.*, Appl. Phys. Express **3**, 026601 (2010).
[4] T.Yasue et.al., Rev. Sci. Instrum., 85, 043701 (2014).
[5] M.Suzuki et.al., J.Phys.Condens.Matter. **25**, 406001 (2013).
[6] K.Kudo et.al., J.Phys. Condens.Matter. **25**, 395005 (2013).

Recent technology advancements in SPM based electrical probing at low temperatures

Markus Maier, Jürgen Koeble, Jürgen Chrost

Scienta Omicron GmbH, Limburger Str. 75, 65232 Taunusstein, Germany
(corresponding author: M. Maier, e-mail: Markus.Maier@scientaomicron.com)

A major challenge in the development of novel devices in nano- and molecular electronics is their interconnection with larger scaled electrical circuits. Local electrical probing by multiple probes with precision on the atomic scale can significantly improve efficiency in analyzing electrical properties of individual structures on the nano-scale without the need of a full electrical integration.

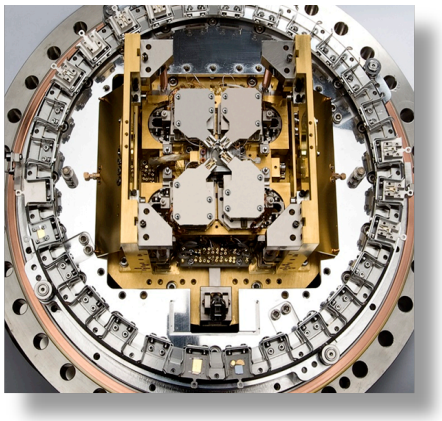

The LT NANOPROBE is a dedicated microscope stage that merges the requirements of a SEM navigated 4-probe STM and at the same time satisfies the needs for high performance SPM. Besides SEM/SPM probe fine navigation, the excellent STM/NC-AFM imaging performance with atomic resolution at T<5K,expands applications to tunneling spectroscopy and even the creation of atomically precise structures. We will present measurements that prove the performance level of the instrument, specifically the low thermal drift, which allows for sufficient measurement time on extremely small structures as well as QPlus AFM measurements, which become important if nanostructures are deposited on an insulating substrate for a better electrical decoupling. We will also show the newest technology improvements and challenges as well as application and scientific drivers for this type of scientific instrumentation.

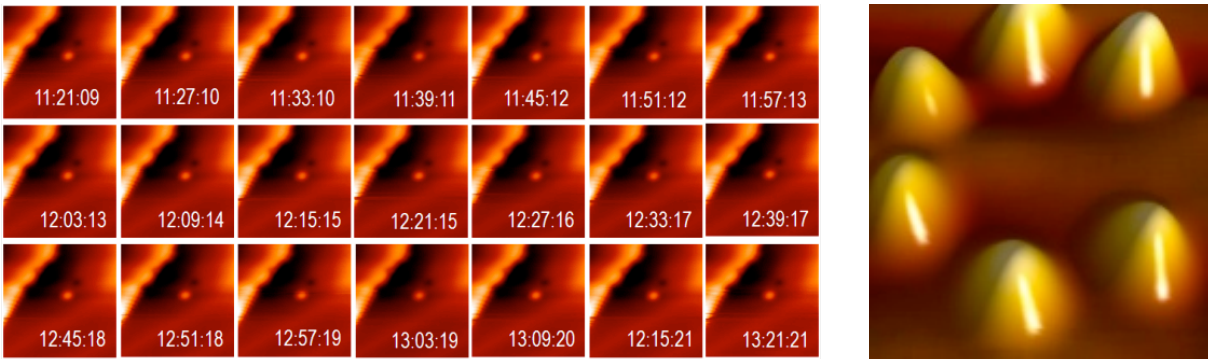

Drift measurements at T< 5K (left) and atom manipulation on Au(111) (right).

Spin-resolved time-of-flight momentum microscopy

Thorsten U. Kampen[1,2], Andreas Oelsner[3], C. Tusche[4], Gerd Schönhense[5]

[1]*SPECS Surface Nano Analysis GmbH, Voltastrasse 5, 13355 Berlin, Germany*

[2]*Institu für Festkörperphysik, Technische Universität Berlin, 10623 Berlin, Germany*

[3]*Surface Concept GmbH, Am Sägewerk 23a, 55124 Mainz, Germany*

[4]*Max Planck Institute for Microstructure Physics, Weinberg 2, 06120 Halle, Germany.*
[5]*Institut für Physik, Johannes Gutenberg-Universität, Staudingerweg 7, 55099 Mainz, Germany*

Our newly developed time-of-flight momentum uses an optimized lens design which provides simultaneously highest energy, angular and lateral resolution. The lens provides a full 2π solid acceptance angle with highest angular resolution. in contrast to standard ARPES measurements with a conventional hemispherical analyzer, electronic structure data from and beyond the 1st Brillouin zone is recorded without any sample movement. in addition the lens of such an instrument can work in a lateral imaging mode for microscopy as well. this enables navigation on the sample and reduces the size of the area under investigation in ARPES down to a few micrometers in diameter. This combination of large acceptance angle, high angular resolution and small acceptance area, makes this instrument the ideal tool for electronic structure studies on small samples or sample areas. the design is compact with a straight optical axis. Operation modes are (k_x,k_y,E_k) data aquisition by operation in energy filtered k-space imaging, ToF-PEEM mode, energy-filtered real space imaging and micro-spectroscopy mode.

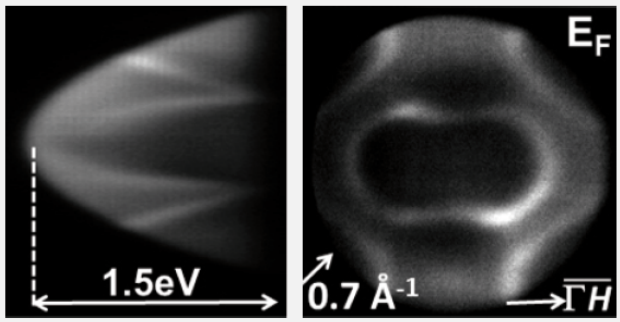

The k-space sections show the bands in an E-k‖ plane (left picture) and a cut through the Fermi surface (right picture) of Mo(110), taken with 2PPE excitation by 3.3eV photons from a Ti:Sa laser.

The 3D (k_x, k_y, E_k) data recording is done with a 2-dimensional delayline detector, with a time resolution of 150 ps and count rates up to 8 Mcps. It uses channelplates with 40 µm spatial resolution. While the x,y position of an incoming electron is converted into k_x,k_y wave vector, the kinetic energy E_k is determined from the flight time t. Spin-resolved imaging is achieved by electron reflection at a W(100) spin-filter crystal prior to the 2-dimensional delayline detector. Electrons are reflected in the [010] azimuth at 45° reflection angle. Varying the scattering energy one can choose positive, negative, or vanishing reflection asymmetry. We will present data taken on different materials like Mo(110) and ferroelectric α-GeTe(111) films.

Friction without dissipation

R. Hu and J.W.M. Frenken

Advanced Research Center for Nanolithography, Science Park, Amsterdam, The Netherlands

(corresponding author: J.W.M. Frenken, e-mail: frenken@arcnl.nl)

We have developed a new microscopic description of frictional processes on the atomic scale. Central to our theoretical model is that we explicitly leave out dissipation and concentrate on the dissipationless, classical phonon dynamics. Our approach contrasts with the conventional theoretical description of atomic-scale friction.

Classical atomic friction theory [1] typically simplifies the process by describing the dynamics of atoms in a solid in terms of a Langevin-type equation of motion with an explicit dissipation term, $\eta\dot{x}(t)$, in which the dissipation rate η is related to the fluctuation-dissipation theorem, $< R(t)R(t') > \sim \eta k_B T\delta(t-t')$. Here $R(t)$ is the randomly fluctuating force, appearing in the Langevin dynamics, and "<>" stands for the mean.

In our model, we follow a dual approach. Our first approach is to perform a molecular dynamics simulation on an initially locally deformed body-centered-cubic (bcc) lattice with a (100) surface, where the lattice is described as an ensemble of point masses, interacting via dissipationless, harmonic springs. In this way, we model the simplest possible, mono-atomic slip contact and compute the time-dependent atomic displacements and velocities. Our second approach is to associate the simulation with a separate calculation of the phonon dispersion relations. While in the molecular dynamics simulation we track the local energy and momentum *flowing* from the deformed area to the whole lattice, in the phononic calculation we track the dephasing of the phonon normal modes. Our model provides a meaningful description of the redistribution of momentum and energy involved in atomic-scale stick-slip motion without the need for thermalization of the phonon system. In this way, we show that friction arises without the need of explicit dissipation. We argue that the mechanism of phonon dephasing naturally leads to typical frictional behavior with typical rates of frictional energy loss.

[1] S. Krylov, and J. W. M. Frenken, Phys. Status Solidi B, 251, 711 (2014)

HIM characterization of noble metal nanostructures for surface-enhanced Raman spectroscopy

H. Takei[1,2], N. Bessho[1], S. Yoneda[1], T. Okamoto[3], A. Beyer[4], H. Vieker[4], A Gölzhäuser[4]

[1]*Department of Life Sciences, Toyo University, Itakura, Gunma 374-0193, Japan*
(corresponding author: H. Takei, e-mail: h_takei@toyo.jp)

[2]*Bio-Nano Electronics Research Centre, Toyo University, Kawagoe, Saitama 350-8585, Japan*

[3]*RIKEN, 2-1 Hirosawa, Wako, Saitama 351-0198, Japan*

[4]*Physics of Supramolecular Systems and Surfaces, University of Bielefeld, D-33615 Bielefeld, Germany*

Surface-enhanced Raman spectroscopy (SERS) has been receiving much attention as an optical analytical technique capable of providing detailed information of surface adsorbed molecular species [1, 2]. To a large extent, SERS is based on the intensified electromagnetic field of a near field generated in the vicinity of noble metal nanostrucutres upon excitation by light of the resonant frequency. The near field is generated by collective oscillation of free electrons and is greatly influenced by the general size and dimension of the nanostructure as well as the local interaction among neighboring nanostructures [3]. Quite often, gaps separate electrically isolated nanostructures over a distance less than ten nm [4]. For observation of such structures the scanning electron microscope is not ideally suited as pre-coating of the sample with an electrically conducting layer inevitably alters the morphology. On the other hand, helium ion microscopes (HIM) are ideally suited because of its capability to neutralize the helium ion beam with electrons, thus precluding the need for pre-coating [5].

In this paper we describe two types of nanostructures for SERS analysis. With one type, a monolayer of quasi-monodisperse SiO_2 nanospheres, with the diameter ranging from 50 to 200 nm, is formed on a substrate, which is subsequently coated with a thin layer of noble metals with the thickness ranging from 5 to 30 nm [6]. When the layer is thin, numerous metal islands isolated from each other are formed on individual nanospheres. As the thickness is increased, these islands begin to merge with each other. Eventually, a semicontinuous metal layer is formed over the nanosphere monolayer [7]. The second type of metalic nanostructures is formed by galvanic displacement reaction which is based on a difference in ionization tendency in various metal. More specifically, immersion of a copper block in a $AgNO_3$ solution results in formation of silver dendrites, for example. Recently, it was reported that use of copper nanoparticles in place of bulk copper lead to formation of silver nanostructures

with various morphologies [8, 9]. We show that copper nanostructrues as well as those of other base metals, formed according to the method of the first type, can be used as seeds for galvanic displacement reaction. In particular, use of copper nanostructures results in nanofilaments some 100 nm in diameter and extending well over 10 μm in length. The growth process is terminated naturally when copper is depleted. They have been found suitable for SERS analytis.

We will characterize various nanostructures formed by the two methods described above, principlly by HIM, optical absorbance, and SERS. Morphological information obtained by HIM observations is used to calculate the spatial field strength of the near-field generated in the vicinity, the method of calculation being the finite difference time domain (FDTD) method. There are many fascinating local regions that promise to provide favorable "hot spots", regions of an intense near-field. A gap among adjacent cap-shaped noble metal nanoparticles, two opposite ends of a dimer structure, a kink in an individual nanofilament, and a crossing of two nanaofilaments are such nanostrucutres. It is hoped that detailed investigation of these nanostructures will lead to a better understanding of behavior of surface atoms which determines the stability of these structrures under chemically harsh environments as well as improvement in a wide range of analytical techniques that exploit plasmonic properties of noble metal nanostructures [10].

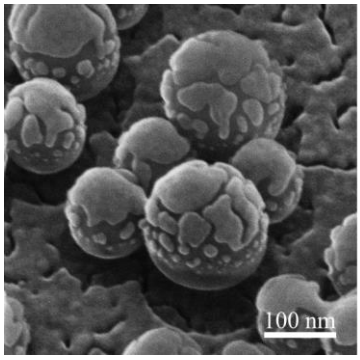

Type 1 Nanostructure

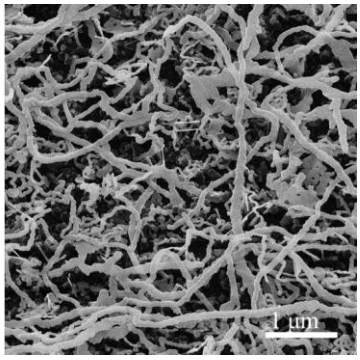

Type 2 Nanostructure

Part of this study has been supported by a Grant for the Programme for the Strategic Research Foundation at Private Universities S1101017 from the Ministry of Education, Culture, Sports, Science and Technology (MEXT), Japan

[1] M. E. Stewart, C. R. Anderton, L. B. Thompson, J. Maria, S. K. Gray, J. A. Rogers, and R. G. Nuzzo, Chem. Rev. 108, 494 (2008)

[2] J. A. Dieringer, K. L. Wustholz, D. J. Masiello, J. P. Camden, S. L. Kleinman, G. C. Schatz, and R. P. Van Duyne, J. Am. Chem. Soc. 131, 849 (2009)

[3] M. A. Garcia, J. Phys. D: Appl. Phys. 44, 1 (2011)

[4] B. W. Ward, J. A. Notte, and N. P. Economou, J. Vac. Sci. Technol., B: Microelectron. Nanometer Struct. 24, 2871 (2006)

[5] S. S. Aćimović, M. P. Kreuzer, M. U. González, and R. Quidant, ACS Nano 3, 1231 (2009)

[6] M. Himmelhaus and H. Takei, Sens. Actuators, B 63, 24 (2000)

[7] H. Takei, N. Bessho, A. Ishii, T. Okamoto, A. Beyer, H. Vieker, and A. Gölzhäuser, Langmuir 30, 2297 (2014)

[8] Y.-N. Wang, W.-T. Wei, C.-W. Yang, and M. H. Huang, Langmuir 29, 10491 (2013)

[9] R. Liu and A. Sen, Chem. Mater. 24, 48 (2012)

[10] H. Takei and T. Yamaguchi, Phys. Chem. Chem. Phys. 12, 4505 (2010)

Attosecond Delays in the Photoemission from the Layered Crystals Bi_2Te_3 and Non-Centrosymmetric BiTeCl

Sergej Neb[1], Christian Oberer[1], Walter Enns[1], Norbert Müller[1], J.-Hugo Dil[2,3], Evgueni V. Chulkov[4,5], Pedro M. Echenique[4], Walter Pfeiffer[1], Ulrich Heinzmann[1]

[1] *Molecular and Surface Physics, Faculty of Physics, Bielefeld University, 33615 Bielefeld, Germany*
[2] *Paul-Scherrer-Institut, Villigen, Switzerland*
[3] *Institute of Condensed Matter Physics, École Polytechnique Fédérale de Lausanne, CH-1015 Lausanne, Switzerland*
[4] *Donostia International Physics Center (DIPC) and Unidad de Fisica de Materiales CSIC-UPV/EHU, Basque Country, Spain5*
[5] *Tomsk State University, Russian Federation*

E-mail: uheinzm@physik.uni-bielefeld. de

The availability of single attosecond (as) XUV pulses allows investigating ultrafast electron dynamics on the as time scale by recording slight temporal shifts of the photoelectron streaking in a simultaneously present strong IR field [1,2]. The physical origin of the observed small delays is not yet understood and controversial theoretical models coexist demonstrating our still limited understanding of the fundamentals of the photoemission process [3-5].

Here we report on as-time-resolved photoemission from the layered crystals Bi_2Te_3 and non-centrosymmetric BiTeCl. The lack of inversion symmetry allows studying relative photoemission delays on differently terminated but well-defined surfaces. Due to reversed layer stacking, photoelectron propagation effects such as the mean free path and the internal effective potential can be determined. However, the measured relative delays cannot be explained by electron propagation alone. Hence effects beyond pure propagation through the layers influence the photoemission dynamics.

References

[1] A.L. Cavalieri, N. Müller, Th. Uphues, V.S. Yakovlev, A. Baltuska, B. Horvath, B. Schmidt, L. Blümel, R. Holzwarth, S. Hendel, M. Drescher, U. Kleineberg, P. M. Echenique, R. Kienberger, F. Krausz and U. Heinzmann, "Attosecond spectroscopy in condensed matter", Nature 449, 1029 - 1032 (2007)
[2] S. Neppl, R. Ernstorfer, A.L. Cavalieri, C. Lemell, G. Wachter, E. Magerl, E.M. Bothschafter, M. Jobst, M. Hofstetter, U. Kleineberg, J.V. Barth, D. Menzel, J. Burgdörfer, P. Feulner, F. Krausz, R. Kienberger, "Direct observation of electron propagation and dielectric screening on the atomic length scale", Nature 517, 342–346 (2015)
[3] for a review see U. Heinzmann, "Attosecond Time-Resolved Photoemission Spectroscopy in Condensed Matter – Photoelectron Wave Phase Shifts and Time Delays", Chapter 13 of "Attosecond Physics" Springer Series in Optical Sciences 177 (Eds. L. Plaja et al.), p. 231-253, DOI 10.1007/978-3-642-37623-8, Springer-Verlag Berlin (2013)
[4] U. Heinzmann and J.-H. Dil, topical review, J. Phys. Condens. Matter 24, 173001 (2012)
[5] R. Pazourek, S. Nagele and J. Burgdörfer, Rev. Mod. Phys. 87, 765 (2015)

Angle resolved Photoemission from Cu single crystals; New insights into the Photoemission Process

F. Roth[1], C. Lupulescu[2], E. Darlatt[3], A. Gottwald[3], W. Eberhardt[1,2]

[1] *Center for Free Electron Laser Science (CFEL), DESY, Notkestr. 85, D-22607 Hamburg, Germany*
Corresponding author e-mail: wolfgang.eberhardt@desy.de

[2]*Inst. for Optics and Atomic Physics, TU Berlin, Strasse des 17. Juni 135, D-10623 Berlin, Germany*

[3] *Physikalisch Technische Bundesanstalt (PTB), Abbestr. 2-12, D-10587 Berlin, Germany*

We present angle resolved photoemission spectra for Cu(100) and Cu(111) single crystals in normal emission geometry, taken at tightly spaced intervals for photon energies between 8 eV and 150 eV. This systematic collection of spectra gives unprecedented insight into the influence of the final states to the photoemission process as well as the band structure and lifetimes of highly excited electrons in Cu. These data also serve as a well-defined test case for full photoemission calculations as they have become possible recently.

Measuring the initial state bandstructure of Cu has been the 'gold standard' of angle resolved photoemission spectroscopy. Here we are interested in the final states. Up to at least 100 eV final state energy a multitude of clear and well-defined final states determines the photoemission process and even beyond these energies direct interband transitions are still detectable. The spectra are shown in a false color representation in Fig. 1 for the Cu(111) surface orientation. The color scale is linear and the spectra are normalized to the photoemission current taken from the Au coated refocussing mirror, the final optical element in front of the sample.

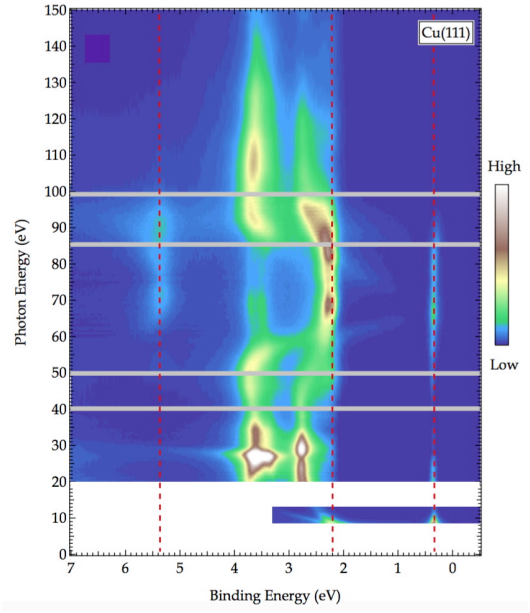

Fig. 1 Normal emission photoemission from the (111) surface, displaying the band dispersion along the Λ- axis.

In Fig. 1 the well known (111) surface state shows an intensity maximum at low photon energies as well as near 70 eV photon energy. The d-band emission displays intensity maxima for emission from initial states near the Γ and L points. Momentum conservation leads to the assignment and -- taking the photon energy into account -- the location of the final state bands involved in these direct transitions. The free electron like final state approximation works reasonably well as a first approximation, but on the other hand there are also other transitions, due to Umklapp scattering, contributing to the spectra. This is a definite manifestation that band structure mapping by angle resolved photoemission indeed works as pronounced by the protagonists of this technique. Inelastic electron scattering, the so-called inelastic mean free path, does not overpower these observations. As the intensity variations demonstrate, even at kinetic energies around 50 to 70 eV, the direct transition related signal is a factor of 5-10 larger than the background.

The measured width of the final states in the observed transitions can be evaluated by plotting the data shown in Fig. 1 at constant initial state energy as indicated by the red dashed lines. The width observed in the peaks of these curves is attributed to the electron self energy or lifetime. A plot of the values thus obtained is shown here as Fig. 2 as function of the final state energy. The widths seem to increase with final state energy whereas a free electron gas model (blue curve), calculated with the parameters of Cu (1) predicts a saturation. On the other hand, the values measured here are in approximate agreement with an estimate derived by Goldmann et al. (2) (yellow line in Fig. 2) earlier.

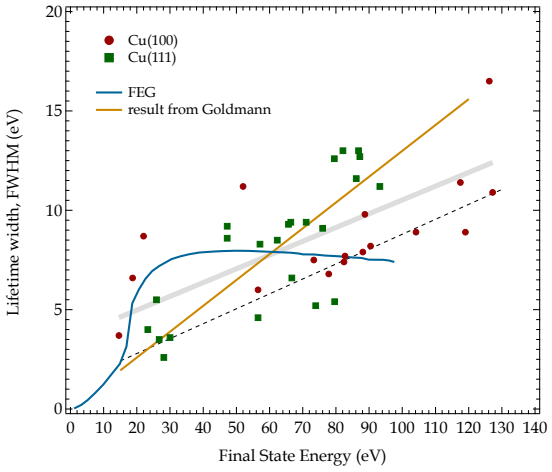

Fig. 2 Observed width of the direct transitions compared with calculations for a Free Electron Gas (1), blue curve, and an earlier estimate (2), (yellow line).

This work was funded within the program ‘Structure of Matter’ of the Helmholtz Association of Research Centers in Germany.

This paper has been accepted for publication in the Journal of Electron Spectroscopy.

(1) P.M. Echenique, J.M. Pitarke, E.V. Chulkov, A. Rubio, ***Chem. Phys. 251***, 1 (2000)
(2) A. Goldmann, W. Altmann, V. Dose, ***Solid State Comm. 79***, 511 (1991)

Determination of the photoelectron interaction time by spin-resolved ARPES

M. Fanciulli[1,2], H. Volfova[3], S. Muff[1,2], J. Minar[3], J. H. Dil[1,2]

[1]*Institut de Physique de la Matière Condensée, Ecole Polytechnique Fédérale de Lausanne, CH-1015 Lausanne, Switzerland*

[2]*Swiss Light Source, Paul Scherrer Institute, 5232 Villigen, Switzerland*

[3]*Department of Chemistry, Ludwig Maximillian University, D-81377 Munich, Germany*

(corresponding author: Hugo Dil: hugo.dil@epfl.ch)

Initially spin- and angle-resolved photoemission spectroscopy (SARPES) was conceived for the study of the band structure of magnetic materials. However, over the last decade it reached a breakthrough in the study of systems with large spin-orbit interaction (SOI). It has played a crucial role in the identification of topological insulators, and in the understanding and identification of complex Rashba systems. Based on these, and older experiments, it has been realised that any spin polarisation measured by SARPES does not necessarily reflect the initial state spin properties [1]. This is often regarded as a nuisance, but can also be explicitly used to determine certain properties. We have. for example, recently used such information to demonstrate that the picture of pure singlet or triplet superconductivity breaks down in Sr_2RuO_4 [2].

Here we will show results for one of the most fascinating aspects of using the spin signal of spin degenerate bands, namely the determination of the photoelectron interaction time. The fact that kinetic energy dependent spin polarisation and photoemission time delay are intimately connected via the phase shift between different matrix elements, as illustrated in the figure, has been known for a long time [references in 1]. However, the model was purely designed for atomic-like targets, and application was limited because of the need to vary the photon energy during the experiment, thereby introducing further dependencies. We have now for the first time applied this concept to angle-resolved measurements with fairly good energy resolution (60 meV) on single crystal samples.

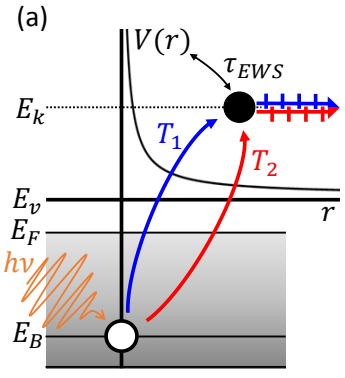

The band dispersion allows us to use a single, well chosen, photon energy to vary the kinetic energy by just measuring at different binding energies. To interpret the data we revisited the original atomic model [3] and adapted it to dispersing bands. Supported by

state-of-the-art one step photoemission calculations we could simplify the model to the following expression:

$$\tau > 0.72\hbar \left| \frac{\partial(\mathbf{P} \cdot \hat{\mathbf{n}})}{\partial E_b} \right|$$

Where τ is the Eisenbud-Wigner-Smith (EWS) time delay in photoemission, and $\mathbf{P} \cdot \hat{\mathbf{n}}$ is the measured spin polarisation normal to the scattering plane.

As with all new measurement concepts it is important to start with a model system, and we chose the well-known bulk sp-band of Cu(111). In the figure below the normal spin component (P_y) is shown as a function of binding energy. From the slope we can determine a photoemission delay time of 62 attosecond, which is in good agreement with expectations from the comparison of attosecond time resolved experiments and theory [4]. However, in contrast to time-resolved measurements our SARPES-based method is sensitive to an absolute time scale, and not only to time differences.

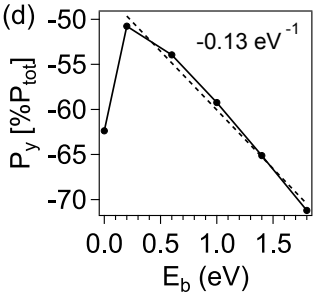

Besides these proof-of-principle measurements on Cu(111) [5] results obtained on graphene will also be shown. In this case a much longer time delay is measured, which could reflect the more collective nature of the valence electrons. It will also be discussed how this method can be applied to determine additional parameters for correlated electron systems and thus assisting their increased understanding.

Further improvements of both the model and experimental capabilities will open up a whole new realm of possibilities to determine interaction times in solids. These results will be complimentary to attosecond time-resolved photoemission techniques. Together, these extremely difficult experiments could further boost the use of photoemission for solving complex physical problems.

In depth discussions with Ulrich Heinzmann are gratefully acknowledged.

[1] U. Heinzmann and J. H. Dil, Journal of Physics: Condensed Matter 24, 173001 (2012).

[2] C.N. Veenstra et al. Physical Review Letters 112, 127002 (2014).

[3] N. Cherepkov, Advances in Atomic and Molecular Physics, Vol. 19 (Elsevier, 1983) pp. 395–447.

[4] M. Lucchini et al. Physical Review Letters 115, 137401 (2015).

[5] M. Fanciulli, submitted to Physical Review Letters

Spatial in-homogeneity and temporal dynamics of a 2D electron gas in interaction with a 2D adatom gas

F. Cheynis[1], S. Curiotto[1], F. Leroy[1], P. Müller[1]
[1] *Centre Interdisciplinaire de Nanoscience de Marseille, CINaM*
Aix Marseille Université - CNRS
Email: cheynis@cinam.univ-mrs.fr

Owing to their fascinating properties, 2D electron gas systems (2DEG) have recently generated major breakthroughs in the field of condensed matter physics. For instance, the occurrence of a conductive 2D phase at the surface of oxides paves the way for the emerging field of functional oxide electronics[1]. 2D Dirac electron gas observed in graphene has been shown to surpass the long-standing 2DEG confined at the GaAs/AlGaAs interface to determine the Planck constant h using Quantum Hall resistance measurements[2]. Apart from homogeneous 2DEG systems, a growing need for nanostructured electron gas is observed. For instance 1D channels obtained by lithographic approaches are building blocks for single-electron meso-transport studies[3].

We focus on a 2DEG that is interestingly created by a charge transfer from a 2D adatom gas (2DAG) to an electronic surface state. More particularly, the 2DAG induced by Ag deposition (Ag-2DAG) onto a Si(111)$\sqrt{3}\times\sqrt{3}$-Ag reconstructed surface shows an electron doping property of the so-called S_1 surface state[4]. A single mesoscopic imaging technique (low-energy electron microscopy, LEEM) is used to characterize independently both atomic and electronic components of the system.

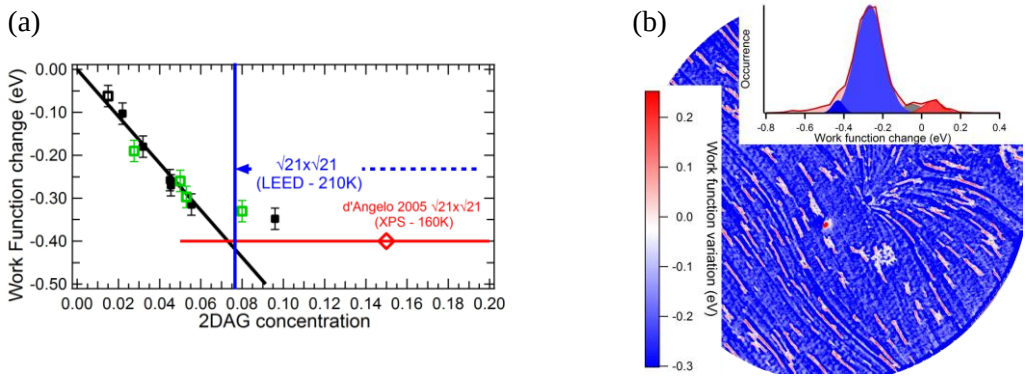

Fig. 1*: (a) Surface work function vs Ag-2DAG concentration relationship as determined by LEEM. (b) Spatially inhomogeneous work function regime induced by the nucleation of growing Ag-3D island colonies (red contrast, field-of-view=25µm).*

In this study [5], a linear relationship between the surface work function and the Ag-2DAG concentration is demonstrated. A breakdown of this dependence is evidenced as a consequence of the occurrence of the Si(111)$\sqrt{21}\times\sqrt{21}$-Ag surface reconstruction below RT [Fig. 1(a)]. Uncommon in-homogeneous spatial and temporal distributions of the 2DEG observed for deposition below RT are discussed in details [Fig. 1(b)]. Explanations of the origin of a 2DEG structured on individual terraces and its associated time-related charge/discharge behaviour are tentatively provided.

[1] A. F. Santander-Syro, *et al.*, Nature **469**, 189 (2011).
[2] R. Ribeiro-Palau, FC, *et al.*, Nature Nanotech. **10**, 965 (2015).
[3] S. Hermelin *et al.* Nature **477**, 435 (2011).
[4] Y. Nakajima *et al.* Phys. Rev. B **56**, 6782 (1997).
[5] F. Cheynis *et al.* Submitted to Phys. Rev. Lett.

Tuesday

Model catalysts for reforming and oxidation reactions: ultrathin films of zirconium oxide and cobalt oxide

Günther Rupprechter, Hao Li, Kresimir Anic, Christoph Rameshan, Andrey Bukhtiyarov

Institut für Materialchemie, Technische Universität Wien, A-1060 Wien, Austria
(corresponding author: G. Rupprechter, e-mail: guenther.rupprechter@tuwien.ac.at)

It is well accepted that surface science based planar model catalysts are well-suited for fundamental studies of surfaces processes, despite the inherent differences between model and technological catalysts [1-3]. Classical ultrahigh vacuum (UHV) based experiment are still indispensable but methodological developments also allow to examine active functioning model catalysts under operando conditions, at (near) atmospheric pressure and at elevated temperature. Frequently applied methods encompass polarization-modulation infrared reflection absorption spectroscopy (PM-IRAS), sum frequency generation (SFG) laser spectroscopy and near atmospheric pressure X-ray photoelectron spectroscopy (NAP-XPS). Most of the current operando studies were performed at synchrotron sources (BESSY (DE), MaxLab (SE), SLS (CH)), and in lock-step with theory. In the current contribution two oxides that are relevant for Solid Oxide Fuel Cell (SOFC) technology are discussed: (i) Ni-ZrO_2 SOFC „cermet" anodes for CH_4 reforming to H_2 and/or H_2 oxidation, and (ii) Co_3O_4, a potential catalysts for cleaning H_2 feeds from CO traces via preferential CO oxidation (PROX).

In order to model SOFC anodes well-ordered ultrathin films of ZrO_2 were grown in UHV by oxidation and annealing of $Pt_3Zr(0001)$ single crystals [4,5]. Ni was deposited by physical vapor deposition. Low Energy Electron Diffraction (LEED), Scanning Tunneling Microscopy (STM), high resolution X-ray Photoelectron Spectroscopy (XPS) and Density Functional Theory (DFT) indicated the formation of a well-structured ZrO_2 trilayer film, corresponding to the (111) facet of cubic ZrO_2. Whereas the interaction of the film with CO or CO_2 was very weak (desorption temperatures of 155 and 117 K, respectively), its interaction with water was very strong (desorption temperature of 485 K). NAP-XPS was thus applied to examine water adsorption and the hydroxylation of the film (Fig. 1, left). Once hydroxylated the film exhibited exceptional activity for reaction with CO_2 (wheras the non-hydroxylated film did not). IRAS, using formic acid (HCOOH) and formaldehyde (HCHO) as reference, was then used to identify the functional groups of the formed species. CO_2 and H_2O codosing induced the formation of formaldehyde, dioxymethylene and formate on hydroxylated ZrO_2.

Low temperature fuel cells rely on clean hydrogen, since CO traces in the feed would poison the catalyst. Cobalt oxide is highly active for low temperature CO oxidation and PROX and holds potential for replacing noble metals and/or rare earth oxides. Nevertheless, the origin of the high cobalt oxide activity is still not thoroughly understood. Thin cobalt oxide films,

Co_3O_4(111) or CoO(111), with well-defined structure were thus grown on Ir(100) by Co physical vapor deposition in O_2 background and subsequent post-oxidation [6].

The interaction of 6 ML thick Co_3O_4(111) or CoO(111) films with CO was again examined by TPD, XPS and PM-IRAS (200 to 700 K, UHV to 100 mbar). Upon CO exposure, weakly bonded CO, carbonates and elementary carbon were observed. Upon desorption and repeated adsorption/desorption cycles, (partial) reduction of cobalt oxide occurred. Interestingly, for CO oxidation (mbar pressure, up to 650 K) operando NAP-XPS in the valence band region revealed the same active state of the catalyst, independent of the original composition (Co_3O_4 or CoO), which is in line with corresponding operando studies on technological „powder“ Co_3O_4 catalysts that were also performed by our group [7].

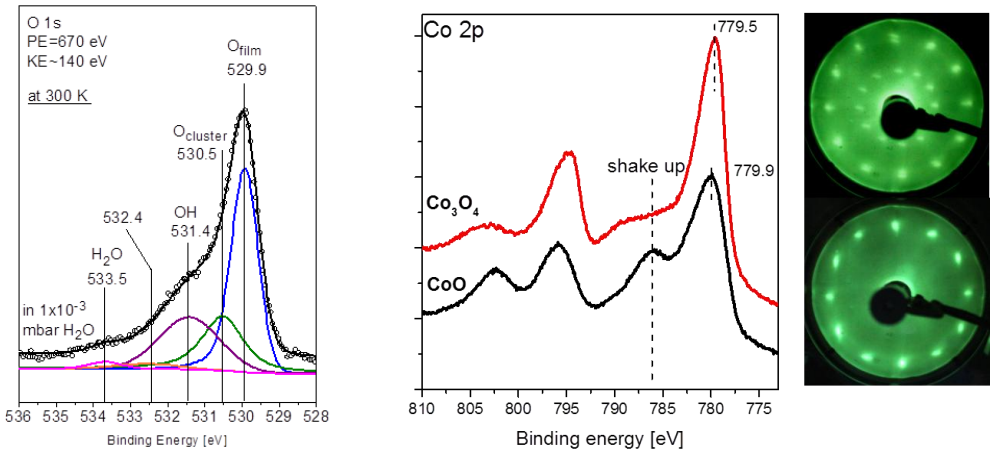

Figure 1. (NAP-) XPS spectra of hydroxylated ZrO_2 (left) and of cobalt oxide thin film model catalysts (right). For the latter, LEED patterns are included.

For both oxide model catalysts, ZrO_2 and Co_3O_4, potential reaction mechanisms and their relevance for technological catalysis will be discussed.

Support by the Austrian Science Fund (FWF SFB-F45 FOXSI & DACH Project ComCat) is gratefully acknowledged.

[1] G. Rupprechter, Advances in Catalysis, 51 (2007) 133-263.

[2] K. Föttinger, G. Rupprechter, Accounts of Chemical Research, 47 (2014) 3071−3079.

[3] Y. Suchorski, G. Rupprechter, Surface Science, 643 (2016) 52-58.

[4] M. Antlanger, W.Mayr-Schmölzer, J. Pavelec, F. Mittendorfer, J. Redinger, P. Varga, U. Diebold, M. Schmid, Phys. Rev. B., 86 (2012) 03451.

[5] H. Li, J.J. Choi, W. Mayr-Schmölzer, C. Weilach, C. Rameshan, F. Mittendorfer, J. Redinger, M. Schmid, G. Rupprechter, Journal of Physical Chemistry C, 119 (2015) 2462–2470.

[6] W. Meyer, D. Hock, K. Biedermann, M. Gubo, S. Müller, L. Hammer, K. Heinz, Phys. Rev. Lett., 101 (2008) 016103.

[7] J. Yang, L. Lukashuk, J. Akbarzadeh, M. Stöger-Pollach, H. Peterlik, K. Föttinger, G. Rupprechter, U. Schubert, Chemistry – A European Journal, 21 (2105) 885-892.

Non-Band-gap Photoexcitation of Hydroxylated TiO_2

Y. Zhang, D.T. Payne, C.L. Pang, H.H. Fielding, G. Thornton

London Centre for Nanotechnology, University College London,
20 Gordon Street, London WC1H 0AJ, UK
(Corresponding author: G. Thornton, e-mail g.thornton@ucl.ac.uk)

This TiO_2 is a prototypical light-harvesting semiconductor showing promising potential in the application of photocatalysis. Nevertheless, it has proven difficult to establish the detailed processes involved in photocatalysis, partly because the excited states involved are difficult to study. Here, we present evidence for the existence of hydroxyl-induced states in the conduction band region that may also play a role in photocatalysis. In the two-photon photoemission (2PPE) experiment on rutile TiO_2(110), an electron in the well-known defect states about 0.8 eV below E_F is excited into an intermediate state by absorbing a photon, from which it is further excited above the vacuum level by a second photon. By varying the photon energy from about 3 to 4 eV, we observe a pronounced resonant enhancement of the 2PPE intensity when the photon energy is about 3.5 eV as shown in the Figure (a). It indicates an intermediate state at about 2.7 eV above E_F marked by the green peak in the Figures. Further investigations show that this state is induced by the hydroxyls on the TiO_2 surface with a lifetime shorter than 15 fs. The intensity of the resonance can be greatly enhanced by the adsorption of molecular water at 100 K. The energy of the hydroxyl-induced state is found to be 2 eV lower and less-influenced by the water adsorption than that expected for a hydroxylated TiO_2(110) surface.

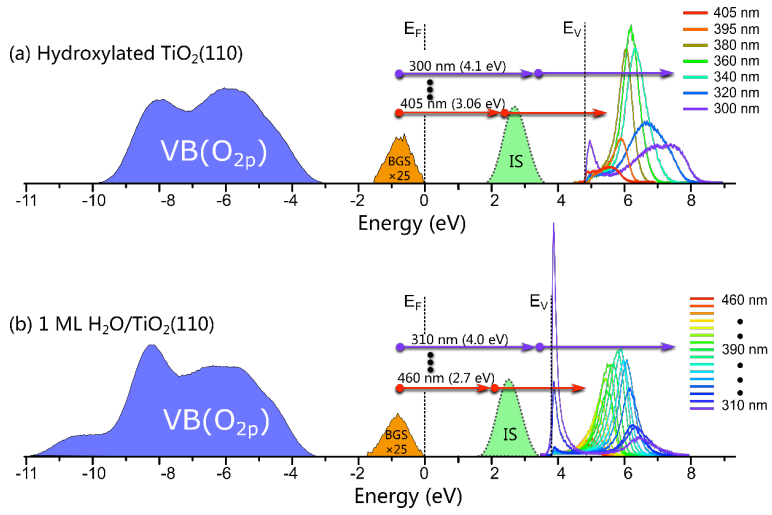

Figure 1. Schematic of 2PPE transitions.

1. Y. Zhang, D.T. Payne, C.L. Pang, H.H. Fielding, G. Thornton, J. Phys. Chem. Lett. 6 (2015) 3391-3395.

Molecular adsorption influences the quantum structure of oxide-supported gold nanoparticles: Chemisorption versus physisorption

Christian Stiehler,[1] Florencia Calaza,[1] Wolf-Dieter Schneider,[1,2]
Niklas Nilius,[1,3] Hans-Joachim Freund [1]

[1]*Fritz-Haber-Institut der Max-Planck-Gesellschaft, Faradayweg 4-6, 14195 Berlin, Germany*
[2]*Ecole Polytechnique Fédérale de Lausanne (EPFL), Institute of Condensed Matter Physics, CH-1015 Lausanne, Switzerland*
[3]*Carl von Ossietzky Universität Oldenburg, Institut für Physik, D-26111 Oldenburg, Germany*
(e-mail: wolf-dieter.schneider@epfl.ch)

Electron quantization is a fundamental phenomenon that accompanies the transition from bulk metals to nanoclusters. The associated opening of a gap at the Fermi level crucially affects various properties of the nanostructures, e.g., its electrical and optical behavior and its performance in catalytic reactions [1]. Using STM conductance spectroscopy and mapping, we have investigated the electronic structure of 2D Au islands, containing between 50-200 atoms, on MgO/Ag(001) thin films [2]. The bare islands exhibit characteristic quantum well states (QWS), arising from the spatial confinement of the Au-6p-orbitals. To explore the impact of molecular adsorption on the quantized structure of individual metal nanoparticles, isophorone ($C_9H_{14}O$) and CO_2, as prototype molecules for physisorptive and chemisorptive binding, were dosed onto monolayer Au islands grown on MgO thin films. The molecules attach exclusively to the metal-oxide boundary, while the interior of the islands remains pristine. The Au quantum well states are perturbed due to the adsorption process and increase their mutual energy spacing in the CO_2 case but move together for isophorone adsorption [3]. The shifts disclose the nature of the molecule-Au interaction, which relies on electron exchange for the CO_2 ligands but on dispersive forces for the organic species. Our experiments reveal how molecular adsorption affects individual quantum systems, a topic of utmost relevance for heterogeneous catalysis.

All experiments were carried out with an ultrahigh-vacuum STM operated at 5K. The sample electronic structure was probed with differential conductance (dI/dV) spectroscopy using a lock-in technique (V_{mod} *=15 mV rms*). The MgO films were prepared by reactive Mg deposition onto a sputtered and annealed Ag(001) surface in 5×10^{-7} mbar O_2 at 550 K [4]. The procedure resulted in atomically flat oxide layers, exposing large rectangular terraces delimited by nonpolar step edges. About 0.06 ML of gold was evaporated at 300 K onto the MgO surface, where it aggregated into quasi hexagonal islands of monolayer height. This peculiar 2D growth regime was earlier explained with an electron transfer from the low-

workfunction MgO/Ag support through the MgO spacer into the highly electronegative Au islands [5]. The extra charges localize at the island perimeter, as this configuration minimizes repulsive electron-electron interactions [6]. Isophorone (0.5 L) was dosed at room temperature from a flask containing the liquid compound, while CO_2 (50 L) was supplied by backfilling the chamber with 1×10^{-7} mbar at 250 K sample temperature. After preparation, the sample was immediately transferred into the cryonic microscope to avoid contamination from the rest gas.

The perturbation of a confined electronic system by molecular adsorbates is not only of academic interest, but directly affects our understanding of heterogeneous catalysis. In many cases, ground-state properties are used to analyze the role of catalyst particles in chemical processes, although their quantum structure gets modified under reaction conditions. Our experiments demonstrate how the impact of molecular ligands on the properties of metal nanostructures can be investigated on a mechanistic level.

This work has been supported by the DFG Excellence Project ‘UNICAT’. C. S. is grateful for a fellowship of the „Studienstiftung des Deutschen Volkes“. F. C. thanks the Humboldt Foundation for a Georg-Foster Fellowship.

[1] M. Valden, X. Lai, D. W. Goodman, Science **281**, 1647 (1998).

[2] C. Stiehler, Y. Pan, W.-D. Schneider, P. Koskinen, H. Häkkinen, N. Nilius, and H.-J. Freund, Phys. Rev. B **88**, 115415 (2013).

[3] C. Stiehler, F. Calaza, W.-D. Schneider, N. Nilius, and H.-J. Freund, Phys. Rev. Lett. **115**, 036804 (2015).

[4] S. Schintke, S. Messerli, M. Pivetta, L. Libioulle, F. Patthey, M. Stengel, A. De Vita, and W.-D. Schneider, Phys. Rev. Lett. **87**, 276801 (2001).

[5] G. Pacchioni, L. Giordano, M. Baistrocchi, Phys. Rev. Lett. **94**, 226104 (2005)

[6] X. Lin, N. Nilius, M. Sterrer, P. Koskinen, H. Häkkinen, H.-J. Freund, Phys. Rev. B **81**, 153406 (2010)

Interplay between steps and oxygen vacancies on curved TiO_2(110)

Luis A. Miccio[1,2], Martin Setvin[3], Moritz Müller[4], Mikel Abadía[1], Ignacio Piquero[1], Jorge Lobo-Checa[1], Frederik Schiller[1], Celia Rogero[1], Michael Schmid[3], Daniel Sánchez-Portal[1,2], Ulrike Diebold[3], J. Enrique Ortega[1,2,5]

[1] *Centro de Física de Materiales (CSIC-UPV/EHU), San Sebastián, Spain*

[2] *Donostia International Physics Center (DIPC) San Sebastián, Spain*

[3] *Institute of Applied Physics, Vienna University of Technology, 1040 Vienna, Austria*

[4] *CIC nanoGUNE, Ave. Tolosa 76, 20018 San Sebastián, Spain*

[5] *Departamento de Física Aplicada, Universidad del País Vasco (UPV/EHU), San Sebastián, Spain*

Vicinal surfaces exhibit distinct chemical and physical properties due to their high density of atomic steps, being also useful as nanoscale templates to control the growth of low dimensional structures, such as nanodots or nanostripes. In this context, a vast majority of studies on the chemistry and electronic properties of rutile r -TiO_2(110) have been carried out flat surfaces, whereas much less effort has been focused on stepped planes. Moreover, as low atomic coordination sites, the step edges are chemically and electronically very active, and hence stepped surfaces may become technologically relevant, e.g., as a way of tailoring new chemical properties of r-TiO_2. Using a curved r-TiO_2(110) crystal with a smooth variation of the density of atomic steps parallel to the [1-10] direction, we have performed a combined (STM-ARPES) and systematic study of stepped r-TiO_2(110) with [1-10]-oriented steps.

By means of Scanning Tunneling Microscopy (STM) we analyze the structure and distribution of steps and vacancies as a function of the average deviation (miscut α) from the (110) surface, at the centre of the sample (Fig. 1 a). We observe the surface to smoothly evolve from wide terraces, containing O_{br} vac´s (Fig. 1 b), toward narrow (110) terraces, depleted of O_{br} vac´s (Fig. 1 c). We also observe the step edge morphology changing across the sample, from [1-11] zig-zag faceting to straight [1-10] steps The [1-10] steps terminate with a pair of two-fold coordinated O atoms, which give rise to bright, triangular protrusions (S_t). The statistical analysis of the terrace width variation across the sample allows us to detect a step-bunching phase with a large α range, triggered by an optimal d~2.8 nm (110) terrace width, where all bridge-bonded O atom vacancies (O_{br} vac´s) vanish, but S_t-featured steps remain.

With Angle-Resolved Photoemission (ARPES) we focused on the Ti 3d-derived gap state (Fig. 1 d). The gap state intensity is observed to remain constant across the curved surface, directly correlating with the total density of S_t protrusions plus O_{br} vac´s measured with STM. This observation indicates that individual S_t protrusions (at steps) and O_{br} vac´s (at terraces) contribute to the crystal doping equally. The scan across the curved surface also reflects the

transition from large O_{br}-filled terraces to the high density of S_t-featured steps through a 110 meV shift in apparent binding energy, which in turn suggests differences in the polaronic relaxation at terraces and steps. Density functional theory (DFT) calculations predict that S_t protrusions of [1-10] step edges are favorable sites for the formation of O_{br} vac's in r-TiO_2(110), in accordance with previous studies on [1-11] steps [1]. Moreover, DFT indicates that the observed electron doping at the stepped part of the sample is not intrinsic to the step-edge, but stems from the presence of one O_{br} vacancy per S_t site.

We acknowledge financial support from the Spanish Ministry of Economy (grant MAT2013-46593-C6-4-P and MAT2013-46593-C6-2-P) and the Basque Government (grant IT621-13 and IT756-13), the ERC Advanced Grant "OxideSurfaces"., and the Marie Curie ITN "THINFACE".

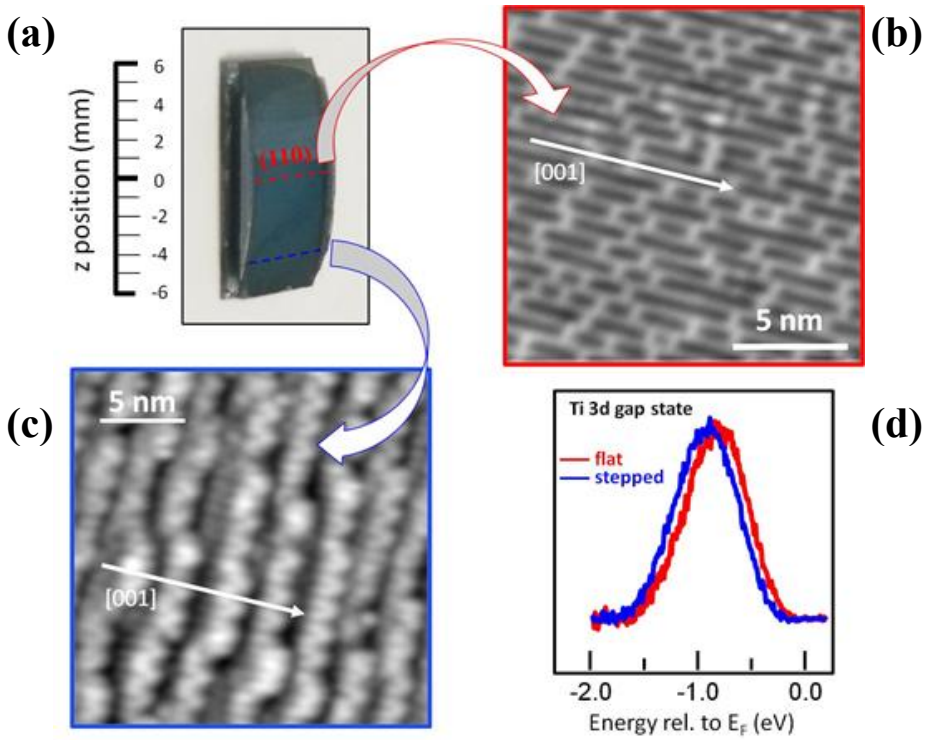

Figure 1. *(a) Photography of the curved TiO_2(110) crystal used in the present work. Marked are the center of the crystal, with large (110) terraces and O_{br} vacancies [measured with STM in panel (b)], and the edge of the crystal, with a high density of steps featured with bright triangular protrusions [measured in panel (c)]. Despite the strong structural differences from flat to stepped areas of the crystal, the Ti 3d gap state peak [measured in ARPES and shown in panel (d)], shows no intensity change,, but a small 110 meV binding energy shift.*

[1] U. Martinez, et al., Phys. Rev. Lett. **109**, 155501 (2012).

Water Interaction with Oxide Surfaces studied with Single-Crystal Adsorption Calorimetry

P. Dementyev, J. Seifert, K.-H. Dostert, F. Ivars-Barcelo, C. P. O'Brien, F. Mirabella, S. Schauermann[1], H.-J. Freund

Fritz-Haber-Institut der Max-Planck-Gesellschaft, Faradayweg 4–6, 14195 Berlin (Germany)
(corresponding author: J. Seifert, e-mail: jseifert@fhi-berlin.mgp.de)

[1] *Institute of Physical Chemistry, Christian-Albrechts-Universität zu Kiel, Max-Eyth-Str. 2, 24118 Kiel (Germany)*

The knowledge of reaction enthalpies for elementary steps catalysed at solid surfaces is crucial for a detailed understanding of heterogeneous catalysis. Aside from theoretical modelling using density function theory (DFT) temperature programmed desorption (TPD) is widely used to determine this quantity experimentally. However, for this technique the adsorption process needs to be fully reversible and therefore systems involving dissociative or reactive adsorption cannot be studied quantitatively. Here we apply a recently developed UHV single-crystal adsorption calorimeter (SCAC) based on molecular beam techniques to directly measure adsorption and dissociation energies as a function of surface coverage [1]. We present results for adsorption of water molecules on the surfaces of well-defined $Fe_3O_4(111)$ and $Fe_3O_4(100)$ as well as CaO(100) thin films grown on Pt crystals [2]. Spectroscopic identification of the surface species was performed by infrared reflection absorption spectroscopy (IRAS). We show that the adsorption energy (101 kJ mol^{-1}) of water on $Fe_3O_4(111)$ is considerably higher than all previously reported values obtained by indirect desorption-based methods. By employing ^{18}O-labeled water molecules, we prove that the generally accepted simple model of water dissociation to form two individual OH groups per water molecule is not correct.

[1] H. M. Ajo, H. Ihm, D. E. Moilanen, C. T. Campbell, Rev. Sci. Instrum. 75, 4471 (2004); J.-H. Fischer-Wolfarth, J. Hartmann, J. A. Farmer, J. M. Flores-Camacho, C. T. Campbell, S. Schauermann, H.-J. Freund, Rev. Sci. Instrum. 82, 024102 (2011)

[2] P. Dementyev, K.-H. Dostert, F. Ivars-Barcelo, C. P. O'Brien, F. Mirabella, S. Schauermann, X. Li, J. Paier, J. Sauer, H.-J. Freund, Angew. Chem. Int. Ed. 54, 13942 (2015)

Counting the Electrons: Metal Support Interactions in Catalysis and Nanoscience

J. Libuda, Y Lykhach, S. M. Kozlov[1], T. Skála[2], A. Tovt[2], V. Stetsovych[2], N. Tsud[2], F. Dvořák[2], V. Johánek[2], A. Neitzel, J. Mysliveček[2], A. Bruix[1], I. Matolínová[2], M. Vorokhta[2], K. Ševčíková[2], R. Fiala[2], M. Václavů[2], K. C. Prince[3], S. Bruyère[4], V. Potin[4], A. Migani[1], T. Staudt, G. P. Petrova[5], G. N. Vayssilov[5], F. Illas[1], S. Fabris[6], V. Matolín[2], K. M. Neyman[7]

Universität Erlangen-Nürnberg, Department Chemie und Pharmazie, D-91058 Erlangen, Germany
(corresponding author: J. Libuda, e-mail: joerg.libuda@fau.de)

[1]*Departament de Química Física and IQTCUB, Universitat de Barcelona, 08028 Barcelona, Spain*
[2]*Charles University, Department of Plasma and Surface Science, 18000 Prague 8, Czech Republic*
[3]*Sincrotrone Trieste, 34149 Basovizza, Trieste, Italy*
[4]*LICB, UMR 6303 CNRS-Université de Bourgogne, F-21078 Dijon Cedex, France*
[5]*Faculty of Chemistry, University of Sofia, 1126 Sofia, Bulgaria*
[6]*CNR-IOM DEMOCRITOS, IOM, CNR and SISSA, I-34136, Trieste, Italy*
[7]*Institucio Catalana de Recerca i Estudis Avançats (ICREA), 08028 Barcelona, Spain*

Interactions between metal nanoparticles and oxide supports control the functionality of nanomaterials. For three types of metal support interactions we demonstrate that these surprising phenomena can be understood at the atomic level.[1-3] In specific, we consider (i) electronic metal support interactions, (ii) adsorbate spillover between the support and the supported particle and (iii) anchoring of metals on the oxide support (see Figure 1).

(i) **Electronic metal support interactions (EMSI) [1]:** For more than 30 years, electronic metal support interactions have been among the most controversially discussed topics in catalysis. One open question was the charge transfer (CT) between supported nanoparticles and the oxide support, which could never be quantified experimentally. In this work we measured this charge transfer quantitatively on a well-defined platinum/ceria catalyst at particle sizes relevant for heterogeneous catalysis. Upon contact of the Pt metal with the oxide surface, the EMSI leads to electron transfer across the metal/oxide interface. The transferred electrons are taken up by Ce^{4+} ions at the interface which, thereby, are reduced to Ce^{3+}. These Ce^{3+} centers can be detected with outstanding sensitivity by resonant photoemission spectroscopy (RPES). Combining this information with structural data from STM and XPS, we are able to "count" the number of electrons which are transferred

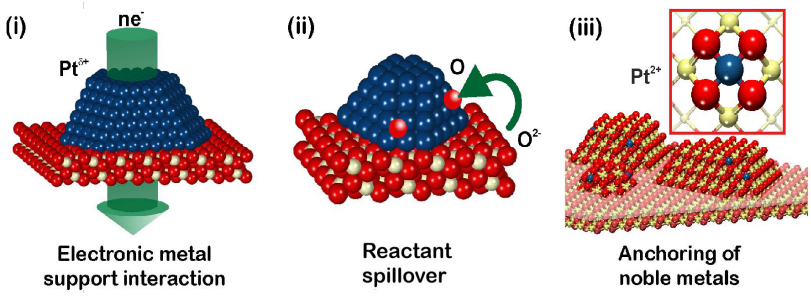

Figure 1: *Three types of metal support interaction on Pt/CeO_2: (i) electronic metal support interaction; (ii) oxygen reverse spillover; (iii) anchoring of ionic Pt species on CeO_2.*

across the metal/oxide interface (see Figure 2). We show that the CT reveals a characteristic size dependence and reaches a maximum for particles between 30 and 70 atoms, where up to 0.11 electrons are transferred per Pt atom ($Pt^{\delta+}$ with $\delta \approx 0.11$) For smaller particles, nucleation at defects hinders the CT whereas the support limits the CT for larger particles. All trends are rationalized by DF calculations. The results show that the CT can be tuned by adjusting the particle size, the structure and the properties of the support.

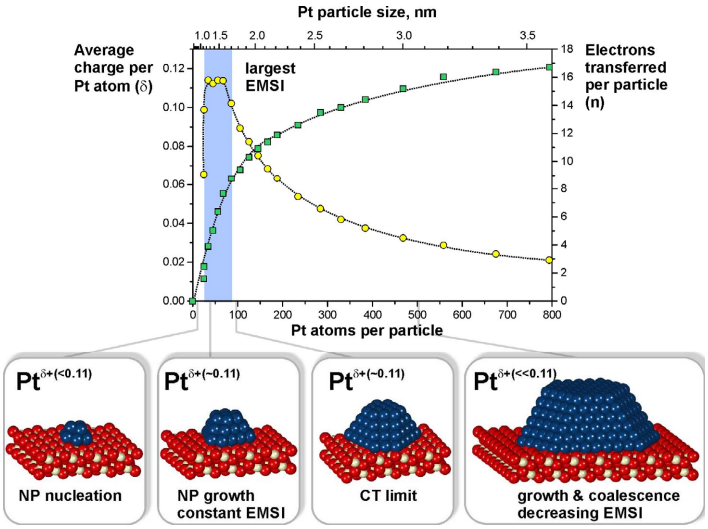

Figure 2: *Electronic metal support interaction for Pt particles on CeO_2(111) leading to charging transfer from the Pt nanoparticles to the support; average charge per Pt atom (yellow symbols) and charge per Pt particle (green symbols).*

(ii) **Reactant spillover and reverse spillover [2]**: Besides the electronic metal support interaction, the second interaction phenomenon is "spillover", i.e. oxygen transfer from ceria to Pt. We show that the oxygen transfer requires the presence of nanostructured ceria in close contact with Pt and, thus, is inherently a nanoscale effect. This explains the extraordinary structure-activity dependence of ceria-based catalysts. Using similar techniques as in (i) we quantify the effects using RPES in combination with XPS.

(iii) **Anchoring of noble metals [3]:** Platinum can be anchored to CeO_2 materials in ionic form with exceptionally high stability. Using DF calculations we identify a specific structural element, a ceria "nanopocket", which binds Pt^{2+} so strongly that it withstands sintering and bulk diffusion. Both on model catalysts and on real Pt-CeO_2 thin film catalysts, which show very high Pt efficiency in proton exchange membrane fuel cells, we identify these anchoring sites and confirm the theoretically predicted stability. Upon reduction the Pt^{2+} is partially reduced und forms ultra-small Pt aggregates. By means of IR spectroelectrochemistry we show that these Pt nanoaggregates on CeO_2 show enhanced stability towards sintering under conditions of varying electrode potential.

This work was financially supported by: European Community (FP7-NMP.2012.1.1-1 project chipCAT, Reference No. 310191), Deutsche Forschungsgemeinschaft (DFG), Excellence Cluster "Engineering of Advanced Materials", MINECO (grant CTQ2012-34969), Generalitat de Catalunya (grants 2014SGR97 and XRQTC), Czech Science Foundation (grant 15-06759S), CERIC-ERIC, COST Action CM1104, Red Española de Supercomputación. Spanish Ministerio de Educación FPU Grant AP2009-3379.

[1] Y. Lykhach, S.M. Kozlov, T. Skála, A. Tovt, V. Stetsovych, N. Tsud, F. Dvořák, V. Johánek, A. Neitzel, J. Mysliveček, S. Fabris, V. Matolín, K.M. Neyman, J. Libuda, Nature Materials 10.1038/nmat4500 (2016)

[2] A. Bruix, Y. Lykhach, I. Matolínová, A. Neitzel, T. Skála, N. Tsud, M. Vorokhta, V. Stetsovych, K. Ševčíková, J. Mysliveček, K. C. Prince, S. Bruyère, V. Potin, F. Illas, V. Matolín, J. Libuda, K. M. Neyman, Angew. Chem. Int. Ed. 53, 10525 (2014)

[3] N. Vayssilov, Y. Lykhach, A. Migani, T. Staudt, G. P. Petrova, N. Tsud, T. Skála, A. Bruix, F. Illas, K. C. Prince, V. Matolín, K. Neyman, J. Libuda, Nature Materials 4, 310 (2011)

Spatio-temporal pattern evolution in oscillating H_2 oxidation on Rh

M. Datler, I. Bespalov, J. Zeininger, G. Rupprechter, Y. Suchorski

Institut für Materialchemie, Technische Universität Wien, A-1060 Vienna, Austria
(corresponding author: Y. Suchorski, e-mail: yuri.suchorski@tuwien.ac.at)

Surface chemical reactions such as CO oxidation on platinum metal surfaces may exhibit oscillating variations of partial coverages of reactants and of the reaction rate even if external reaction parameters are constant [1]. Simultaneous formation of numerous adsorption nucleation centers combined with the spatial coupling of different surface regions lead on extended surfaces to a formation of variety of spatio-temporal patterns, such as e.g. spiral waves, target patterns, standing waves, and chemical turbulence, which can be visualized in real time by PEEM [2]. Till now such heterogeneous oscillating patterns were observed, in particular for the CO oxidation, mainly on macroscopic single crystal surfaces, whereas oscillations showing a synchronized behavior of the whole reacting surface were observed also on the nanotips [3].

We present herewith the first *in situ* observations of the oscillating spatio-temporal behaviour in the H_2 oxidation on a polycrystalline Rh foil consisting of differently oriented µm-sized domains. Until now the oscillating H_2 oxidation reaction on Rh was observed merely on the nanotip surfaces in the presence of high electric fields [4], thus the actual study is also the first successful attempt to detect the oscillating behaviour of H_2 oxidation on plane Rh surfaces.

Experimentally, the polycrystalline Rh foil (10x10 mm) was cleaned in UHV by repeated sputtering and annealing and was exposed then at isothermal conditions to oxygen at 1.1×10^{-6} mbar and hydrogen at 8.4×10^{-7} mbar. The resulting H_2 oxidation reaction was visualized by PEEM and video-monitored (Fig. 1). Due to the higher work function, the oxygen covered Rh surface appears as dark in the PEEM image, the reduced by hydrogen surface, in turn, as bright. The chemical composition of the sample could be proven *in situ* by XPS which is an integral part of the apparatus.

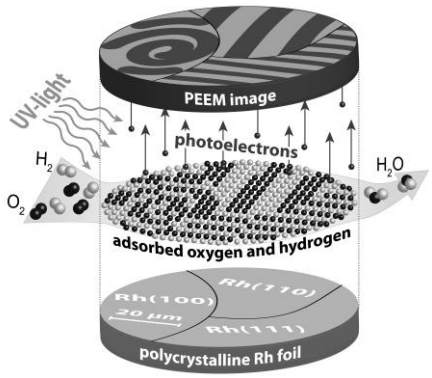

Fig.1. Schema of the experiment: the PEEM chamber is used as a flow reactor for the H_2 oxidation on Rh at partial pressures in the 10^{-6} mbar range. The spatial variations of the surface coverage during the ongoing reaction are reflected via the local work function as local PEEM image intensities and are video-monitored *in situ*.

After the induction period of a few minutes, the PEEM image showed the variety of rotating spiral-shaped waves and apparently irregular wave fronts moving in a complex "turbulent-like" way. Detailed examination of the PEEM video-files shows that the spiral-shaped waves

originate periodically from localised nucleation centers and propagate across the surface with an approximately constant velocity. The spreading waves collide with each other and annihilate upon collisions creating the cusp shaped formations. Figure 2a shows a screen shot of the ongoing H_2 oxidation on a polycrystalline Rh foil at 433 K. The nucleation centers oscillate with a frequency varying for different domains between $2.0x10^{-3}$ and $4.8x10^{-3}$ sec^{-1} producing wavelengths in the range of 12 to 25 µm.

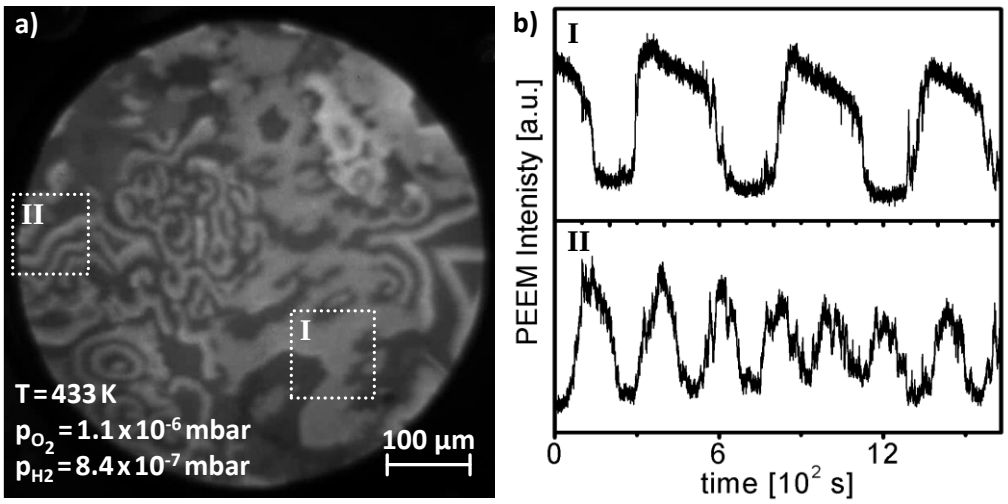

Fig. 2. PEEM monitoring of the hydrogen oxidation on a polycrystalline Rh foil: **(a)** Turbulence-like picture of ongoing H_2 oxidation at 433 K; **(b)** Oscillations of the local PEEM intensity in the (100)- and (110)-type regions. Note the approximate doubling of the frequency in the region (II) in comparison with the region (I).

The digital evaluation of the local intensity from the PEEM video-frames allows spatially-resolved monitoring of the oscillations on individual domains of the polycrystalline sample. A comparison of the local PEEM intensity variations for two crystallographically different Rh domains, shown in Fig. 2, reveals the difference in the frequency of the simultaneously occurring oscillations by factor of approximately two. This documents the terminating role of the grain boundaries in the spatial coupling of surface reactions on polycrystalline surfaces during the self-sustaining oscillations. A similar role of the grain boundaries was already observed in the catalytic ignition during CO oxidation on polycrystalline Pt and Pd [5]. On the basis of the present observations and of our previous experience with the oscillating CO oxidation on Rh [6], a model which includes the Rh surface oxide formation as a presumable feedback mechanism leading to the appearance of oscillations in a bistable H_{ad}/O_{ad}/Rh system will be discussed.

This work was supported by the Austrian Science Fund (FWF) within SFB F45 “FOXSI” (Project Part F4504/05). Technical support by Johannes Frank (TU Vienna) is cordially acknowledged.

[1] G. Ertl, Angew. Chem. Int. Ed. 47 (2008) 3524
[2] H.H. Rotermund, Surf. Sci. 603 (2009) 1662 and references therein
[3] Y. Suchorski, in: "Surface Science Tools for Nanomaterials Characterization", S. Kumar (Ed.) Springer, 2015, S. 2 - 43 and references therein
[4] J.-S. McEwen, P. Gaspard, T. Visart de Bocarme, and N. Kruse, J.Phys.Chem. C 113 (2009) 17045
[5] Y. Suchorski and G. Rupprechter, Surf. Sci. 643 (2016) 52
[6] V. Medvedev, Y. Suchorski, J. Block, Surf. Sci. 343 (1995) 169.

Ambient pressure x-ray photoelectron spectroscopy

J. Åhlund

Scienta Omicron, P.O. Box 15120,, SE-75015, Uppsala Sweden
(corresponding author: J. Åhlund, e-mail: john.ahlund@scientaomicron.com)

Ambient Pressure X-ray Photoelectron Spectroscopy (APXPS) is a rapidly developing technique with applications in a wide range of fields ranging from fundamental surface science and catalysis to energy materials, environmental science and biology [1]. Here we present the design and performance of the Scienta Omicron ambient pressure photoelectron spectrometers capable of recording photoelectron spectroscopy at mbar pressure.
The transmission performances, as well as a general discussion about sample to first aperture distance [2] for APXPS systems [3] are illustrated using Ag 3d at nitrogen and water mbar pressures for various lens modes [4], such as the newly developed swift acceleration mode [4,5], as well as application examples [6].
New lens modes including the spatial mode of the newly developed HiPP-3 analyser is evaluated. The spatial mode tests are performed on a sample of well-defined gold stripes on a silicon oxide. For the Au 5d 5/2 core level a spatial resolution of better than 5 μm is demonstrated under vacuum conditions as well as for high APXPS measurements of 1 mbar.

The Scienta HiPP-2 analyzer was developed with funding from Swedish Governmental Agency for Innovation Systems (VINNOVA).

[1] D. E. Starr, Z. Liu, M. Hävecker, A. Knop-Gericke and H. Bluhm, Chem. Soc. Rev., 42, 5833 (2013)

[2] J. Matthias Kahk, Ignacio J. Villar-Garcia, L. Grechy, P. J.K. Bruce, P. E. V., S. K. Eriksson, H. Rensmo, M. Hahlin, J. Åhlund, M. O.M. Edwards, D. J. Payne, Journal of Electron Spectroscopy and Related Phenomena 205, 57, (2015)

[3] S. K. Eriksson, M. Hahlin, J. M. Kahk, I. J. Villar-Garcia, M. J. Webb, H. Grennberg, R. Yakimova, H. Rensmo, K. Edström, A. Hagfeldt, H. Siegbahn, M. O. M. Edwards, P. G. Karlsson, K. Backlund, J. Åhlund, and D. J. Payne, Review of Scientific Instruments 85, 075119 (2014)

[4] J. T. Newberg, J. Åhlund, C. Arble, C. Goodwin, Y. Khalifa, and A. Broderick, Review of Scientific Instruments 86, 085113 (2015)

[5] M. O.M. Edwards, P. G.Karlsson, S. K.Eriksson, M. Hahlin, H. Siegbahn, H. Rensmo, J. M.Kahk, I. J.Villar-Garcia, D. J.Payne, J Åhlund, NuclearInstrumentsandMethodsinPhysicsResearchA785 191 (2015)

[6] J. Maibach, C. Xu, S. K. Eriksson, J. Åhlund, T. Gustafsson, H. Siegbahn, H. Rensmo, K. Edström, and M. Hahlin, Review of Scientific Instruments 86, 044101 (2015)

Lithium-oxygen cells – how a surface science view helps to explain a next-generation battery system

A. Rinaldi[1], O. Wijaya[1,2], and H. E. Hoster[1,2,3]

Department of Chemistry, Lancaster University, LA1 4YB, United Kingdom
(corresponding author: H. E. Hoster, e-mail: h.hoster@lancaster.ac.uk)

[1] *Technische Universität München, TUM CREATE, Singapore 138602, Singapore*

[2] Energy Research Institute at Nanyang Technological University, Singapore 637141, Singapore

[3] *Energy Lancaster, Lancaster University, LA1 4YB, United Kingdom*

Their high theoretical gravimetric energy density makes metal-oxygen systems such as lithium-oxygen (Li-O_2) promising candidates for the next generation of rechargeable batteries for mobile applications [1-5]. Li-O_2 cells convert the free energy of the spontaneous reaction $2\,Li + O_2 \rightarrow Li_2O_2\,(s)$ into electricity (Figure 1). However, the theoretically high energy densities are not yet achieved even under idealized laboratory conditions, and re-charging the system with reasonable capacity retention remains challenging.

Figure 1 is drawn to highlight that this particular type of battery relies on principles of crystal growth and of coupled liquid-phase and surface-phase reactions. The Li_2O_2 product grows on the surface of a porous carbon electrode.

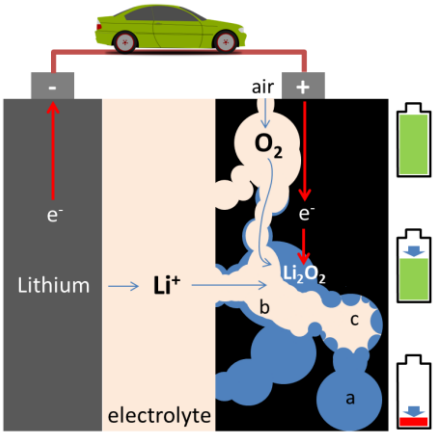

Figure 1 | Principle of a Lithium oxygen battery. Ideal scenario: discharge stops when pores are filled with Li_2O_2 (a). Real scenario: discharge stops earlier, when Li_2O_2 film blocks electron transport (b,c). Two scenarios: Li_2O_2 film grows everywhere (b) vs. Li_2O_2 particles grow at certain sites but close the gaps at some point (c).

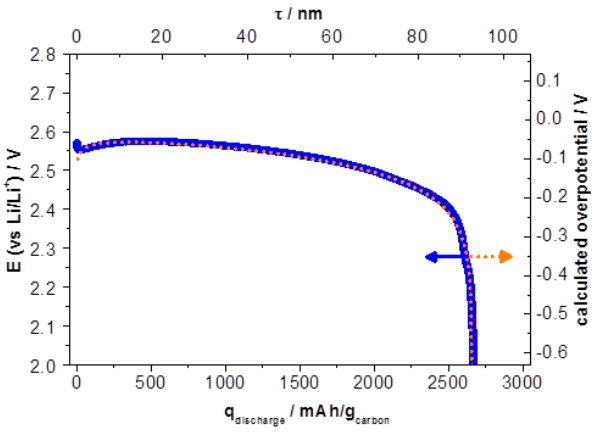

Figure 2 | Voltage profile during constant-current discharge of a Li-O_2 cell. Bottom x-axis: charge; top x-axis: average thickness of the deposited Li_2O_2 film. Measured (solid line) and calculated (dotted line) voltage profiles agree well. Experiment: graphitized carbon nanofibres in O_2 saturated 0.1 M $LiClO_4$/DME electrolyte

Li_2O_2 is a poor electron conductor; hence its growth will eventually block the ongoing discharge, because the reaction $2Li^+ + O_2 + 2e^- \rightarrow Li_2O_2\,(s)$ at the positive electrode (cathode) involves (at least) one electrochemical step. Until very recently, the Li_2O_2 film was imagined to possess rather homogeneous thickness (layer-by-layer growth) and to be the electrode surface for the ongoing electrochemical reaction [6,7]. However, the formation of interfaces between Li_2O_2 and basal plane carbon is energetically rather expensive. In this picture, the overgrowth of the electronically conducting carbon surface is rather an accidental side process, i.e., the lateral component of a three-dimensional growth.

In this presentation, we will demonstrate that some key features of Li-O_2 batteries are indeed better understood if the “language” of surface science and film growth is applied instead of the terminology from the battery community, which is more suitable for the solid-state (electro-)chemical bulk phenomena that govern intercalation-based batteries.

A characteristic fingerprint of a given cell is the voltage-vs.-charge profile recorded during discharge at constant current (Figure 2). We will demonstrate that such profiles can be summarized in a single analytic formula with two key parameters. The formula is based on the principles of crystalline thin-film growth, involving an electrochemically generated intermediate. Considering the two fundamental equations of interfacial electrochemistry (Nernst and Tafel equation), the film growth kinetics can be directly translated into the voltage profiles. For the first time, it explains a frequently observed, yet paradox part of the voltage-profile, where the voltage initially increases while the cell discharges (see initial part of Figure 2). It also rationalizes the typical fingerprint of the so-called "sudden death" of both battery cell types, which denotes the observation that the discharge process seizes long before the theoretical discharge capacity is reached.

We will demonstrate that the found principles are rather universal for this type of battery and can be transferred to Na-O_2 and in certain aspects even to Lithium-sulphur systems.

Support by the National Research Foundation (Singapore) through its “CREATE” programme is gratefully acknowledged.

[1] K.M. Abraham and Z. Jiang, J. Electrochem. Soc. 143, 1 (1996).

[2] T. Ogasawara, A. Débart, M. Holzapfel, P. Novák, and P.G. Bruce, J. Am. Chem. Soc. 128, 1390 (2006).

[3] G. Girishkumar, B. McCloskey, A.C. Luntz, S. Swanson, and W. Wilcke, J. Phys. Chem. Lett. 1, 2193 (2010)Y. Hasegawa and Ph. Avouris, Phys. Rev. Lett. 71, 1071 (1993)

[4] J.-S. Lee, S. Tai Kim, R. Cao, N.-S. Choi, M. Liu, K.T. Lee, and J. Cho, Adv. Energy Mater. 1, 34 (2011).

[5] J. Christensen, P. Albertus, R.S. Sanchez-Carrera, T. Lohmann, B. Kozinsky, R. Liedtke, J. Ahmed, and A. Kojic, J. Electrochem. Soc. 159, R1 (2012).

[6] A. Rinaldi, O. Wijaya, H.E. Hoster, and D.Y.W. Yu, ChemSusChem 7, 1283 (2014).

[6] J. Højberg, B.D. McCloskey, J. Hjelm, T. Vegge, K. Johansen, P. Norby, and A.C. Luntz, ACS Appl. Mater. Interfaces (2015).

Transition metal/oxide hybrid chain structures on Ir(100) - is there a general trend?

P. Ferstl[1], M. Gubo[1], C. Sobel[1], K. Heinz[1], M.A. Schneider[1], and L. Hammer[1]

[1] *Lehrstuhl für Festkörperphysik, Univ. Erlangen-Nürnberg, 91085 Erlangen, Germany*

F. Mittendorfer[2], and J. Redinger[2]

[2] *Institut für Angewandte Physik & CMS, TU Wien, 1040 Wien, Austria*

Bulk transition metal (TM) oxides show a wide diversity of structural, electronic, magnetic and catalytic properties which makes this material class interesting for tailor-made technological applications. This spectrum of properties can even be expanded by changing the dimensionality of the oxides towards one- or two-dimensional nanostructures. Moreover, together with the usually metallic substrate, these oxide nanostructures form a completely new class of metal/oxide hybrid systems, which are vastly unexplored so far. Here, we present for different TM oxides – MnO_2, CoO_2, FeO_2 and NiO_2 – the self-organized growth and ordering of oxide chains on the Ir(100) surface as well as their detailed structural characterization.

The deposition of 1/3 monolayer of different transitions metals (Mn, Co, Fe and Ni) on the Ir(100) surface under oxygen rich conditions and elevated temperatures leads in all cases to the formation of quasi-one-dimensional oxide chains. These wires grow exclusively with a threefold lateral spacing on the plain terraces creating an almost defect-free 3x1 superstructure proven both by STM and LEED, see Figure 1a,b. Both the TM coverage of 1/3 monolayer needed for optimal phase formation as well as atomically resolved STM images (see Fig. 1c) suggest a mono-atomic metal wire as the core of the oxide nanostructures. Similar oxide wires could be produced so far only in low density and poorly ordered at vicinal surfaces via step decoration [1, 2]. Here, the high degree of lateral order of the one-dimensional structures allows for a quantitative determination of the crystallographic structure by means of full-dynamical LEED-IV analyses.

For each structural phase a huge intensity data basis between 10,000 eV and 20,000 eV was collected for nominally normal incidence of the primary electron beam and energies ranging up to 800 eV. The final best-fit structures yield an excellent agreement between experimental and calculated spectra expressed by Pendry R-factors in the range of 0.090-0.116. Furthermore, all structural findings are independently confirmed by DFT calculations where the geometric parameters of the respective model coincide with those derived from LEED within the picometer range.

The quantitative structure determination confirms that all investigated TMs form oxide wires with mono-atomic metal cores and further reveals a unique TMO_2 stoichiometry. The most surprising finding, however, is that the TMO_2 stripes bind only via the oxygen atoms towards the substrate (see schematic model in Fig.1d), while the central TM core is sterically decoupled from its Ir neighbours (Fig. 1e). The only notable difference between the various metal-oxide hybrid structures is the relative height of the TM-atom above the first Ir layer that varies between 1.1 and 0.7 Å. Therefore this structural configuration seems to be a general trend for the transitions metals on the Ir(100) surface.

Besides the modification of the metal oxide wires by changing the central metal species the oxidic character of the stripes can also be varied by the chemical environment which is exemplarily demonstrated for the CoO_2 case. Exposing these stripes to the strongly oxidizing agent NO_2 leads to the formation of wires with CoO_3 stoichiometry where the additional oxygen is located right below every Co atom. Even more, both types of oxide wires can be completely reduced by hydrogen to give an ordered, purely metallic Ir_2Co surface alloy where the Co wires are now embedded in the outermost iridium layer. Hence, this great flexibility in the chemical composition and oxidation state makes the various TM nanowires on the Ir(100) surface prototypical systems to study the magnetic and chemical properties of low dimensional hybrid structures.

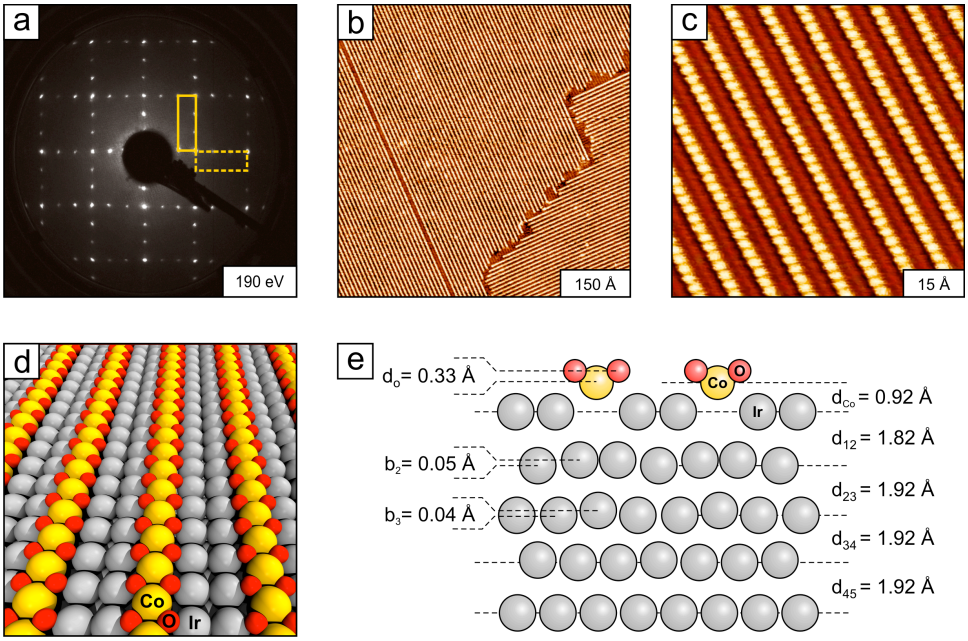

Figure 1: a) LEED pattern, b,c) STM images and d,e) ball models of the Ir(100)-3x1-CoO_2 phase

[1] F.P. Netzer, Surf. Sci. **604** (2010) 485
[2] Li *et al*. Surf. Sci. **604** (2010) L43
Email: *pascal.ferstl@fau.de*

Localized Surfaces Plasmons: Does an ultrathin oxide film matter?

L. Břínek, T. Šamořil, O. Tomanec, M.Kvapil, R. Kalousek, M. Hrtoň, J. Čechal, P. Dub, J. Spousta, P. Varga, and T. Šikola

Inst. of Physical Engineering., Brno University of Technology, Technická 2, 616 69 Brno, Czech Rep. (corresponding author: T. Šikola, e-mail: sikola@fme.vutbr.cz)

CEITEC BUT, Brno University of Technology, Technická 10, 61669 Brno, Czech Republic

One of the most straightforward applications of FIB technology is fabrication of plasmonic nanoantennas by milling their shapes out of metallic thin films (Fig. 1). However, we have found that the Mid-IR Au rectangular antennas show different behaviour according to their fabrication origin. These antennas prepared by EBL on transparent samples (e.g. Si) possessed linear scaling of resonance frequency with their arm length. Contrary to that, those prepared by Ga (Xe) FIB milling of the Au layer (60 nm) revealed more complex behaviour (Fig. 2). In principle, the resonant peak of relative reflectance of antennas (measured by FTIR) was split into two sub-peaks separated by a dip at $\lambda \approx 8.2$ μm.. The short-wavelength sub-peak was moving with the antenna arm length towards higher wavelengths until its motion almost stopped at higher arm lengths. However, the long-wavelength sub-peak almost did not move with the antenna arm length for shorter arm lengths and then started to move towards higher wavelengths. The same behaviour was found for antennas fabricated by FIB using Xe ions. It means that this effect was not caused by Ga contamination.

In the presentation such an unexpected effect will be explained and the proofs for it given. Our previous work [1] indicated that this complex behaviour can be related to a strong coupling of antenna plasmons to the absorbing substrate modified by ions. X-ray Photoelectron Spectroscopy revealed the presence of a silicon-oxide layer having an enhanced thickness (6 nm) with respect to the native oxide (≈ 2 nm) at the silicon surface in the vicinity of antennas fabricated by Ga or Xe ions. FDTD simulations (Lumerical) proved that such an ultrathin oxide layer absorbing in Mid-IR was able to cause the splitting of the resonant peak. Finally, removing the oxide layer by HF etching the dip in the MID-IR resonant peaks disappeared and the antennas started permanently to show up the same spectra like in case of the EBL antennas. The mechanism of the formation of such an oxide layer will be explained well.

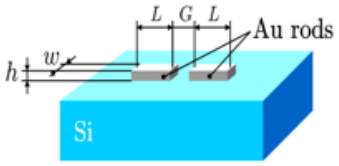

Fig. 1. Schematic of the antenna setup and the corresponding dimension parameters (w = 0.4μm, h = 60 nm, G = 0.4μm).

a)

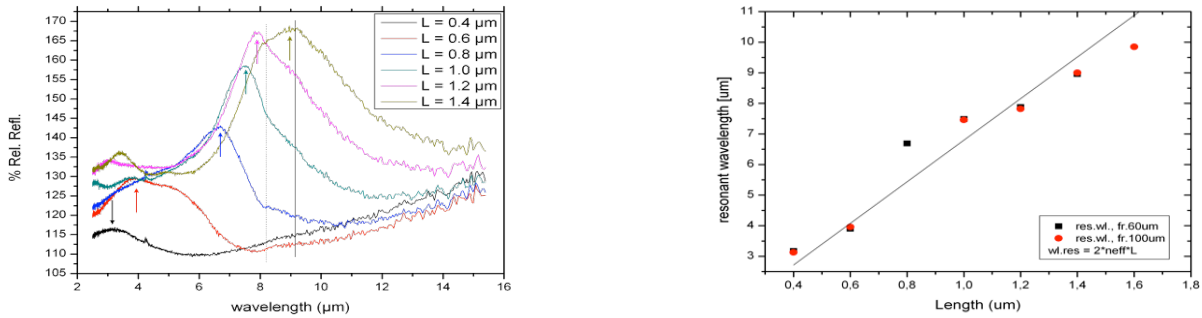

b)

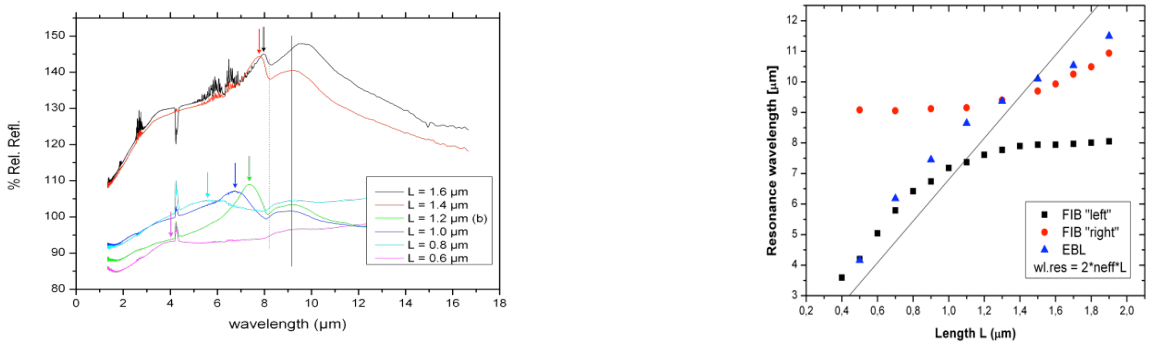

Fig. 2. FTIR spectra (left) and resonant wavelength as a function of the antenna arm length (right) for plasmonic antenna arrays fabricated by EBL (a) and Ga FIB (b).

[1] T. Šikola, R. D. Kekatpure, E. S. Barnard, J. S. White, P. Van Dorpe , L. Břínek, O. Tomanec, J. Zlámal, D. Lei, Y. Sonnefraud, S. A. Maier, J. Humlíček, M. L. Brongersma: *Appl. Phys. Lett.* **95** (2009), 253109.

Wednesday

Surface energies and equilibrium crystal shapes of wurtzite crystals

C. Draxl[1], H. Li[1,2], L. Geelhaar[2], and H. Riechert[2]

[1] *Institut für Physik und IRIS Adlershof, Humboldt-Universität Berlin, D-12489 Berlin, Germany*
(corresponding author: C. Draxl, e-mail: claudia.draxl@physik.hu-berlin.de)

[2] *Paul-Drude-Institut für Festkörperelektronik, 10117 Berlin, Germany*

Crystal morphologies are important for the design and functionality of devices based on low-dimensional nanomaterials. The equilibrium crystal shape (ECS) is a key quantity in this context. It is determined by surface energies, which are hard to access experimentally but can generally be well predicted by first-principles methods. Unfortunately, this is not necessarily so for polar and semipolar surfaces of wurtzite crystals. We show that the ECSs can nevertheless be obtained for this class of materials [1].

To this extent, we introduce a generalization of the Wulff construction, based on combinations of surface energies. We demonstrate this principle by taking GaN as a technologically important example. The wide-band-gap semiconductor GaN is a key material in today's white-light-emitting diodes for general illumination, blue lasers, and high-power and high-frequency electronics. GaN readily grows in the form of nanowires (NWs) in molecular beam epitaxy (MBE) [2,3] and metal-organic chemical vapor deposition (MOCVD) [4,5]. However, different shapes are observed, depending on the growth temperature, pressure, and chemical environment [6–10].

We identify different crystal shapes depending on the chemical potential [1]. The crystal exhibits a rod-like shape along the polar c axis, with top and bottom geometries depending on the chemical potential, while the side walls are formed by both types of nonpolar surfaces. Our results can well explain the experimentally observed NW shapes. Beyond that, it opens a perspective to gain insight into morphologies of the entire class of wurtzite materials.

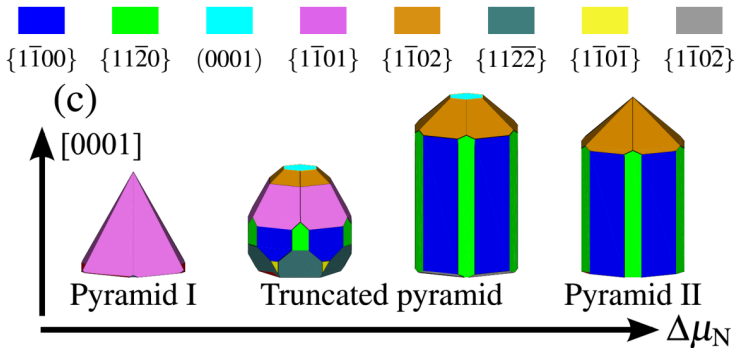

Fig. 1: Equilibrium crystal shape of wurtzite GaN under thermodynamic equilibrium conditions as a function of the nitrogen chemical potential.

[1] H. Li, L. Geelhaar, H. Riechert, and C. Draxl, Phys. Rev. Lett. **115**, 085503 (2015)
[2] L. Geelhaar,et al., IEEE J. Sel. Top. Quantum Electron. 17, 878 (2011).
[3] V. Consonni, Phys. Status Solidi RRL 7, 699 (2013).
[4] S. D. Hersee, X. Sun, and X. Wang, Nano Lett. 6, 1808 (2006).
[5] X. J. Chen, et al., Appl. Phys. Lett. 97, 151909 (2010).
[6] D. Du, D. J. Srolovitz, M. E. Coltrin, and C. C. Mitchell, Phys. Rev. Lett. 95, 155503 (2005).
[7] V. Jindal and F. Shahedipour-Sandvik, J. Appl. Phys. 106, 083115 (2009).
[8] B. N. Bryant, A. Hirai, E. C. Young, S. Nakamura, and J. S. Speck, J. Cryst. Growth 369, 14 (2013).
[9] A. Urban, J. Malindretos, J.-H. Klein-Wiele, P. Simon, and A. Rizzi, New J. Phys. 15, 053045 (2013).
[10] M. Jin, H. Shu, P. Liang, D. Cao, X. Chen, and W. Lu, J., Phys. Chem. C 117, 23349 (2013).

Electronic Friction for Surface Dynamical Processes: Beyond the Independent Atom Approximation

K. Reuter

Lehrstuhl für Theoretische Chemie, Technische Universität München, D-85747 Garching, Germany
(corresponding author: K. Reuter, e-mail: karsten.reuter@ch.tum.de)

The role of electron-hole pair excitations during dynamical surface processes on metal substrates has been controversially discussed. While adiabatic first-principles calculations often provide a satisfactory description, an abundance of such excitations is generally suggested by the continuum of electronic states around the Fermi level. With high-level non-adiabatic calculations still intractable for extended metal surfaces, the concept of electronic friction within the local density friction approximation (LDFA) offers numerically efficient, but approximate insight [1,2].

The numerical efficiency of LDFA-based friction coefficients stems from an intrinsic decomposition and mapping of the interacting system to independent atoms that are embedded in a homogeneous electronic density. Concomitantly, this inherent simplicity has also raised concerns about the accuracy of this theory. It has been heavily criticized not to capture subtle changes in the electronic structure of molecules interacting with metal surfaces, resulting in a wrong description of non-adiabatic energy losses in gas-surface dynamics [3]. Measurements of vibrational lifetimes on metal surfaces have been invoked as accurate "key observables" a non-adiabatic theory is challenged to reproduce [4].

In order to clarify the situation we thus apply the LDFA to the non-adiabatic damping of adsorbate vibrations on transition metal surfaces, and specifically to the internal stretch mode of two systems which have been studied most extensively and conclusively by experiments: CO adsorbed on Cu(100) and Pt(111). Despite the largely different surface frontier orbital locations and concomitant hybridizations at the transition and noble metal surface, we find the LDFA in the prevalent independent atom approximation (IAA) to already exhibit a good qualitative performance with respect to the experimental and high-level theoretical benchmark data. Rather than an explicit account of the surface band structure, our analysis suggests missing intramolecular contributions as reason for the remaining differences. Approximately incorporating such contributions through a numerically efficient atoms-in-molecules (AIM) charge partitioning indeed yields consistent lifetimes for a range of diatomic adsorbate systems [5].

With this confidence we further apply this approach to surface diffusion, where non-adiabatic energy losses compete with energy losses due to phononic coupling. We compare our LDFA-based molecular dynamics simulations for various alkali-metal adsorbates on Cu(111) to experimental signatures obtained from 3He spin echo measurements [6]. This comparison

allows to decompose empirically obtained friction coefficients into electronic and phononic contributions for the first time.

Support by the Deutsche Forschungsgemeinschaft and ample supercomputing time at the Leibniz Rechenzentrum der Bayerischen Akademie der Wissenschaft is gratefully acknowledged.

[1] J.I. Juaristi, M. Alducin, R. Díez Muiño, H.F. Busnengo, and A. Salin, Phys. Rev. Lett. 100, 116102 (2008)

[2] M. Blanco-Rey, J.I. Juaristi, R. Díez Muiño, H.F. Busnengo, G.J. Kroes, and M. Alducin, Phys. Rev. Lett. 112, 103203 (2014)

[3] A.C. Luntz, I. Makkonen, M. Persson, S. Holloway, D.M. Bird, and M.S. Mizielinski, Phys. Rev. Lett. 102, 109601 (2009)

[4] P. Saalfrank, Chem. Rev. 106, 4116, (2006)

[5] S.P. Rittmeyer, J. Meyer, J.I. Juaristi, and K. Reuter, Phys. Rev. Lett. 115, 046102 (2015)

[6] D.J. Ward, PhD thesis, University of Cambridge (2013)

Angular distribution of ^{13}C atoms reflected from W surfaces

M. Hellwig[1], H. R. Koslowski[1], Ch. Linsmeier[1], Ch. Schwab[2], R. A. De Souza[2]

[1]*Forschungszentrum Jülich GmbH, Institut für Energie- und Klimaforschung – Plasmaphysik, 52425 Jülich, Germany*

[2]*Institute of Physical Chemistry, RWTH Aachen University, Landoltweg 2, 52074 Aachen, Germany*

(corresponding author: M. Hellwig, e-mail: m.hellwig@fz-juelich.de)

Plasma-facing components made of bulk tungsten for future fusion experiments will have a castellated tile structure in order to better withstand the consequences of cyclic heat and particle loads: thermal expansion and crack propagation, as well as the reduction of eddy currents. The retention of hydrogen in the gaps between adjacent tiles is of concern. Experiments in the tokamaks TEXTOR and DIII-D have shown that deposited layers of hydrogen and carbon in the gaps are close to the top surface and decay quickly with depth [1]. Since the utilised tungsten components had technically finished surfaces, the surface roughness has been identified as a one potential reason for the observed deposition patterns [2].

In order to study the influence of W surface roughness on the angular distribution of reflected and sputtered atoms, a dedicated experiment using a UHV apparatus with a mass selected ion source and a specially constructed target holder is performed [2]. A beam of $^{13}C^+$ ions with an energy of 950 eV is produced by electron impact ionisation of ^{13}CO. The ions are mass filtered in a 90° magnetic sector field and guided under incidence angles of 30° and 80° (with respect to the surface normal) onto the W surface. The reflected atoms from the surface are collected on a semi-cylindrical Ti catcher foil which is mounted on top of the W sample. Ion beam penetration has been enabled by 2 mm holes under the respective angles. The surface density of collected ^{13}C atoms (relative to ^{12}C) is analysed by Time-of-Flight Secondary Ion Mass Spectrometry (ToF-SIMS), exploiting its mass selective high sensitivity.

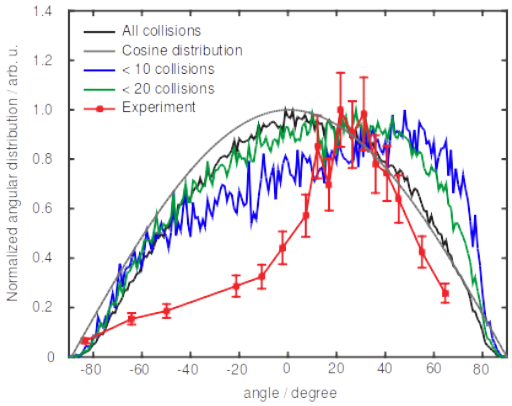

Fig. 1: Angular distribution of reflected and sputtered C atoms on Ti catcher foil.

The W samples are prepared with two different levels of surface roughness. All samples are chemically etched in a mixture of HNO_3 and HF. The surface of "rough" samples is not further modified. The "smooth" samples are polished in consecutive steps with FEPA P silicon carbide paper with decreasing grain sizes down to 6 µm, followed by diamond suspension with 1 µm grains and a final polishing with silica suspension of 0.04 µm.

The ion beam exposure duration for each sample is adjusted to ensure an average deposited areal density of reflected ^{13}C atoms of $10^{20}m^{-2}$ to allow for sufficient sensitivity of the SIMS measurements. This results in ion bombardment times up to 470 hours.

Modelling of the experimental results is performed using the SDTrimSP code [3]. The surface roughness is considered by pre- and post-processing algorithms simulating the surface morphology by a statistical variation of the angle of incidence according to the distribution of surface normals determined by AFM for the various samples.

A comparison between experiment and modelling for 30° incidence angle on a smooth W surface is shown in Fig. 1. The experiment shows a mainly specular reflection (note that the incident ions in the reference system of Fig. 1 are at -30°). The left wing of the distribution could be caused by deposited and sputtered ^{13}C atoms from the surface which should exhibit a cosine distribution [4] and amounts to approximately 10% in this experiment. The modelling shows a much broader and almost cosine shaped distribution and does not well reproduce the experiment. A much better agreement is reached for an incidence angle of 80° on a smooth W surface. This behaviour can be explained by an analysis of the collision cascades. The momentum of the incoming particle parallel to the surface is better conserved when the collision cascade has a smaller number of collisions. This can be seen in Fig.1 where the distribution of reflection and sputtering events with collision cascades shorter than 10 collisions (blue curve) yields a better agreement of the maximum but is still much broader than the experiment. In order to confirm the SDTrimSP calculations, the binary collision code MARLOWE [5] is applied to calculate reflection angles and collision cascade statistics of reflected ^{13}C atoms. Fig. 2 shows the frequency distributions of the number of collisions for incidence angles of 30° and 80°. The more grazing the incidence angle to the surface is, the smaller is the number of collisions. The angular distribution of reflected atoms show specular behaviour for 80° incidence angle, and a broad, almost cosine, distribution around 0° for 30° angle of incidence, in agreement with the SDTrimSP results. Rough surfaces show the opposite behaviour. At 30° angle of incidence the measured angular distribution of reflected atoms agrees well with the measurement, whereas at 80° the experiment shows a predominant backscattering which could not be reproduced in the modelling.

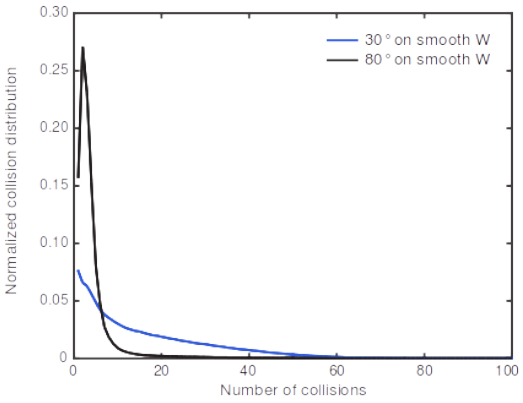

Fig. 2: Distribution of number of collisions in the collision cascade.

[1] A. Litnovsky, M. Hellwig, D. Matveev et al., J. Nucl. Mater. 463, 174-179 (2015)
[2] M. Hellwig, Dissertation, Ruhr-Universität Bochum (2016)
[3] W. Eckstein, R. Dohmen, A. Mutzke, and R. Schneider, Technical Report IPP 12/3, MPI-IPP (2007)
[4] R.A. Langley, J. Bohdansky,W. Eckstein, et al., Nucl. Fusion 24, S9 (1984)
[5] M. T. Robinson, Phys. Rev. B 40, 10717 (1989); M. T. Robinson, Radiat. Eff. 130/131, 3 (1994)

Electronic stopping of slow hydrogen ions in oxides

D. Roth[1], B. Bruckner[1], A. Mardare[2], C. McGahan[3], R.F. Haglund Jr.[3], D. Primetzhofer[4], Iñaki Juaristi[5], and P. Bauer[1,5]

[1] *Institut für Experimentalphysik, Johannes Kepler Universität Linz, A-4040 Linz, Austria (corresponding author: P. Bauer, e-mail: peter.bauer@jku.at)*

[2] *Institut für Chemische Technologie Anorganischer Stoffe, Johannes Kepler Universität Linz, A-4040 Linz, Austria*

[3] *Dept. Physics and Astronomy, Vanderbilt University, Nashville, Tennessee 37235, USA*

[4] *Dept. Physics and Astronomy, Uppsala University, P.O. Box 516, SE 751 20, Uppsala, Sweden*

[5] *Donostia International Physics Center DIPC, P. Manuel de Lardizabal 4, 20018 San Sebastián, Spain*

Electronic interaction between fast ions and solids ($v >> v_0$) is well understood, while the mechanisms of electronic interactions are still unclear for very low ion velocities, $v << v_0$ (v_0 = c/137 where c is the speed of light). At low velocities, electronic stopping measurements were conducted for many metals, semiconductors, and insulators, in order to gain insight into the prevailing stopping mechanisms. While electron-hole pair excitation is commonly accepted as dominant mechanism in electronic stopping of slow H ions in metals and semiconductors like germanium, electron promotion processes are considered important for ionic crystals like LiF [1, 2, 3]. Here, we present the results from a systematic study of electronic stopping of slow H ions in various oxides with different electronic properties, including VO_2 in its metallic and semiconducting states, ZnO as large band gap semiconductor (~ 3.4 eV band gap) and insulators like Ta_2O_5, HfO_2, Al_2O_3 and SiO_2, with band gaps in the range 4.5 to 8.9 eV. Apart from the obvious differences in their electronic structures, the more global properties like valence electron densities, as reflected by the plasmon energies, are quite similar. Thus, one may expect to obtain an answer to the question, whether the unperturbed band structure is reflected in the electronic stopping behavior or whether the band structure is so strongly perturbed by the presence of the ion that detailed band properties cease from being important while only the number of participating electrons is relevant ("metallization").

For the experiments, nanometer films were prepared where possible, otherwise thick oxide layers were used. The energy loss was evaluated either from the widths of the backscattering spectra or from the heights at energies close to the high energy onset, corresponding to scattering depths close to the surface [4]. The influences of nuclear collisions and multiple scattering were eliminated by use of Monte-Carlo simulations using the TRBS code [5]. Where possible, both techniques were applied and found to yield concordant results.

For electronic stopping in compounds, the question arises what would be the best way to present the data. While for a Free Electron Gas (FEG), the stopping power, $S = dE/dx$, is the only reasonable quantity, for gases and solids, the stopping cross section (SCS) $\varepsilon = S/n$ is used, with the atomic density n. For compounds like oxides, on the one hand the smallest meaningful unit is M_xO_y, where M stands for the metal, and x and y for the stoichiometric abundancies. On the other hand, in this case different numbers of electrons are involved in units of different size which makes it difficult to compare oxides of different stoichiometry. In the regime of the stopping power maximum, it has been found adequate for oxides to consider the electronic SCS per O atom, ε/y, which yields consistent results for quite different oxides like for H_2O ice, SiO_2, Al_2O_3 and $LiNbO_3$, when the inner shell contributions are subtracted [6]. Therefore, this approach has been applied to the results obtained in the range of very low velocities, i.e. $0.1\ v_0 < v < 0.65\ v_0$. The results presented in Figs. 1a and 1b indicate that indeed at velocities below $0.25\ v_0$, all data fall on top of each other within experimental accuracies (± 10 %). This result indicates that in this context neither the density of valence electrons nor the band gap are of importance, and that either band structure perturbation is so strong that only the number of valence electrons per O is relevant, or a mechanism different from electron-hole pair excitation in a Coulomb collision is the prevailing mechanism.

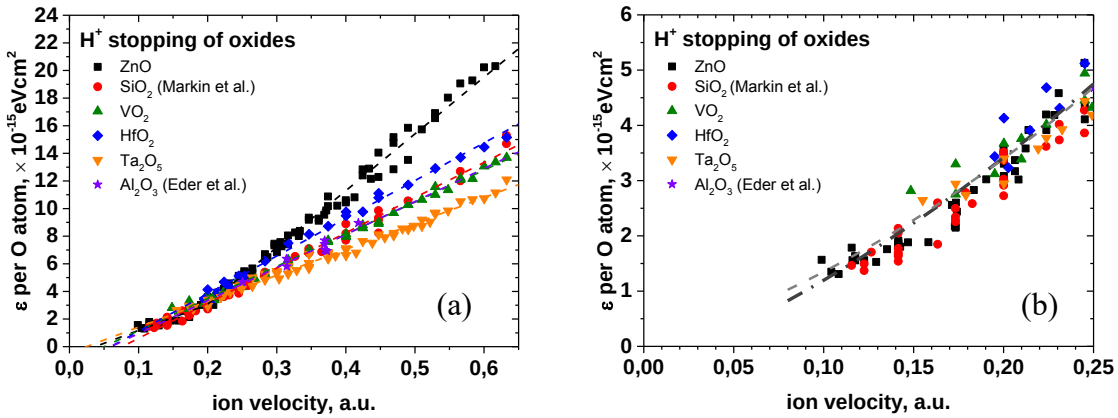

Figs. 1a and 1b: SCS per O atom for H ions in various oxides (see insert) as a function of ion velocity in the range $0.1\ v_0$ to $0.65\ v_0$ and $0.1\ v_0$ to $0.25\ v_0$ (Fig. 1a and 1b, respectively).

Support by the Austrian Science Fund FWF within project P25704 is gratefully acknowledged.

[1] M.A. Zeb, J. Kohanoff, D. Sanchez-Portal, A. Arnau, J.I. Juaristi, and E. Artacho, Phys. Rev. Lett. 108, 225504 (2012), and D. Goebl, W. Roessler, D. Roth, and P. Bauer, Phys. Rev. A90, 042706 (2014).

[2] R. Ullah, F. Corsetti, D. Sanchez-Portal, and E. Artacho, Phys. Rev. B91, 125203 (2015).

[3] P.A.Z. van Emmichoven, A. Niehaus, P. Stracke, F. Woegershaus, S. Krischok, V. Kempter, A. Arnau, F.J.G. de Abajo, and M. Penalba, Phys. Rev. B59, 10950 (1999).

[4] D. Roth, D. Goebl, D. Primetzhofer, and P. Bauer, Nucl. Instr. Meth. B317, 61 (2013).

[5] J.P. Biersack, E. Steinabuer, and P. Bauer, Nucl. Instr. Meth. B61, 77 (1991).

[6] P. Bauer, R. Golser, F. Aumayr, D. Semrad, A. Arnau, E. Zarate, and R. Diez-Muiño, Nucl. Instr. Meth. B125, 102 (1997).

Postersession

Breaking time-reversal symmetry at the topological insulator surface by metal-organic coordination networks

M. M. Otrokov,[1,2,3] E. V. Chulkov,[1,4,3] and A. Arnau[1,4]

(corresponding author: A. Arnau , e-mail: andres.arnau@ehu.eus)

[1] *Donostia International Physics Center, E-20018 Donostia-San Sebastián, Spain*

[2] *Tomsk State University, 634050 Tomsk, Russia*

[3] *Saint Petersburg State University, 198504 Saint Petersburg, Russia*

[4] *Departamento de Fisica de Materiales UPV/EHU and Material Physics Center (MPC), Centro Mixto CSIC-UPV/EHU, E-20018 Donostia - San Sebastián, Spain*

We propose a way to break the time-reversal symmetry at the surface of a three-dimensional topological insulator that combines features of both surface magnetic doping and magnetic proximity effect. Based on the possibility of organizing an ordered array of local magnetic moments by inserting them into a two-dimensional matrix of organic ligands, we study the magnetic coupling and electronic structure of such *metal-organic coordination networks (MOCN)* on a topological insulator surface from first principles. In this way, we find that both Co and Cr centers, linked by the tetracyanoethylene-like organic ligand, are coupled ferromagnetically and, depending on the distance to the topological insulator substrate, can yield a magnetic proximity effect. This latter leads to the Dirac point gap opening indicative of the time-reversal symmetry breaking, as shown in the inset of the figure below with the electronic band structure for the Cr-MOCN [1].

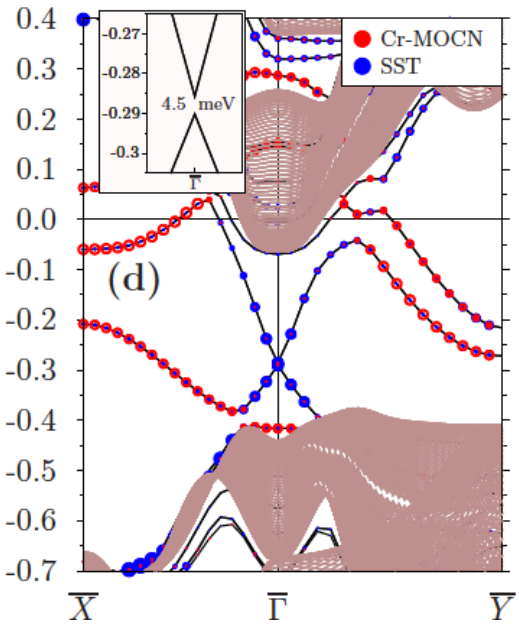

[1] M. M. Otrokov, E. V. Chulkov and A. Arnau, Phys. Rev. B 92, 165309 (2015).

Recent Results in Ultra Low Temperature STM

T. Berghaus*, Y. Miyatake**

** nanoscore gmbh, 61479 Glashütten, Germany, www.nanoscore.de*
(corresponding author: T. Berghaus, e-mail: t.berghaus@nanoscore.de)
*** UNISOKU Co., Ltd., Osaka, Japan, www.unisoku.com*

There is a growing number of Ultra Low Temperature SPM (ULT-SPM) installations yielding an increasing number of publications on quantum phenomena, nano magnetic effects, and super conductivity. In our poster we present recent results of various (ultra) low temperature STMs which have been delivered by UNISOKU.

Superconductivity above 100K has been observed in single-layer FeSe films on doped SrTiO3 with a USM1300 ULT-STM by Xue, Jia and coworkers[1]. Conductance was measured with a 4-point probe at varied temperature and varied magnetic field of up to 10Tesla.

S. Loth and co-workers have reported on the *Control of quantum magnets by atomic exchange bias*[2]. Iron trimers were assembled on top of a mono layer of Cu_2N on Co(100) by STM manipulation of iron atoms. The trimers a antiferromagnetic which was proven by spin polarised STM. Under the presence of an external magnetic field, the magnetic tip an electronic pump probe signal the trimers can be magnetised, re-magnetised, and their spin states can be controlled. Data have been taken with USM1300 UHV vector magnet STM with 3He cooling at 0.5K.

Further the combination of optical spectroscopies and STM in situ is becoming of wider interest. We present *Tip Enhanced Raman Spectroscopy (TERS) spectra of single wall carbon nanotubes* (CNT) on Au which have been taken in UHV[3]. A single CNT has been imaged with STM and with spatially resolved Raman spectroscopy revealing images spectrally filtered in the G-, 2D, and D-bands and showing a local defect.

Further we present STM images and TERS spectra of 1,2-di(4-pyridyl)ethylene (BPE) on Au. Observation over time reveals a degradation of the mono film during scanning at room temperature. In contrast the mono film stays intact whilst STM imaging and spectroscopy measurement at 78K.

---

[1] Superconductivity above 100 K in single-layer FeSe films on doped SrTiO3,
nature materials LETTERS. ONLINE: 24 NOVEMBER 2014 | DOI: 10.1038/NMAT4153, Jian-Feng Ge, Zhi-Long Liu, Canhua Liu, Chun-Lei Gao, Dong Qian, Qi-Kun Xue, Ying Liu, Jin-Feng Jia

[2] Control of quantum magnets by atomic exchange bias
Nature nanotechnology LETTERS,. ONLINE: 15 DECEMBER 2014 | DOI: 0.1038/NNANO.2014.281 Shichao Yan, Deung-Jang Choi, Jacob A. J. Burgess, S. Rolf-Pissarczyk, Sebastian Loth

[3] Data taken by UNISOKU during factory and final acceptance test with a UNISKU USM1400 UHV STM and a NanoFinder Flex Raman spectrometer

Strain induced conversion of adsorption states of small benzene derivatives on Pt(111)

S.N. Filimonov, L.N. Nikitina, and R. Sparks

Department of Physics, Tomsk State University, 634050 Tomsk, Russia
(corresponding author: S.N. Filimonov, e-mail: filimon@phys.tsu.ru)

It is well known that electronic and optical properties of small aromatic molecules adsorbed on metal and semiconductor surfaces may experience drastic changes when the molecule change its adsorption configuration, e.g. switching from the chemisorbed to physisorbed state. Therefore the possibility to control relative stability of different adsorption configurations is very important from the point of view of potential applications of molecules in organic microelectronics.

One way to tune relative stability of physisorbed and chemisorbed states is to play with the molecule constitution or/and the metal substrate [1,2]. In this way the physisorbed state, commonly referred to as a weakly bound and short living, can be made long living and equally stable with the chemisorbed state, as, for instance, in the case of tetrachloropyrazine (C4Cl4N2) on Pt(111) [1].

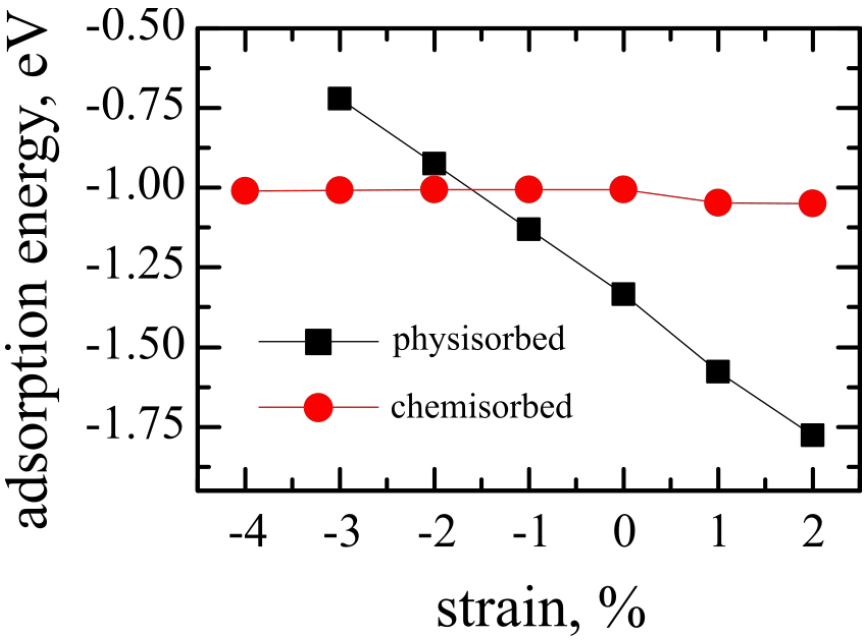

Fig. 1 Adsorption energy of tetrachloropyrazine on Pt(111) as function of the lattice strain.

In the present work we show by first principles density functional theory calculations that fine tuning of the molecule-substrate interactions is also possible by applying strain to the metal substrate. Our calculations show that the physisorbed state of tetrachloropyrazine on Pt(111) is almost not affected by the strain. However, in the chemisorbed state the adsorption energy of tetrachloropyrazine decreases linearly with increasing lattice constant of Pt. When a strong compressive strain is applied the chemisorbed state of tetrachloropyrazine becomes energetically less favorable than the physisorbed state.

We also show that the strain induced conversion of the energetically most stable adsorption states is not unique for tetrachloropyrazine on Pt(111), but should be observed for a number of different benzene derivatives and different substrates.

Financial support by the Russian Science Foundation (project #14-12-00813) is gratefully acknowledged.

[1] W. Liu, S. Filimonov, J. Carrasco, and A. Tkatchenko, Nat. Commun. 4:2569 (2013)
[2] R. Peköz K. Johnston and D. Donadio, J. Phys. Chem. C 118, 6235 (2014)

Adsorption of Water and Oxygen on $Ca_3Ru_2O_7(001)$

Daniel Halwidl[1], Bernhard Stöger[1], Florian Mittendorfer[1,2], Wernfried Mayr-Schmölzer[1,2], Michael Schmid[1], Josef Redinger[1,2], Ulrike Diebold[1]

[1]Institute of Applied Physics, TU Wien, Wiedner Hauptstraße 8-10, A-1040 Vienna, Austria
(corresponding author: D. Halwidl, e-mail: halwidl@iap.tuwien.ac.at)

[2]Center for Computational Materials Science, TU Wien, Wiedner Hauptstraße 8-10, A-1040 Vienna, Austria

Complex ternary perovskite oxides are increasingly used in solid oxide fuel cells and catalysis [1]. Therefore it is highly desirable to obtain a better understanding of their surface chemical properties. We use low-temperature STM, XPS and DFT to investigate the adsorption of water and oxygen on $Ca_3Ru_2O_7$.

Dosing small amounts of water on the clean surface at 105 K leads to bright dots sitting on the bright lines of the substrate. We propose that water dissociates and that the bright dots correspond to OH groups sitting on Ca bridge sites. The OH groups are immobile, in contrast to the interesting dynamic behavior observed on the $Sr_3Ru_2O_7(001)$ surface [2]. At higher doses various superstructures are formed, with long-range order that depends on the coverage, dosing temperature and annealing time.

Oxygen adsorbs weakly and is moved around by the STM tip. At higher coverages the oxygen becomes partially immobile and can be imaged by STM. Upon adsorption of oxygen the O*1s* XPS spectrum shows a peak at 532.7 eV binding energy, 3.7 eV above the bulk oxygen peak. We attribute the peak to molecularly adsorbed O_2, in agreement with our DFT calculations.

This work was supported by the Austrian Science Fund (FWF project F45) and the ERC Advanced Grant “OxideSurfaces”.

[1] M. A. Pena, and J. L. G. Fierro, Chem. Rev. **101,** 1981 (2001)
[2] D. Halwidl et al., Nature Mater. (2015), doi:10.1038/nmat4512

Reliability of LEED analyses for complex systems

Lutz Hammer, Pascal Ferstl, and Alexander Schneider

Lehrstuhl für Festkörperphysik, Univ. Erlangen-Nürnberg, 91085 Erlangen, Germany

A quantitative surface structure determination, i.e. a precise localisation of atomic coordinates within the surface unit mesh, is only possible by an evaluation of diffraction intensities. In case of electron diffraction (LEED) spot intensities are measured as a function of the electron energy (LEED-IV spectra) and subsequently compared to the results of full-dynamical intensity calculations for various reasonable models, whereby for each model all relevant structural parameters have to be varied in order to optimise the experiment-theory correspondence. Quantitative measures for the quality of this correspondence are so-called reliability factors (R-factors), whereby nowadays the Pendry R-factor R_P [1] is the most common. Best-fit values in the range R_P = 0.2 - 0.3 or even somewhat larger are generally accepted as a proof for the correctness of the underlying structural model. This assignment, however, has been established decades ago in the early days of LEED analyses, where sample preparation and data acquisition were often quite poor and intensity calculations strongly limited by low computing power. In those days even for structurally quite simple systems like clean metal surfaces or mono-atomic adsorbates an R-factor value around R_P = 0.2 was the optimum which could be achieved. Nowadays, we are able to reach R-factor values as low as R_P = 0.06 - 0.10 for well defined systems and so it is about time to set new standards what is called a *trustworthy R-factor*. This holds the more in the case of rather complex surface structures, where crystallographically different models may vary by the presence (or absence) of only one or a few atoms within a large unit cell containing tens or even hundreds of atoms.

In this case study we have investigated the fit quality which can be achieved for different structural modifications of the correct c(2×2) surface reconstruction of Fe_3O_4(100) [2]. The key features of the correct reconstruction model are two subsurface Fe vacancies within the second B-layer of the Fe_3O_4 spinel structure as well as a Fe interstitial in the A-layer above bridging the vacancies (cf. Fig. 1 left). This in total leads to a slight Fe depletion of one Fe ion per surface unit mesh. With this structural model the huge experimental data set of 40 beams (cumulated energy range ≈10,000 eV) could be reproduced with an R-factor of R_P = 0.125 [2] though the geometrical distortions due to the Verwey transition were neglected in the analysis.

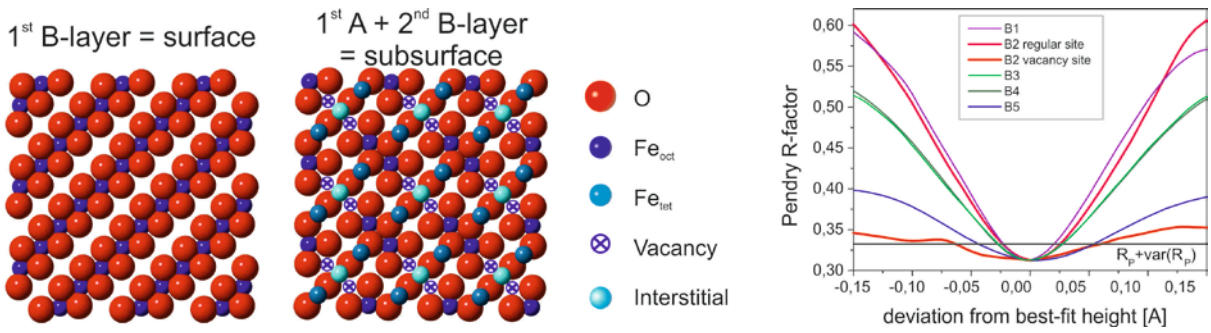

Figure 1: Left: Ball model for the Fe_3O_4(100)-c(2×2) Fe vacancy and interstitial structure. Right: R-factor as a function of the displacement from the best-fit values (for pairs of Fe ions).

Testing alternative plausible models, which either neglect one or both of the vacancies or/and the interstitial ion of the correct model, we found still so-called acceptable R-factors between 0.159 and 0.313, see Tab. 1. The reason for this low structural sensitivity lies qualitatively in the relatively small scattering contribution of a particular atom to the total wave field produced by the large surface unit cell. The situation becomes even worse by the fact that a comparable R-factors will result even for the correct model, when the parameter space for the structural search is reduced (cf. Tab. 2). Then, the local positional distortions induced by the vacancies and interstitials are not completely modelled in the fit. Therefore, the experimental data base has to be always large enough to allow for an extended analysis of the substrate strain field. A similar rise of the R-factor level will be caused by an imperfect surface preparation, where random defects locally disturb the structure and deteriorate the corresponding wave field. Overall, this means that for complex structures incomplete models become more and more indistinguishable from imperfect preparations or calculations and thus other criteria for the validity of a certain structural model have to be regarded.

A simple consistency check provided by the LEED-IV analysis itself is the examination of error margins determined from the variance of the R-factor [1]. Whenever a certain parameter is moved away from its best-fit value the R-factor will increase leading to the typical parabolic "error curves". Extra atoms within the model, which do not belong to the correct structure, disturb the wave field always, regardless of their position, and hence they hardly show a pronounced positional preference as demonstrated in Fig. 1 (right part) for the incorrect "bulk truncation model" [3]. Here, the extra Fe atoms on actual vacancy sites produce an only minor z-dependence of the R-factor in stark contrast to the Fe ions at regular sites. Unfortunately, this procedure cannot give any hint about missing atoms.

A much more powerful tool to detect inconsistencies in the structural model is the inspection of the strain field within the substrate. The LEED fit usually tends to move as many scatterers as possible into the correct position - at least when the redundancy of the analysis is high enough - irrespective whether these positions are physically reasonable within the chosen model or not. Hence, a check of the reasonability of the deduced atomic position (e.g. bond lengths) - or much better a comparison with a fully relaxed DFT structure for the same basic model - might help to reveal structural faults in a tested model.

Model	**Off-stoichiometry**	**R_P -factor**
2 vacancies, 1 interstitial ("correct" model [2])	-1 Fe	**0.125**
1 vacancy,1 interstitial ("correct" model with half-filled vac.)	none	**0.159**
No vacancy, 1 interstitial	+ 1 Fe	**0.257**
2 vacancies, no interstitial	-2 Fe	**0.217**
No vacancy, no interstitial ("bulk truncation model" [3])	none	**0.313**

Table 1: Quality of LEED fit for various structural models

"Correct" model fitted up to the	**Fit parameters**	**R_P -factor**
6th bilayer	58	**0.125**
5th bilayer	52	**0.131**
4th bilayer	47	**0.142**
3rd bilayer	35	**0.169**
2nd bilayer	23	**0.447**

Table 2: Dependence of the quality of the LEED fit on the parameter space used.

[1] J.B. Pendry, **Journal of Physics C 13** (1980) 937
[2] R. Bliem et al., **Science 346** (2014) 1215.
[3] R. Pentcheva et al., **Surface Science 602** (2008) 1299.

Temperature programmed desorption studies of metal oxide surfaces

Jan Hulva, Jiří Pavelec, Martin Setvín, Thomas Simschitz, Michael Schmid, Gareth Parkinson, Ulrike Diebold

Institut für Angewandte Physik, TU Wien, Wien, Austria
(hulva@iap.tuwien.ac.at)

Temperature programmed desorption (TPD) is a traditional surface science technique used to investigate interactions of surfaces and adsorbed molecules [1]. Analysis of TPD spectra provide basic information about desorption mechanisms and kinetics. Here we present a combined TPD and X-ray photoelectron spectroscopy (XPS) study of several metal oxide surfaces using our recently developed ultra high vacuum setup equipped with molecular beam source, mass spectrometer, liquid helium cryostat, x-ray, and ultraviolet photoelectron spectroscopy setup. We investigate adsorption and desorption behavior of CO and formaldehyde on TiO2 anatase (101); a technologically relevant surface of titanium dioxide with only few basic TPD studies published [2]. Next, we show TPD spectra of CO2 on Fe_3O_4 magnetite (001), an important metal oxide model surface [3].

CO on anatase (101) is physisorbed at low temperatures, as confirmed by XPS, and desorbs between 100 and 140 K. The desorption peak shows a first order kinetics with repulsive interaction of adsorbed molecules which results into a coverage dependent desorption energy [4]. Molecular beam sticking coefficient measurement shows unusual coverage dependent behavior – a sharp minimum of sticking coefficient appears around one monolayer coverage. This suggests formation and consequent destabilization of an ordered phase of CO molecules.

Formaldehyde is adsorbed on anatase at 50K and main TPD peak is located around 250K and shows a first order behavior with attractive interaction between formaldehyde molecules. XPS shows a significant change of the O1s and C1s peak position after between measurement at 50K and 140K indicating thermally activated interaction between formaldehyde molecules.

CO_2 desorbs from Fe_3O_4 with a first order kinetics and a weak attractive interaction between CO2 molecules from regular lattice sites with the peak position around 115 K. We assign a small peak around 125 K to surface defect sites and its size provide quantitative information about the surface defect concentration. The desorption peak of the second CO2 layer shows unusual behavior pointing towards the existence of two distinct CO_2 phases at certain coverages.

[1] D.A. King, Surf. Sci. 47, (1975): 384-402
[2] U. Diebold. Surf.Sci.Rep. 48.5 (2003): 53-229.
[3] R. Bliem, et al.. Science 346 (2014): 1215-1218.
[4] M. Setvin, et al., JPCC, 119.36 (2015): 21044-21052.

Near Field Interference Patterns of Surface Plasmon Polaritons

P. Dvořák, Z. Édes, M. Hrtoň, R. Kalousek, and T. Šikola

Institute of Physical Engineering and CEITEC, Brno University of Technology, Technická 2 Brno 616 69, Czech Republic
(corresponding author: R. Kalousek, e-mail: kalousek@fme.vutbr.cz)

Scanning near-field optical microscopy (SNOM) has become a powerful technique for the experimental study of the electromagnetic field penetrating out from the surfaces of materials with high conductivity [1-3]. This electromagnetic field originates in surface collective oscillations of the free electron gas in the material and, thus, the quasiparticles connected with these oscillations are called the surface plasmon polaritons (SPPs). Depending on the spectral region of the detected field various types of SNOM probes are convenient. In the infrared region scattering from a metal aperture-less SNOM (called the s-SNOM) tip represents the most suitable technique, while in the visible region an aperture SNOM (a-SNOM) probe is commonly used [4,5]. The a-SNOM probe consists of an optical fiber etched at its end into a tip coated with a metal except a small aperture at its apex. After the probe has been approached to a surface the observed near electromagnetic field is coupled into the optical fiber of the probe. However, the presence of the tip strongly affects the resultant distribution of the near field [6,7]. Therefore, understanding of the interaction between the SNOM tip and the near field is crucial to correctly interpret the field distribution from the SNOM images.

Much effort has been invested in the study of surface plasmon polaritons freely propagating along smooth metal-dielectric interfaces. Due to the fact that only the time-averaged power flux of the electromagnetic field is detected by SNOM, SPPs at the optical frequencies (order of 10^{15} Hz) cannot be visualized by this technique [8]. This difficulty can be overcome by detection of standing waves of SPPs excited e.g. on plasmonic interference structures. The resultant interference pattern can be controlled via geometry of the structures and also the optical properties of the exciting illumination (i.e. wavelength, phase) [9-11]. The application and utilization of plasmonic interference structures can be found in bio- and chemical sensoring [12-14], 2D optics [15,16], and in manipulation with nanoobjects [17]. The dependences of interaction parameters between SNOM tip and the near field are as a rule interpreted by dispersion relations, i.e. dependence of the frequency of the electromagnetic field propagating through a material on the wavelength [18].

The aim of this contribution is to further unfold the fundamental questions of the near-field imaging using a-SNOM probe depending on basic physical parameters. A similar work on the detection capabilities of s-SNOM tips has been published just recently [19].

We excite the interfering SPPs by illumination of square-like structures formed by four slits prepared into a 200-nm gold film deposited on quartz. The sensitivity of the a-SNOM probe on individual near-field components is demonstrated with SPP-interference patterns measured at various wavelengths of the illuminating light. Furthermore, using simulations we provide the parameters affecting the sensitivity of the a-SNOM probe on the components of the near electromagnetic field.

This work was supported by the Czech Science Foundation (project No. 15-21581S), the Technology Agency of the Czech Republic (TE 01020233: AMISPEC), and the European Regional Development Fund (CEITEC-CZ.1.05/1.1.00/02.0068).

[1] D. W. Pohl, Near-Field Optics and Surface Plasmon Polaritons, Ed. by S. Kawata, Springer-Verlag Berlin Heidelberg 2001, 1-13

[2] D. W. Pohl, W. Denk, M. Lanz, Appl. Phys. Lett. 44, 651 (1984)

[3] L. Novotny, B. Hecht, Nano Today 1, 41 (2006)

[4] R. Hillenbrand, Ultramicroscopy 100, 421 (2004)

[5] J. Aizpurua, T. Taubner, F. J. Garcíja de Abajo, M. Brehm, R. Hillenbrand, Opt. Express 16, 1529 (2008)

[6] R. Esteban, R. Vogelgesang, K. Kern, Phys. Rev. B 75, 195410 (2007)

[7] B. Hecht, B. Sick, U. P. Wild, V. Deckert, R. Zenobi, O. J. F. Martin, D. W. Pohl, J. Chem. Phys. 112, 7761 (2000)

[8] W. L. Barnes, T. W. Preist, S. C. Kitson, J. R. Sambles, Phys. Rev. B 54, 6227 (1996)

[9] P. Dvořák T. Neuman, L. Břínek, T. Šamořil, R. Kalousek, P. Dub, P. Varga, T. Šikola, Nano Lett. 13, 2558 (2013)

[10] G. Obara, N. Maeda, T. Miyanishi, M. Terakawa, N. N. Nedyalkov, M. Obara, Opt. Express 19, 19093 (2011)

[11] J. Lin, J. P. B. Mueller, Q. Wang, G. Yuan, N. Antoniou, X.-C. Yuan, F. Capasso, Science 340, 331 (2013)

[12] J. N. Anker, W. P. Hall, O. Lyandres, N. C. Shah, J. Zhao, R. P. Van Duyne, Nat. Mater. 7, 442 (2008)

[13] C. Valsecchi, A. G. Brolo, Langmuir 29, 5638 (2013)

[14] S. Zeng, D. Baillargeat, H.-P. Ho,K.-T. Yong, Chem. Soc. Rev. 43, 3426 (2014)

[15] M. C. Quong, A. Y. Elezzabi, Opt. Express 16, 8198 (2008)

[16] N. Yu, F. Capasso, Nat. Mater. 13, 139 (2014)

[17] M. L. Juan, M. Righini, R. Quidant, Nat. Photonics 5, 349 (2011)

[18] J. Mihaljevic, C. Hafner, A. J. Meixner, Opt. Express 21, 25926 (2013)

[19] B. N. Tugchin, N. Janunts, A. E. Klein, M. Steinert, S. Fasold, S. Diziain, M. Sison, E.-B. Kley, A. Tunnermann, T. Pertsch, ACS Photonics 2, 1468 (2015)

Focused electron beam induced processing on surface-anchored metal-organic frameworks

Martin Drost[1], Fan Tu[1], Hartmut Gliemann[2], Christof Wöll[2] and Hubertus Marbach[1]

[1] *Lehrstuhl für Physikalische Chemie II, Universität Erlangen-Nürnberg, Egerlandstr. 3, 91058 Erlangen, Germany,*
(corresponding author: H. Marbach, e-mail: hubertus.marbach@fau.de)

[2] *Institut für Funktionelle Grenzflächen,Karlsruher Institut für Technologie (KIT,) Hermann-von-Helmholtz-Platz 1, D-76344 Eggenstein-Leopoldshafen, Germany*

In this contribution we explore the possibilities to structure surface-anchored metal-organic frameworks (SURMOFs) on the nanometer scale by making use of a focused electron beam to either locally modify the SURMOF substrate itself or adsorbed precursor molecules. The corresponding methods for the lithographic fabrication of extremely small nanostructures are subsumed under Focused Electron Beam Induced Processing (FEBIP).[1] The most prominent FEBIP technique is Electron Beam Induced Deposition (EBID) in which adsorbed precursor molecules are locally dissociated by the impact of the electron beam leaving a deposit of the non-volatile dissociation products on the surface. With our distinct "surface science approach" we are not only able to fabricate clean metallic nanostructures but also expanded the family of FEBIP techniques with the exploration of Electron Beam Induced Surface Activation (EBISA).[2] Thereby, in a first step, the chemical properties of the surface (e.g. oxide interfaces or thin organic layers) itself are modified via the e-beam such that it becomes active towards the decomposition of certain precursor molecules. In a second step the surface is exposed to the precursor which decomposes at the preirradiated areas and eventually continues to grow autocatalytically (AG). To do so a 3 nm wide beam of a scanning electron microscope was applied to locally modify the properties of precursor molecules adsorbed on the SURMOF substrate or the SURMOF substrate itself. First experiments were successful (selective fabrication of pure iron deposits on a SURMOF with 5,15-diphenyl-10,20-di(4-carboxyphenyl) porphyrin as linker molecule and zinc acetate as metal containing building block, (c.f. Fig. 1) as well as on a standard HKUST-1 SURMOF (c.f. Fig. 2) and clearly document the high potential of the proposed FEBIP-based nano-structuring approach. Latest Results will be presented and discussed.

Support by the DFG through grant MA 4246/1-2, MA 4246/2-1/ research Unit funCOS, the Excellence Cluster "Engineering of Advanced Materials" and COST Action CM1301 (CELINA) is gratefully acknowledged.

[1] W. van Dorp et al., **J. Appl. Phys.** 104, 081301 (2008); I. Utke et al., **JVST B**, 26, 1197 (2008); I. Utke, A. Gölzhäuser, **Ang. Chem. Int. Ed.**, 49, 9328 (2010)

[2] H. Marbach, **Appl. Phys. A** 117 (2014) 987, F. Vollnhals et al., **J. Phys. Chem. C**, 117, 17674 (2013), M.-M. Walz et al., **Ang. Chem. Int. Ed**., 49, 4669 (2010)

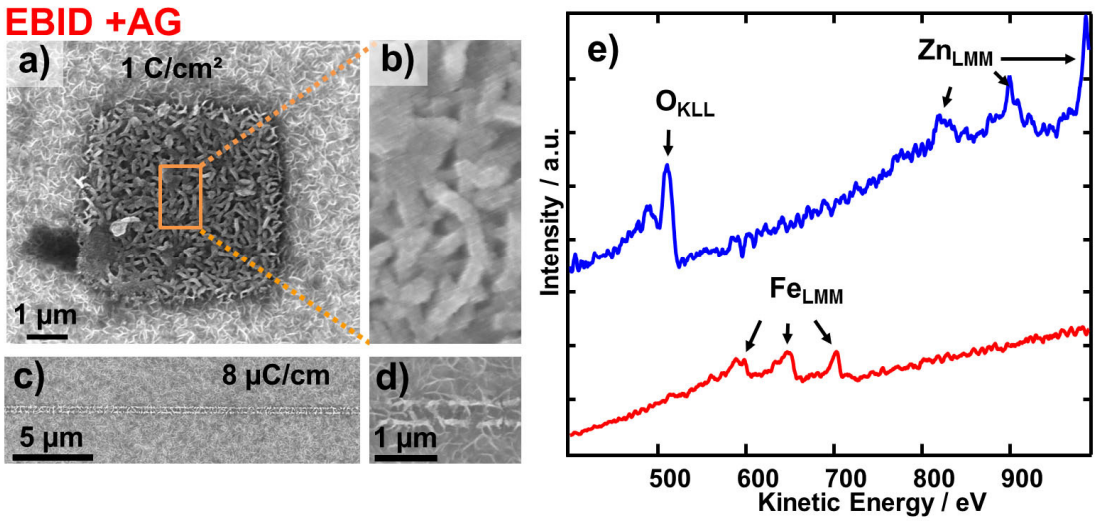

Figure 1: ***a)*** *SEM image of an 4x4 µm² square pattern written via EBID, i.e. in the presence of $Fe(CO)_5$ (p_{BG} = $3x10^{-7}$ mbar), with the indicated electron dose and subsequent exposure to the precursor for approx. 240 min.* ***b)*** *Zoom-in on the iron deposit from a) as indicated.* ***c), d)*** *SE micrographs of a "double line" written via EBID in the same way as the square in a) but with a line dose of 8 µC/cm.* ***e)*** *Auger electron spectra acquired on the EBID square structure shown in a) (red spectrum) and away from the square (blue spectrum) on the non-irradiated SURMOF. The spectra evidence the selective deposition of pure Fe with a sufficient thickness (complete suppression of O and Zn signals) on the electron irradiated area.*

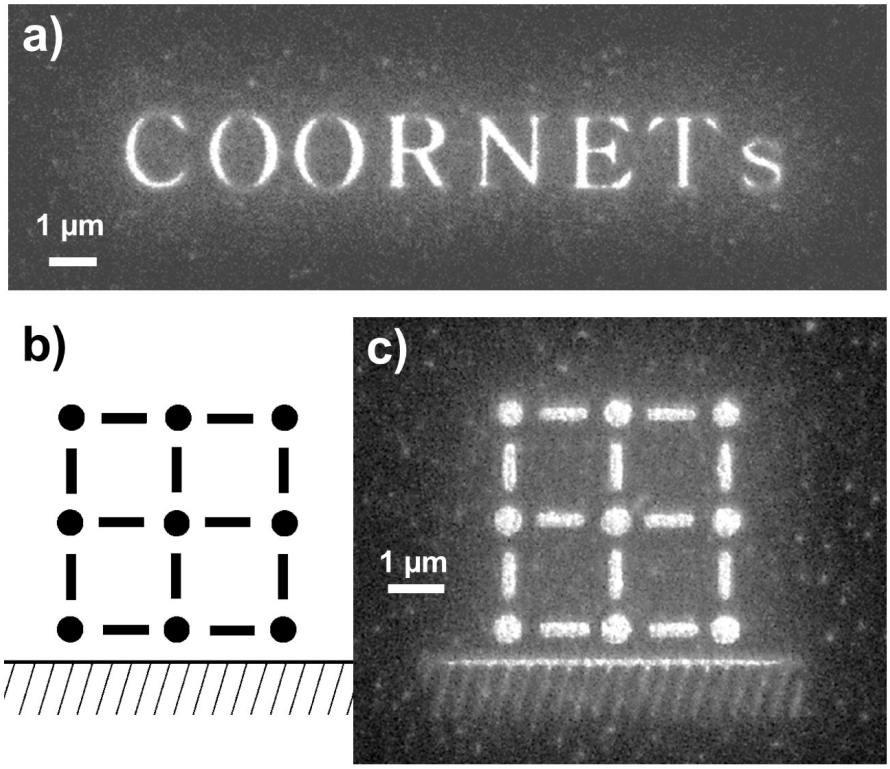

Figure 2: *Selected SEM images of FEBIP deposits from $Fe(CO)_5$ on a HKUST-1 SURMOF. a) "COORNETs" lettering written with EBID and subsequent AG.* ***b)*** *Blueprint for the structure depicted in* ***c)*** *which was again written via EBID and successive AG.*

PEARL – The Photo-Emission and Atomic Resolution Laboratory at the Swiss Light Source

M. Muntwiler[1], J. Zhang[1], R. Stania[1,2], F. Matsui[3], T. Glatzel[4], T. A. Jung[1,4], P. Aebi[5], T. Greber[2], R. Fasel[6]

[1] *Paul Scherrer Institut, 5232 Villigen PSI, Switzerland*
(corresponding author: M. Muntwiler, e-mail: matthias.muntwiler@psi.ch)
[2] *Universität Zürich, Zürich, Switzerland*
[3] *Nara Institute of Science and Technology, Nara, Japan*
[4] *Universität Basel, Basel, Switzerland*
[5] *Université de Fribourg, Fribourg, Switzerland*
[6] *EMPA, Dübendorf, Switzerland*

The Photo-Emission and Atomic Resolution Laboratory (PEARL) is a new synchrotron-based user laboratory for surface science at the Swiss Light Source (SLS). PEARL is designed particularly for studies of atomic and molecular structure at surfaces and interfaces in a variety of systems, for example, surfaces of complex materials, molecular adsorbates, thin films, or nanostructured systems. A major goal has been to implement synchrotron based photoelectron spectroscopy techniques as well as scanning probe microscopy in the same ultra-high vacuum system, allowing for a more complete characterization of the same sample with complementary real and reciprocal space techniques.

The experimental station at PEARL consists of three parts which are connected by sample transfer under ultra-high vacuum: a state of the art angle- and energy-resolved photoelectron spectrometer using synchrotron radiation, a low-temperature scanning tunnelling microscope, and a surface preparation chamber with standard surface cleaning, organic evaporators, and accessory ports. The synchrotron beamline delivers smoothly tunable X-rays from 60 to 2000 eV at a resolving power $E/\Delta E$ of up to 7000. The X-ray optics is optimized for photoelectron diffraction experiments in angle and energy scanned modes (XPD/PhD), while high-resolution XPS, Auger electron spectroscopy, and valence band spectroscopy (at limited resolution) are also supported. PEARL has started operation in 2014, and now also accepts external users.

In this contribution, examples from scientific projects are presented to demonstrate the capabilities of the laboratory. In more detail, a measurement of the adsorption height of hexagonal boron nitride on a Ni(111) surface is discussed as a use case of energy-scanned photoelectron diffraction. Measuring distance along the surface normal has been difficult, as only few techniques are capable and the interpration of the data can be tedious. In such a case, the direct imaging power of STM is helpful as a first step towards a complete (and quicker) three-dimensional characterization with diffraction-based techniques.

Electron emission from single layer graphene induced by impact of highly charged ions

J. Schwestka*, A. Fuchs-Fuchs, L. Rachbauer, and F. Aumayr

Institute of Applied Physics, TU Wien, Wiedner Hauptstr. 8-10/E134, 1040 Vienna, Austria
*(*e-mail: schwestka@iap.tuwien.ac.at)*

Single layer graphene (SLG) is an ultimately thin membrane made of sp^2-hybridized carbon atoms with unique electronic properties. Since its discovery [1], SLG has been considered as an excellent candidate for future nano-electronics. Disorder, as e.g. induced by collisions with energetic electrons or ions, effects the electronic structure and opens the possibility to modify and tailor the properties of this true 2D material. Collision studies between ions and free-standing SLG are also of fundamental interest, because they bridge the gap between atomic collisions in gaseous and those in solid targets.

For the transmission of slow highly charged ions through slightly thicker (1 nm) carbon nano membranes (CNMs) we have recently observed two distinct exit charge state distributions [2]. In addition a strong charge state dependent energy loss [2] and the creation of nano-sized pores for impact of Xe^{q+} projectiles in charge states $q \geq 25$ were found [3]. To learn more about the microscopic interaction mechanism, we have built a new experimental setup (fig. 1), which allows us to determine the numbers statistics of electrons emitted during the transmission of slow multiply charged Ar^{q+} ions through SLG (and CNMs in comparison).

Slow Ar^{q+} ions ($q \leq 11$) are extracted from an ECR-ion source [4], mass analysed and collimated before traversing a free standing SLG or CNM target (mounted on a TEM grid, which is fixed onto a rotatable manipulator) and being registered by a position sensitive multichannel plate detector (MCP). Electrons emitted from the interaction region are extracted by a weak electric field through a highly transparent grid and accelerated onto a surface barrier type detector biased at +30 kV, where their statistical distribution is measured in the usual way (see, e.g. [5, 6]). By changing the orientation of the target film from 45° to 135° with respect to the incident beam direction, electrons emitted from the front (= ion entrance side) and back side (= ion exit side) can be distinguished. To separate electron-emission events caused by ion transmission through SLG from events originating from ion impact on the (solid) TEM grid support, only electrons registered in coincidence with an ion signal on the MCP are counted.

As an example fig. 2 shows the comparison of a coincidence and a non coincidence electron emission statistics spectrum for 18 keV Ar^{9+} ions impinging under an incident angle of 45° onto a SLG target. The coincidence spectrum shows a clearly higher electron yield. Electrons, which are registered in coincidence with transmitted projectile ions, are unambiguously emitted from the graphene sheet (not the support or other sources). The observed number of

emitted electrons is surprisingly high, but consistent with the observation, that the neutralization of a highly charged ion seems to happen on a time scale as short as a few femtoseconds only [7].

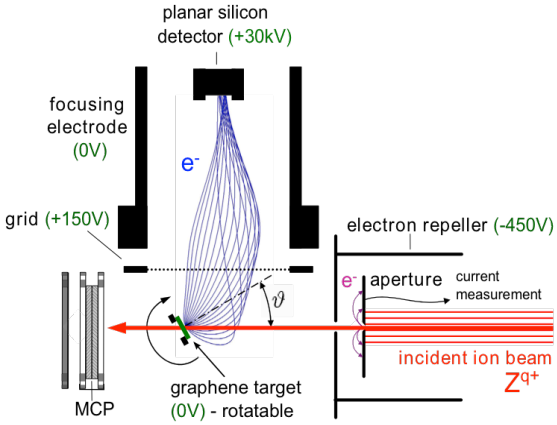

Fig. 1: *Experimental setup for measuring the numbers statistics of electrons emitted during the transmission of slow multiply charged Ar^{q+} ions through SLG.*

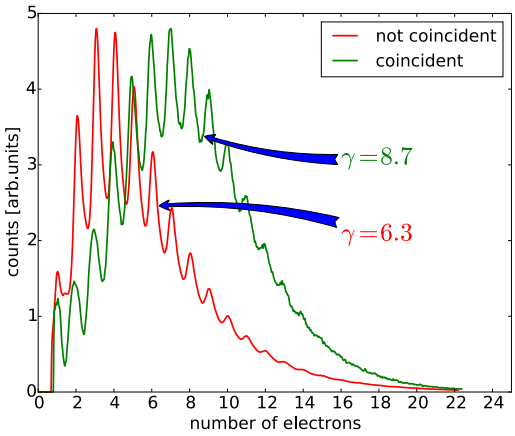

Fig. 2*: Comparison of coincidence and non coincidence electron emission statistics (ES) spectra for 18 keV Ar^{9+} ions impinging under an incident angle of 45° onto a SLG target.*

Since electron emission and projectile charge exchange are closely related, it is planned to register the electrons in coincidence with a particular projectile exit charge state in a next step.

[1] A. K. Geim and K. S. Novoselov, Nature Mater. 6, 183 (2007).
[2] R. A. Wilhelm, et al., Phys. Rev. Lett. 112 153201 (2014).
[3] R. Ritter, et al., Appl. Phys. Lett. 102 06311 (2013).
[4] E. Galutschek et al., J. Phys. Conf. Ser. 58 395 (2007).
[5] F. Aumayr et al., Appl. Surf. Sci. 47 139 (1991).
[6] K. Töglhofer et al., Surf. Sci. 281 143 (1993).
[7] E. Gruber et al. in preparation

Charging Single O_2 Molecules on Anatase TiO_2 (101)

M. Setvin, J. Hulva, T. Simschitz, M. Schmid, and U. Diebold

Institut für Angewandte Physik, TU Wien, A-1040 Wien, Austria
(corresponding author: M. Setvin, e-mail: setvin@iap.tuwien.ac.at)

TiO_2 is a prototypical material used in photocatalysis, e.g. in water remediation or photocatalytic water splitting [1]. Two polymorphs of TiO_2 are used industrially – rutile and anatase, where the anatase is typically preferred in applications. The surface chemistry of oxygen is key in the majority of (photo)catalytic processes on TiO_2.

O_2 adsorption on the anatase TiO_2 (101) surface has been investigated in the temperature range from 4 to 300 K by scanning tunneling microscopy (STM), non-contact atomic force microscopy (nc-AFM), X-ray photoelectron spectroscopy (XPS) and temperature-programmed desorption (TPD). In our previous works [2,3] we have shown that O_2 chemisorbs in the vicinity of subsurface donors and step edges, where the chemisorbed (active) O_2 species accept electrons from the substrate.

Here we show that a full monolayer of O_2 can be adsorbed on the anatase (101) surface at LHe temperature; the corresponding TPD desorption peak for the first monolayer is found at 60 K (Fig. 1c). The O_2 molecules in this monolayer are neutral and thus chemically inactive. The neutral molecules can be directly imaged by nc-AFM at zero sample bias (see Fig. 1a). We show that applying a small positive bias to the tip results in electron transfer into the O_2 molecules, which become singly charged (superoxo) $(O_2)^-$. Such purposely charged $(O_2)^-$ species are stable over time, even though the substrate is metallic (Fig. 1b). The extra electron can be removed from the molecule, either by the STM/AFM tip or by illumination by UV light. This process requires a negative sample bias of -1.5 V and results in desorption of the O_2 molecule from the surface. We attribute the desorption to a Frank-Condon mechanism.

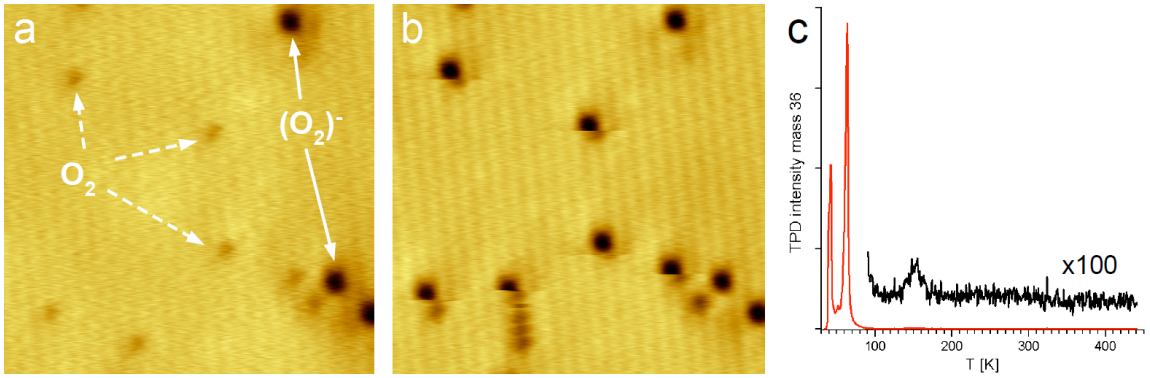

Fig. 1: a) 12x12 nm² AFM image of O_2 molecules adsorbed at the anatase (101) surface. Const. height, measured at V_S = -0.4 V. Dark color denotes higher attractive force. b) The same area imaged at V_S = +0.33 V. Neutral O_2 molecules become charged by the electrons from the tip. c) O_2 TPD spectrum.

Measurements of the force curves above the neutral and charged O_2 molecules directly show a drastic difference in the reactivity of these species: forces measured above the neutral O_2 corresponds to weak chemical interactions, while the forces detected above the $(O_2)^-$ indicate formation of a chemical bond between the tip and the molecule.

The details of charging/discharging of the O_2 molecules were further studied by local Kelvin-probe spectroscopy. The measured shift of the Kelvin parabola maximum is consistent with the charging scheme. Further, we find that the potential barrier required for the O_2 charging grows with the increasing concentration of $(O_2)^-$ species.

The work was supported by the advanced ERC grant "Oxide Surfaces" and the FWF (Project Z250, Wittgenstein Prize). We thank Franz Giessibl for help with the q-Plus AFM technique.

[1] M. A. Henderson, Surf. Sci. Rep. 66, 185 (2011)

[2] M. Setvin *et al*., Science 341, 988 (2013)

[3] M. Setvin *et al*., Angew. Chem. Int. Ed. 53, 4714 (2014)

Structure and adsorption properties FeO(111) on Ag(100) and Ag(111)

M. Shipilin, J. Gustafson, C. Zhang, F. Bertram[1], E. Lundgren, J. Choi[2], M. Vikram[2], J. F. Weaver[2], and L. R. Merte

Division of Synchrotron Radiation Research, Lund University, 22100 Lund, Sweden
(corresponding author: M. Shipilin, e-mail: mikhail.shipilin@sljus.lu.se)

[1] *Deutsches Elektronen-Synchrotron (DESY), D-22603 Hamburg, Germany*

[2] *Department of Chemical Engineering, University of Florida, Gainesville, FL 32611, USA*

Thin metal oxide films have attracted a wide scientific interest as model systems for catalysis to explore properties not present in the corresponding bulk oxides. Two-dimensional iron oxide films in particular have been extensively studied because of their scientific importance not only as model systems for investigations of surface properties but also for technological applications ranging from magnetic devices to heterogeneous catalysis [1,2]. Both structural and electronic properties of such films largely depend on the substrate-film interactions. Thus, by changing the substrate, the chemical properties of the system can be tuned, potentially allowing for a design of novel materials with desired surface properties.

The growth of one-layer thick iron oxide films has been studied recently using different substrates. In particular, the structure analogous to FeO(111) – the stoichiometric structure, which is not stable in the bulk form – was grown on Pt(111) [3,4], Ru(0001) [5], Pd(111) [6], Au(111) [7], Pt(100) [8-10] substrates with lattice constants comparable to the lattice constant of FeO(111). Intriguingly, it was found that the complete iron oxide monolayer on Pt(111) exhibits higher catalytic activity towards CO oxidation than the bare substrate [11,12], under certain conditions.

Recently, we have shown that a monolayer of FeO(111) grown on Ag(100) [13] has very different NO adsorption properties from FeO(111) on Pt(111), due to the difference in the so-called rumpling distance between the Fe and O in the FeO(111) film [14].

In this contribution we present a Surface X-Ray Diffraction (SXRD) study of the atomic positions in the c(2×11) structure formed by the FeO(111) monolayer on Ag(100), paving the way for in situ CO-oxidation investigations. Further, we present experimental results showing that the FeO(111) monolayer can also be grown on Ag(111). The NO adsorption properties studied by Reflection-Absorption Infrared Spectroscopy (RAIRS) and Temperature Programmed Desorption (TPD) of the FeO(111) film on Ag(111) show that the chemical properties are similar to the adsorption properties of the FeO(111) film on Ag(100). Therefore, the chemical properties of the FeO(111) monolayer appear to be determined by the

strength of the substrate-Fe interaction, rather than by the surface orientation of the substrate and differences in the exact moiré geometries of the oxide films.

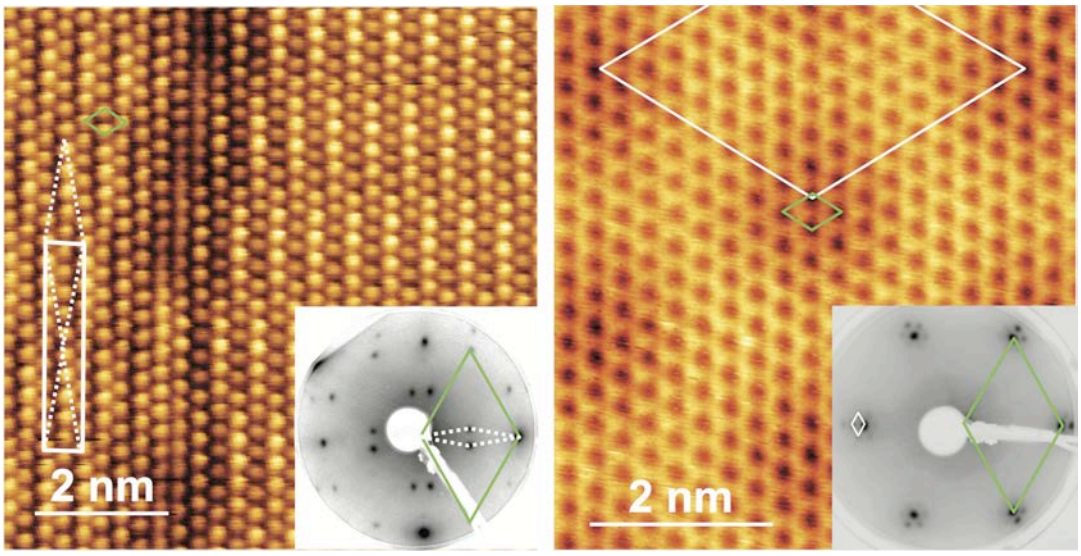

Fig. STM and LEED images of one-layer FeO(111) on Ag(100) (left panel) and Ag(111) (right panel).

The authors would like to acknowledge the Röntgen-Ångström collaboration "Catalysis on the atomic scale". Financial support by the Swedish research council (VR), the Swedish foundation for cooperation and research in higher education (STINT) and the U.S. Department of Energy is gratefully acknowledged.

[1] R. M. Cornell, U. Schwertmann, The Iron Oxides; Wiley-VCH: Weinheim, Germany, 2003

[2] G. Ertl, H. Knözinger, F. Schüth, J. Weitkamp, Handbook of Heterogeneous Catalysis; Wiley-VCH: Weinheim, Germany, 2008

[3] G. H. Vurens, M. Salmeron, G. Somorjai, Surf. Sci. 201, 129 (1988)

[4] W. Weiss, G. A. Somorjai, J. Vac. Sci. Technol. A 11, 2138 (1993)

[5] G. Ketteler, W. Ranke, J. Phys. Chem. B 107, 4320 (2003)

[6] H. Zeuthen et al., J. Phys. Chem. C 117, 15155 (2013)

[7] N. A. Khan, C. Matranga, Surf. Sci. 602, 932 (2008)

[8] G. H. Vurens, V. Maurice, M. Salmeron, G. A. Somorjai, Surf. Sci. 268, 170 (1992)

[9] M. Ritter, H. Over, W. Weiss, Surf. Sci. 371, 245 (1997)

[10] S. Shaikhutdinov, M. Ritter, W. Weiss, Phys. Rev. B 62, 7535 (2000)

[11] Y.-N. Sun, Z.-H. Qin, M. Lewandowski, E. Carrasco, M. Sterrer, S. Shaikhutdinov, H.-J. Freund, Journal of Catalysis 266, 359 (2009)

[12] Y.-N. Sun et al., Angew. Chem., Int. Ed. 49, 4418 (2010)

[13] L. R. Merte, M. Shipilin, S. Ataran, S. Blomberg, C. Zhang, A. Mikkelsen, J. Gustafson, and E. Lundgren, J. Phys. Chem. C 119, 2572 (2015)

[14] L. R. Merte, C. J. Heard, F. Zhang, J. Choi, M. Shipilin, J. Gustafson, J. F. Weaver, H Grönbeck, and E. Lundgren, *submitted*

Description of many-body effects in quasiparticle interference on noble-metal surfaces

V. M. Silkin[1,2,3], P. Sessi[4], I. A. Nechaev[2], Th. Bathon[1], L. El-Kareh[1], E. V. Chulkov[2,3,5], P. M. Echenique[2,3,5], M. Bode[1,6]

Donostia International Physics Center (DIPC), Paseo de Manuel Lardizabal 4, 20018 San Sebastian/Donostia, Spain
(corresponding author: V. M. Silkin, e-mail: waxslavas@ehu.es)

[1]*Donostia International Physics Center (DIPC), Paseo de Manuel Lardizabal 4, 20018 San Sebastian/Donostia, Spain*
[2]*Departamento de Física de Materiales, Universidad del País Vasco, Apartado 1072, 20080 San Sebastián/Donostia, Spain*
3IKERBASQUE, Basque Foundation for Science, 48011 Bilbao, Spain
[4]*Physikalisches Institut, Experimentelle Physik II, Universität Würzburg, Am Hubland, D-97074 Würzburg, Germany*
[5]*Centro de Física de Materiales CFM-Materials Physics Center MPC, Centro Mixto CSIC-UPV/EHU, Paseo de Manuel Lardizabal 5, 20018 San Sebastián/Donostia, Spain*
[6]*Wilhelm Conrad Röntgen-Center for Complex Material Systems (RCCM), Universität Würzburg, Am Hubland, D-97074 Würzburg, Germany*

One of the applications of scanning tunneling microscopy (STM) is the study the electronic density of states is based on a simple approximation that the STM tunneling current is determined by the local density of states of the sample [1,2]. Recently, to take advantages offered by the Fourier transform (FT) of the quasiparticle interference (QPI) imaging in the STM experiments, the experimental and theoretical studies to probe the electron self-energy have appeared [3-5]. It was shown that, in principle, the self-energy can be extracted by examining the properties of the peak attributed to the quasiparticle excitations.

However, the self-energy effects are generally not reduced to a quasiparticle picture, since the many-body spectral function can have other features with lower intensities. Recently, by analyzing the images of the energy dependent standing-wave patterns at Cu, Ag, and Au (111) surfaces, we demonstrated that additionally to the surface-state quasiparticle peak a satellite with certain dispersion emerges [6]. We relay the appearance of this satellite in the STM measurements to the existence of the acoustic surface plasmon on these surfaces [7-12]. Within a proposed approach based on the GW approximation for the self-energy, we describe how the additional plasmon-related peak appears in the FT-QPI. We believe that our approach can be useful in expanding the capabilities of the FT-QPI imaging as an experimental technique to study many-body effects in condensed matter physics.

[1] J. Tersoff and D.R. Hamann, Phys. Rev. Lett. **50**, 1998 (1983).
[2] J. Tersoff and D.R. Hamann, Phys. Rev. B **31**, 805 (1985).
[3] S. Grothe *et al*., Phys. Rev. Lett. **111**, 246804 (2013).
[4] T. Dahm and D.J. Scalapino, New J. Phys. **16**, 023003 (2014).
[5] M. P. Allan *et al*., Nature Phys. **11**, 177 (2015).
[6] P. Sessi *et al*., Nature Commun. **6**, 8691 (2015).
[7] V.M. Silkin *et al*., Europhys. Lett. **66**, 260 (2004).
[8] B. Diaconescu *et al*., Nature **448**, 546 (2007).
[9] S.J. Park and R.E. Palmer, Phys. Rev. Lett. **105**, 016801 (2010).
[10] K. Pohl, Europhys. Lett. **90**, 57006 (2010).
[11] J. Pischel *et al*., J. Chem. Chem C **117**, 26964 (2013).
[12] L. Vattuone *et al*., Phys. Rev. Lett. **110**, 127405 (2013).

Erosion of iron and iron-tungsten films under deuterium ion impact

R. Stadlmayr*, B. M. Berger, D. Blöch, S. Kaser, L. Bergen and F. Aumayr

Institute of Applied Physics, TU Wien, Fusion@ÖAW
Wiedner Hautpstraße 8-10, 1040 Vienna, Austria
*(*e-mail: stadlmayr@iap.tuwien.ac.at)*

For a future fusion reactor, like DEMO, a stable and quiescent plasma has to be assumed. With this presumption, the lifetime of the plasma facing components (PFC) will be dominated by the plasma induced erosion due to ions and energetic neutrals. Since the erosion of high-Z materials is considerably lower than the erosion of low-Z materials at the low energy of ions impinging on plasma-facing surfaces [1] the use of thin tungsten armors as plasma facing components is foreseen in some DEMO design studies [1, 2]. However, the steady-state operation also brings new demands to the heat removal from the PFC. A bonding of the armor directly to the cooled component is necessary, which will probably be expensive and technologically challenging.

One attractive alternative to a tungsten armor for recessed areas would be the use of tungsten containing steels (e.g. EUROFER [3]). Experiments at the linear plasma device PISCES-A have shown a strong decrease in the sputtering yield of EUROFER for low energetic D plasma bombardment at high incident fluences [4]. A tungsten surface enrichment due to preferential sputtering of the lighter elements is observed and correlates with the reduction of the erosion yield [4, 5]. A profound understanding of the tungsten surface enrichment process due to the interaction of deuterium ions with tungsten-containing steels is hence highly desirable.

We have studied the interaction of mono-energetic deuterium projectiles (250 eV/D and 1000 eV/D) with 400 nm thick iron-tungsten (FeW) model films with 1.5 at% tungsten under well defined laboratory conditions and have compared the results to pure Fe films. The experiments were performed at 465 K using a highly sensitive quartz crystal microbalance (QCM) technique [6]. The evolution of the mass change rate of the FeW model films under D ion irradiation was investigated under normal and oblique incidence. After reaching certain D fluences we measured the sputtering yield as a function of ion incident angle (0° - 70° with respect to the surface normal). For low D fluences the mass removal rate of FeW is close to the value of pure Fe. In good agreement with the experimental results reported in [5] a reduction of the sputtering yield with increasing D fluence is observed. The measured angular variation of the sputtering yield for FeW is much weaker than for pure Fe and vanishes at higher fluences (fig. 1a). Dynamic sputtering calculations with SDTrimSP are not able to reproduce this behaviour, which points out, that possible changes in surface topography are

not taken into account. AFM investigations of the irradiated film indeed show a self-organized quasi-periodic patterning [7, 8] of the FeW film (fig. 1b) due to ion bombardment. A very similar surface morphology has been reported for erosion of a polycrystalline Ni surface by low energy Ar ion bombardment [9].

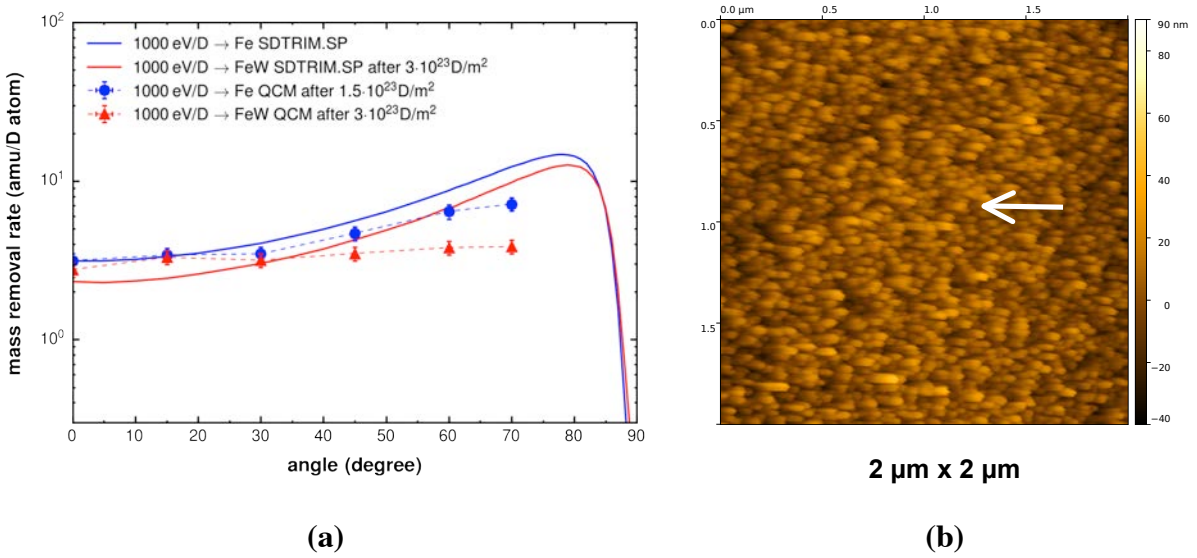

Fig. 1 (a) Sputtering yield of Fe - and FeW - model films under deuterium ion bombardment (1000 eV/D atom) as a function of ion impact angle (with respect to the surface normal). The FeW film was pre-irradiated under normal incidence up to a fluence of 3 x 10^{23} D m^{-2}. **(b)** AFM image of the FeW film after irradiation with 250 eV/D deuterium ions at 60° impact angle (impact direction indicated by the white arrow) up to a total fluence of 3.4 x 10^{23} D m^{-2} (typical ion flux: 4.5 x 10^{17} D m^{-2} s^{-1}).

The authors are grateful to K. Sugiyama (IPP Garching) for preparation oft he Fe-W model film and to M. Schmid (TU Wien) for his continued support with the QCM electronics. This work has been carried out within the framework of the EUROfusion Consortium and has received funding from the Euratom research and training programme 2014-2018 under grant agreement No 633053. The views and opinions expressed herein do not necessarily reflect those of the European Commission. Financial support has also been provided by KKKÖ.

[1] H. Bolt et al., J. Nucl. Mat. **307–311** (2002) 43
[2] D. Maisonnier et al., Fusion Eng. Design **75-79** (2005) 1173
[3] R. Lindau et al., Fusion Eng. Design **75-79** (2005) 989
[4] J. Roth et al., J. Nucl. Mat. **454** (2014) 1
[5] K. Sugiyama et al., J. Nucl. Mat. **463** (2015) 272
[6] G. Hayderer et al., Rev. Sci. Instrum. **70** (1999) 3696
[7] S. Facsko et al. Science **285** (1999) 1551
[8] M.A. Makeev and A.L. Barabasi, Nucl. Instr. Meth. B **222** (2004) 335
[9] T. Skeren, et al., New J. Phys. **15** (2013) 093047

Transformation of paramagnetic fcc Fe into ferromagnetic bcc Fe by Focused Ion Beams

Jonas Gloss[1], Viola Krizakova[2], LukasFlajsman[2], Michal Horky[1,2],Michal Urbanek [2], Peter Varga [1,2]

[1] Institute of Applied Physics (IAP),Vienna Univ. of Techn. (VUT), Austria
[2] Central European Inst. of Techn. (CEITEC) at Brno Univ. of Techn., Czech Republic

It has been show before by LEED and also STM that 8ML Fe films grown on Cu(100) have an fcc structure[1,2,3] and it was known also that such a film is nonmagnetic at room temperature[3]. We could show by high resolution STM and also by LEED that in such a film bcc structured needles are formed by ion bombardment [4]. It could also be unambiguous confirmed by SMOKE [4] that this crystallographic transition is related also to a transition from paramagnetic to ferromagnetic structure. We also demonstrated fabrication of micro- and nanoscale magnetic patterns by ion irradiation. For this purpose, we have grown such metastable face-centered cubic (fcc) Fe layers with a thickness of 22ML and 40ML by stabilizing the metastable ffc Fe by increased CO pressure [5] and for the 40ML thick layer by co-evaporation of Ni (about 20%)[6][7] respectively. On these "metastable" fcc films various magnetic patterns from nm up to mm size were produced by ion beam lithography [8] and focused ion beam (FIB)respectively[9]. Recently we managed to grow such metastable fcc Fe films also on Cu thin films which were grown on hydrogen stabilized Si(100) substrates.

This system will be the starting point to produce magnonic structures [10] often called metamaterials. Magnonic structures represent a new class of metamaterials with periodically modulated magnetic properties. Similarly to the propagation of electromagnetic waves in photonic crystals the propagation of collective spin waves in magnonic crystals is subject to the existence of allowed frequency ranges alternated with forbidden band gaps additionally tunable by external magnetic field. Magnonics offers great opportunity to design and exploit a new generation of spin logic devices, filters, and waveguides operating in GHz and THz frequency range [11]

[1] A.Biedermann, M.Schmid, P.Varga, Phys. Rev. Lett.86 (2001) 464-467
[2] A.Biedermann, R.Tscheließnig, M.Schmid and P.Varga, Phys. Rev. Lett. 87 (2001)
[3] J.Thomassen, F.May, B.Feldmann, M.Wuttig and H.Ibach, Phys.Rev.Lett 69 (1992) 3831
[4] W. Rupp, A. Biedermann, B. Kamenik, R. Ritter, Ch. Klein, E. Platzgummer, M. Schmid, P. Varga, Appl. Phys.Lett. 93 (2008) 063102
[5] A.Kirilyuk, J. Giergiel, J.Shen, J.Kirschner, Phys.Rev.B 52, R116772 (1995)
[6] S. Shah Zaman, H. Oßmer, J. Jonner, Z. Novotný, A. Buchsbaum, M. Schmid, P. Varga, Phys. Rev. B 82 (2010) 235401
[7] S. Shah Zaman, P. Dvorak, R. Ritter, A. Buchsbaum, D. Stickler, H.P. Oepen, M. Schmid, P. Varga. J. Appl. Phys. 110 (2011) 024309
[8] W. Rupp, A. Biedermann, B. Kamenik, R. Ritter, Ch. Klein, E. Platzgummer, M. Schmid, P. Varga, Appl. Phys. Lett. 93 (2008) 063102
[9] J. Gloss, S. Shah Zaman, J. Jonner, Z. Novotny, M. Schmid, P. Varga, M. Urbánek Appl. Phys. Lett. 103 (2013) 262405
[10] Lenk B., Ulrichs H. Garbs F., Münzenberg M., Physics Reports 507 (2011) 107
[11] Kruglyak V., Demokritov S.O.,Grundler D., J.Phys.D: Appl.Phys.43 (2010)246001

Thursday

Combined STM, IETS, and AFM on CO/Cu(111) reveals that single atom tips maximize the intensity of IETS signal

Norio Okabayashi[1,2], Alexander Gustafsson[3], Angelo Peronio[1], Magnus Paulsson[3], Toyoko Arai[2], and Franz J. Giessibl[1], franz.giessibl@ur.de

[1]Institute of Experimental and Applied Physics, University of Regensburg, D-93053 Regensburg, Germany, [2]Graduate School of Natural Science and Technology, Kanazawa University, 920-1192 Ishikawa, Japan, [3]Department of Physics and Electrical engineering, Linnaeus University, 391 82 Kalmar, Sweden

Achieving a high intensity in inelastic scanning tunneling spectroscopy (IETS) is important for precise measurements. The intensity of the IETS signal can vary up to a factor three for various tips without an apparent reason accessible by scanning tunneling microscopy alone. Here, we show that combining STM and IETS with atomic force microscopy (AFM) enables carbon monoxide front atom identification, revealing that high IETS intensities for CO/Cu(111) are obtained for single atom tips, while the intensity drops sharply for multi-atom tips. Adsorbing the CO molecule on a Cu adatom [CO/Cu/Cu(111)] such that it is elevated over the substrate strongly diminishes the tip dependence of IETS intensity, showing that an elevated position channels most of the tunneling current through the CO molecule even for multi-atom tips, while a large fraction of the tunneling current bypasses the CO molecule in the case of CO/Cu(111). Inelastic electron tunneling spectroscopy (IETS) with scanning tunneling microscopy (STM) is an effective method to analyze the vibrational modes of a single adsorbed molecule with sub-nanometer lateral resolution [1,2]. The vibrational energy of a molecule on a substrate strongly depends on the surrounding environment, such as the substrate structure and composition. The intensity is described by the multiplication of the two factors: (1) the ratio of the tunneling current passing through a molecule to the total tunneling current ($I_{molecule}/I_{total}$) and (2) the efficiency of the inelastic process (γ_{inel}). These factors should in principle be affected by the geometrical structure of the substrate and the tip.

The geometrical structure of a metal tip apex can be determined by using carbon monoxide (CO) front atom identification (COFI) provided by AFM [3,4], where the tip apex of a force sensor is probed by a CO molecule that stands upright on a metal surface (inset of Fig. 1(e)). While the STM image of the CO molecule is similar for monoatomic tips (a) and a tetramer tip (c), the COFI images in (d,e) show pronounced differences. The IETS intensity is roughly three times higher for the monotip versus the tetramer tip. This effect is much weaker when the CO molecule is adsorbed on a Cu adatom (see Fig. 2).

We expect that our findings have strong consequences for the spatial resolution of IETS, in addition to the demonstrated impact of tip sharpness on IETS intensity.

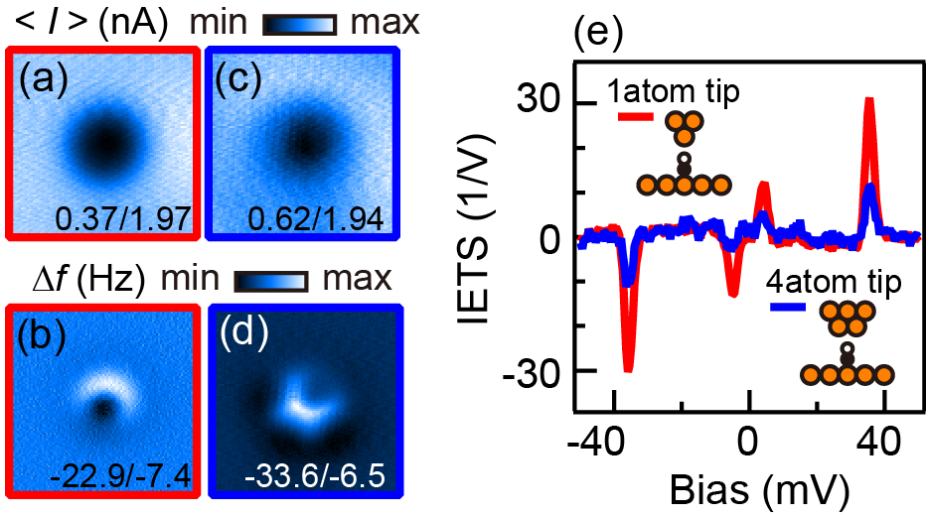

Fig. 1. Constant-height, (a)[(c)] current and (b)[(d)] frequency shift images (1.5 nm×1.5 nm) for a CO molecule adsorbed on Cu(111) by a single-atom tip [four-atom tip]. The tip height is set on the Cu(111) substrate at a sample bias V_t=−1 mV and an average current $\langle I_t \rangle$=1.5 nA. (e) Normalized IETS for a CO molecule at a set-point of V_t=−50 mV and $\langle I_t \rangle$=5 nA, where the IETS on the Cu(111) surface is subtracted.

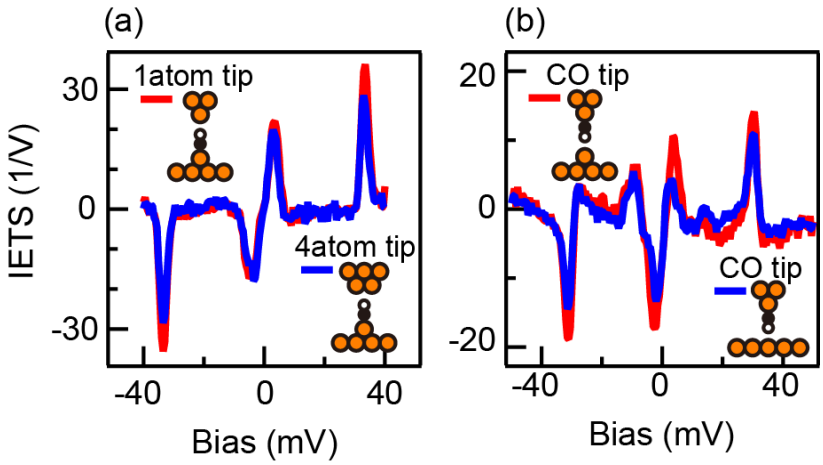

Fig. 2. (a) IETS with the single-atom tips (red) and the four-atom tip (blue) for a CO on a Cu adatom. (b) IETS of a CO-functionalized tip for a Cu adatom (red) and the bare Cu(111) surface (blue). In both cases [(a) and (b)], the tip-height is set at V_t=−50 mV and $\langle I_t \rangle$=5 nA on the measurement points.

References

[1] W. Ho, J. Chem. Phys. **117**, 11033 (2002).

[2] B. C. Stipe, M. A. Rezaei, and W. Ho, Science **280**, 1732 (1998).

[3] J. Welker and F. J. Giessibl, Science **336**, 444 (2012).

[4] T. Hofmann, F. Pielmeier, and F. J. Giessibl, Phys. Rev. Lett. **112**, 066101 (2014).

High-Resolution Imaging with "Scanning Electrochemical Potential Microscopy (SECPM)"

Christoph Traunsteiner[1], Slawomir Sek[2], Kaiyang Tu[1], Julia Kunze-Liebhäuser

Institut für Physikalische Chemie, Universität Innsbruck, A-6020 Innsbruck, Austria
(corresponding author: J. Kunze-Liebhäuser, e-mail: julia.kunze@uibk.ac.at)

[1] *Technische Universität München, James-Franck-Str. 1, 85748 Garching, Germany*

[2] *Department of Chemistry, University of Warsaw, Pasteura 1, 02-093 Warsaw, Poland*

In fuel cell systems and metal-air batteries, the oxygen reduction reaction (ORR) at the cathode side is still one of the performance-limiting factors [1]. ORR active enzymes like laccase are ideal candidates for the investigation of this reaction due to their high redox potentials and their high catalytic activity [2]. To synthesize a model system for ORR studies with laccase, the enzymes have been immobilized on Au(111) surfaces modified with mixed self-assembled monolayers (SAMs) of two different thiols. One of these thiols serves as a linker to the enzyme due to its end group which resembles the enzyme's natural substrate. These linkers are embedded in a matrix of shorter thiols to increase the distance between the linkers and thus improve accessibility to the enzymes. High-resolution electrochemical scanning tunneling microscopy (EC-STM) was used to determine the thiols' molecular arrangement in the SAM. Enzymatic activity measured with cyclic voltammetry was found to be high when the SAM is homogeneously mixed, whereas no activity was observed when the thiols attach in separated phases. The immobilized enzymes can be imaged using EC-STM and a method called scanning electrochemical potential microscopy (SECPM). The latter is a scanning probe technique supposedly detecting the electrical double-layer (EDL) potential, and previously showed high-resolution imaging capabilities of biomolecules [3].SECPM was established in the group of A.J. Bard, who used it to probe potential distance curves of conductive and semiconductive surfaces [4]. In case of laccase imaging, EC-STM and SECPM micrographs show an unexpected degree of similarity.

Therefore, a fundamental study of the working principle of SECPM has been performed. The OH adsorbate structure formed on Cu(111) in alkaline solution is used as a model system for this investigation and reveals a structural parameter of (0.60 ± 0.04) nm when imaged with SECPM, which is in excellent agreement with EC-STM results [5]. This was the first evidence of high-resolution imaging with SECPM [6]. The origin of the potential signal measured with the SECPM probe was then critically investigated and discussed taking into account leakage currents that have to be transported between tip and surface [6]. Two

different approaches are presented to measure these currents; the obtained values are similar to tunneling currents in EC-STM.

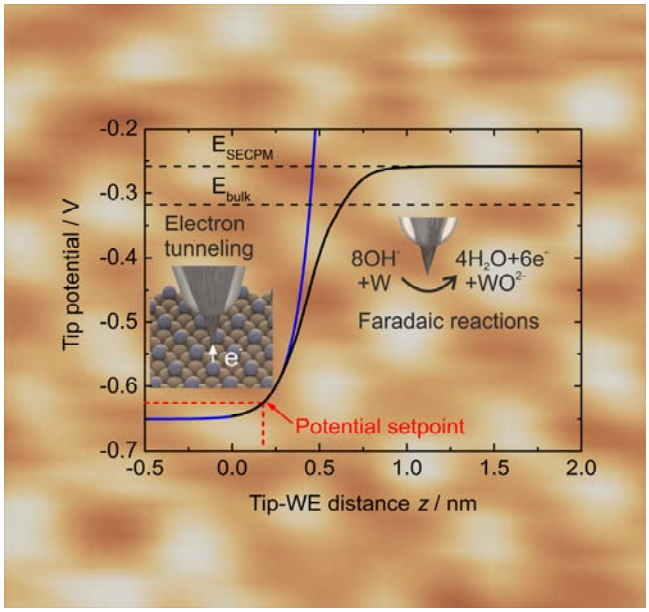

At a probe position far away from the electrode surface, leakage currents are transported via faradaic reactions with the electrolyte. At close tip-surface distances corresponding to potential set-points typical for SECPM surface scans, the potential detected with the tip can be explained by tunneling currents. Thus, the SECPM imaging principle is similar to that of an EC-STM with feedback signal set to potential instead of current and unfortunately cannot deliver information on the EDL potential.

[1] H.A. Gasteiger, S.S. Kocha, B. Sompalli, F.T. Wagner, Appl. Catal. B Environ. 56, 9 (2005).
[2] C.H. Kjaergaard, J. Rossmeisl, J.K. Nørskov, Inorg. Chem. 49, 3567 (2010).
[3] C. Baier, U. Stimming, Angew. Chemie - Int. Ed., 48, 5542 (2009).
[4] C. Hurth, C. Li, A. J. Bard, J. Phys. Chem. C 111, 4620 (2007).
[5] J. Kunze, V. Maurice, L. H. Klein, H.-H. Strehblow, P. Marcus, J. Phys. Chem. B 105, 4263 (2001).
[6] C. Traunsteiner, K. Tu, and J. Kunze-Liebhäuser, ChemElectroChem 2, 77 (2015).

Recent progress in the bottom-up fabrication of graphene nanoribbons: From armchair to zigzag and beyond

Pascal Ruffieux, Shiyong Wang, Bo Yang[1], Jia Liu, Carlos Sanchez, Thomas Dienel, Leopold Talirz, Prashant Shinde, Carlo Pignedoli, Daniele Passerone, Tim Dumslaff[1], Xinliang Feng[1,2], Klaus Müllen[1], Roman Fasel

Empa, Swiss Federal Laboratories for Materials Science and Technology,
8600 Dübendorf, Switzerland
(corresponding author: R. Fasel, e-mail: roman.fasel@empa.ch)

[1] *Max Planck Institute for Polymer Research, Ackermannweg 10, 55124 Mainz, Germany*
[2] *Technical University Dresden, 01062 Dresden, Germany*

Graphene nanoribbons (GNRs) are promising candidates to overcome the low on/off-behaviour of graphene – a zero band gap semiconductor – while still preserving the high charge carrier mobility that is essential for the fabrication of efficient field effect transistors. It has been shown that atomically precise GNRs can be fabricated by an on-surface bottom-up approach [1]. This versatile method has been successfully applied to the fabrication of armchair GNRs (AGNRs) of different widths [1-4] – and consequently different band gaps – as well as more complicated structures like chevron GNRs [1] or heterojunctions [5,6]. However, one of the most interesting types of GNRs has remained elusive: GNRs with zigzag edges (ZGNRs). ZGNRs are predicted to exhibit intriguing electronic properties like the existence of localized edge states with antiferromagnetic ordering across the ribbon width, thus giving rise to spin-polarized edges [7].

Here we will show how the on-surface synthesis approach can be extended to afford the fabrication of a new family of GNRs including atomically precise 6-ZGNRs, edge-modified variants thereof, as well as cove-edged GNRs. Spectroscopic evidence of the zigzag edge state is reported, with a significant energy splitting between occupied and unoccupied states that reflects the strong electron-electron interaction in these one-dimensional materials.

[1] J. Cai et al. Nature 466, 470 (2010).
[2] N. Abdurakhmanova et al. Carbon 77, 1187 (2014).
[3] H. Zhang et al. J. Am. Chem. Soc., 137, 4022 (2015).
[4] Y.-C. Chen et al. ACS Nano 7, 6123 (2013).
[5] Y.-C. Chen et al. Nature Nanotech. 10, 156 (2015).
[6] J. Cai et al. Nat. Nano. 9, 896 (2014).
[7] M. Fujita et al. J. Phys. Soc. Jpn. 65, 1920 (1996)

Fusing tetrapyrroles to graphene edges by surface-assisted covalent coupling

Yuanqin He [1,3], Manuela Garnica [1], Felix Bischoff [1], Jacob Ducke [1], Matthias Batzill [2,3], Willi Auwärter [1] & Johannes V. Barth [1*]

[1] *Physik-Department E20, Technische Universität München, James-Franck-Straße 1, D-85748 Garching, Germany;* [2] *Department of Physics, University of South Florida, Tampa, FL 33620, USA; * e-mail: jvb@tum.de*

Surface-assisted covalent linking of precursor molecules enables the fabrication of low-dimensional nanostructures, including graphene nanoribbons[1–5]. For building functional multicomponent systems the lateral anchoring of organic heteromolecules to graphene is desirable. Here, we demonstrate the dehydrogenative coupling of single porphines to graphene edges on the same metal substrate used for graphene synthesis. The covalent linkages are visualized by scanning probe techniques with sub-molecular resolution, and we directly inspected molecular bond motifs and electronic features. Distinct configurations are identified that can be steered towards entities predominantly fused to graphene edges via two pyrrole rings by thermal annealing. Furthermore we succeeded in concomitant metallation of the macrocycle with substrate atoms and axial ligation of adducts[6]. Combining such processes with graphene nanostructure synthesis has the potential of creating complex materials systems with novel, tunable functionalities.

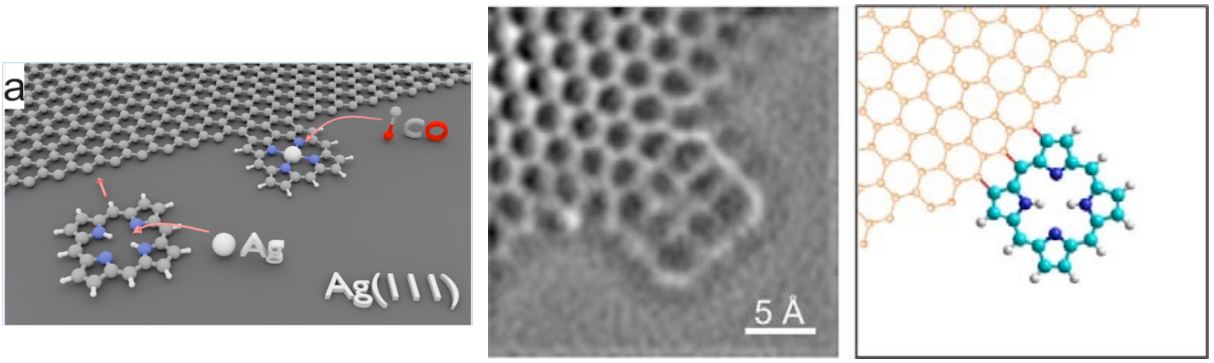

Graphene-anchored tetrapyrrole macrocycles. Left: Scheme illustrating the metallation of fused 2H-P with Ag adatoms to form Ag-P and the reversible ligation of CO to Ag-P. Center & right: AFM data showing covalent bonds of the graphene lattice, the porphine and their interface with schematic model illustrating an exemplary coupling configuration.

1. Cai, J. *et al*. Atomically precise bottom-up fabrication of graphene nanoribbons. *Nature* **466,** 470–473 (2010).
2. Otero, G. *et al*. Fullerenes from aromatic precursors by surface-catalysed cyclodehydrogenation. *Nature* **454,** 865–868 (2008).
3. Méndez, J., López, M. F. & Martín-Gago, J. A. On-surface synthesis of cyclic organic molecules. *Chem. Soc. Rev*. **40,** 4578–4590 (2011).
4. Lafferentz, L. *et al*. Controlling on-surface polymerization by hierarchical and substrate-directed growth. *Nat. Chem*. **4,** 215–220 (2012).
5. Wiengarten, A. *et al*. Surface-assisted dehydrogenative homocoupling of porphine molecules. *J. Am. Chem. Soc*. **136,** 9346–9354 (2014).
6. Auwärter, W., Écija, D., Klappenberger, F. & Barth, J. V. Porphyrins at interfaces. *Nat. Chem*. **7,** 105–120 (2015).

Work supported by European Research Council Advanced Grant MolArt (n° 247299); as well as Munich Centre for Advanced Photonics (MAP) and TUM Institute for Advanced Study funded by the German Research Foundation (DFG) via the German Excellence Initiative & the European Union Seventh Framework Programme under grant agreement n° 291763. W.A. acknowledges funding by the DFG via a Heisenberg professorship and by the European Research Council Consolidator Grant NanoSurfs (n° 615233). MB acknowledges support from the National Science Foundation under award DMR-1204924. MG acknowledges financial support by the Marie Curie Intra-European Fellowship (Project 2D Nano, n° 658070)..

Defects, Strain and Polymorphism in Graphene on Metals

Ka Man Yu, Feifei Wang, M.S. Altman

Department of Physics, Hong Kong University of Science and Technology, Kowloon, Hong Kong
(corresponding author: M.S. Altman, e-mail: phaltman@ust.hk)

The preparation of high quality, microscopic specimens of atomically thin graphene by mechanical exfoliation from graphite opened the door to the discovery of its unique and intriguing electronic, mechanical, chemical and optical properties. One area of active graphene research has focused on the development and optimization of methods to prepare graphene for large-scale integration, as well as on the identification of ways to manipulate graphene's properties. For example, substantial strain-induced effects have been observed that raise prospects for tuning graphene's properties through strain engineering. Renewed interest in chemical vapor deposition (CVD) and bulk segregation on metal surfaces produced advances that underpin current capabilities to fabricate epitaxial graphene over large areas with atomic layer control and transferability to arbitrary substrates. However, structural imperfections, such as point and line defects, are known to be present in epitaxial graphene on metals. These imperfections may undermine the exceptional properties that are vital to graphene-based applications. Alternatively, they may exhibit distinct properties of their own that may be harnessed to tailor graphene's properties or alter its functionality.

We have studied the growth/defect structure of graphene (g) on metals using low energy electron microscopy (LEEM) and micro-low energy electron diffraction (μLEED). In this work, we determine structural information with high spatial resolution based on two-dimensional scanning μLEED measurements. These investigations reveal the proliferation of lattice orientational disorder and small-angle grain boundaries in g/Ru(0001) during conventional ethylene CVD growth at high temperature, due to the random introduction of pentagonal and heptagonal ring defects into the hexagonal carbon lattice [1]. Although orientationally uniform graphene could be produced by a hybrid CVD/segregation method, this layer exhibited significant incommensurability and polymorphism (Fig. 1(a)) [2]. The apparent elasticity of graphene on Ru(0001) is attributed to the coupling of in-plane lateral strain and out-of-plane bending strain in the corrugated graphene lattice. These results contradict an authoritative structure determination of a 25-on-23 periodicity based on surface x-ray diffraction measurements [3]. Therefore, our observations may shed light on controversies over lateral periodicity and corrugation in g/Ru(0001) [3-5]. Interestingly, similar evidence of coupled rotation and lattice strain is also observed in g/Rh(111) in our work.

Two-dimensional strain mapping in g/Ir(111) using scanning μLEED measurements also reveals inhomogeneous strain relaxation by wrinkles, which form during cooling from the high growth temperature due to the differential thermal expansion of graphene and Ir (Fig.

1(b)) [2]. Strain is relaxed only within a distance from wrinkles of about 20% of the mean wrinkle spacing. This suggests that it may be possible to strain-engineer the properties of graphene by a bottom-up approach if wrinkling can be controlled to form desirable strain networks.

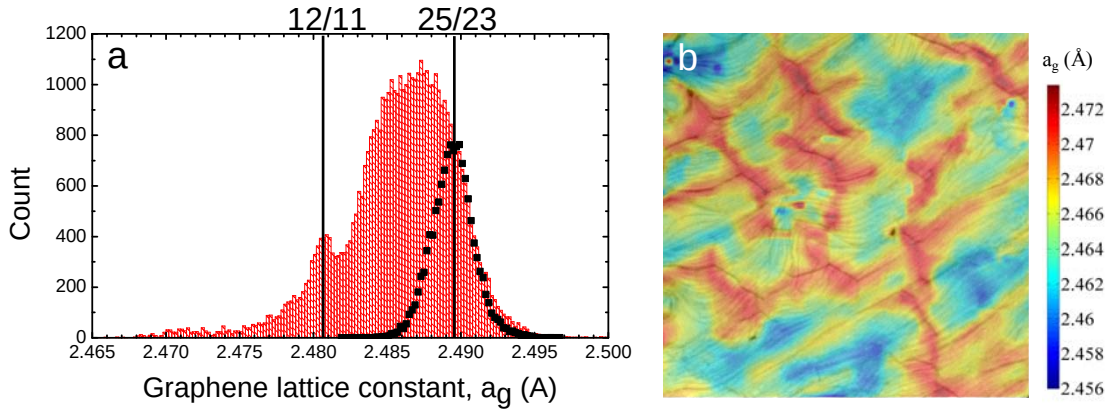

Figure 1. (a) Lattice constant distribution in uniformly oriented graphene (histogram) and orientationally disordered graphene (■) on Ru(0001) determined by scanning μLEED measurements. Lattice constants corresponding to commensurate 25-on-23 (C:Ru) and 12-on-11 periodicities are identified at the top. (b) Scanning μLEED image (6μm) depicts inhomogeneous strain relaxation at wrinkles in g/Ir(111).

Financial support from the Hong Kong Research Grants Council under Grant No. HKUST600113 is gratefully acknowledged.

References

[1] K.L. Man and M.S. Altman, Phys. Rev. B **84**, 235415 (2011).

[2] K.M Yu, F. Wang, M.S. Altman (2016).

[2] D. Martoccia, et al., Phys. Rev. Lett. **101**, 126102 (2008).

[3] Y. Pan, H. Zhang, D. Shi, J. Sun, S. Du, F. Liu, and H. J. Gao, Adv. Mater. **21**, 2777 (2009).

[4] A. L. Vázquez de Parga, at al., Phys. Rev. Lett. **100**, 056807 (2008).

Tailoring the Mechanics of Carbon Nanomembranes for Molecular Separation

A. Beyer[1], V. Chinaryan[1], X. Zhang[1], C. Neumann[1], S. Shishatskiy[2], J. Wind[2], V. Abetz[2], P. Angelova[3], A. Gölzhäuser[1]

[1] Physics of Supramolecular Systems, Bielefeld University, 33615 Bielefeld, Germany
[2] Inst. for Polymer Research, Helmholtz-Zentrum Geesthacht, 21502 Geesthacht, Germany
[3]CNM Technologies GmbH, Herforder Str. 155a, 33609 Bielefeld, Germany

E-mail: ag@uni-bielefeld.de

Carbon Nanomembranes (CNMs) are extremely thin (0.5 – 3.0 nm), synthetic two-dimensional (2D) layers or sheets with tailored physical, chemical or biological function. With their two opposing surfaces they interface and link different environments by their distinct physical and chemical properties, which depend on their thickness, molecular composition, structure and the environment on either side. Due to their minute nanometer thickness and 2D architecture, they can be regarded as "surfaces without bulk" separating regions with different gaseous, liquid or solid components and controlling any materials exchange between them [1].

The fabrication of CNMs involves the formation of a monolayer of aromatic molecules on a solid surface [2]. This precursor layer is exposed to electrons or UV, which leads to a cross-linking between neighboring molecules. The cross-linked monolayer is released from the surface as a self-supporting CNM with properties that are determined by the precursor molecules [3,4]. Fig. 1 shows Helium Ion Micrographs of CNMs from different aromatic molecules; pyrolysis transforms these CNMs into graphene [3,5]. CNMs can be engineered with a controlled thickness, permeability and elasticity [6].

Here, we demonstrate that CNMs can be utilized as *ballistic membranes* for the separation of gas molecules (Fig. 2) [7]. In particular it is shown that CNMs made from of cross-linked 4'-nitro-1,1'-biphenyl-4-thiol show a high selectivity for the permeation of carbon dioxide molecules (Fig. 3). We also report on bulge-test experiments that elucidate a correlation between the flexibility of the precursor molecules and the macroscopic mechanical stiffness of CNMs. CNMs made from rigid and condensed precursors like naphthalene and pyrene thiols exhibit higher Young's moduli (15-20 GPa), than CNMs from less condensed oligophenyls (~10 GPa). In CNMs of less densely packed monolayers, the presence of defects and nanopores plays an important role in determining their mechanical properties.

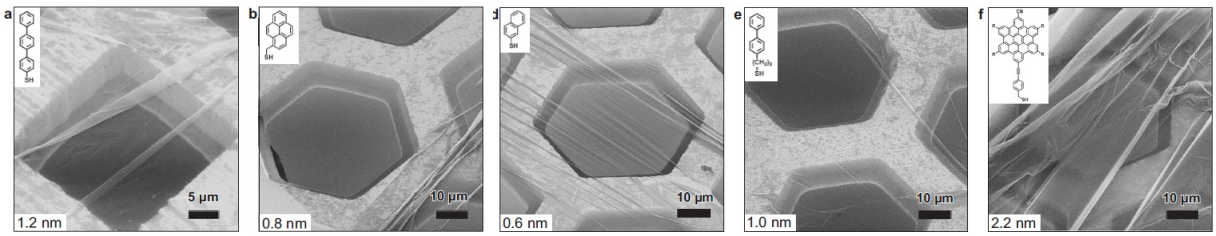

Fig. 1: Helium Ion Micrographs of free-standing carbon nanomembranes from different aromatic molecules. The CNMs are suspended over quadratic (a) and hexagonal (b-f) openings in thin metal grids. The parenting precursor molecule is shown in the upper left insert, the CNM thickness is shown in the lower left insert (from ref. 3).

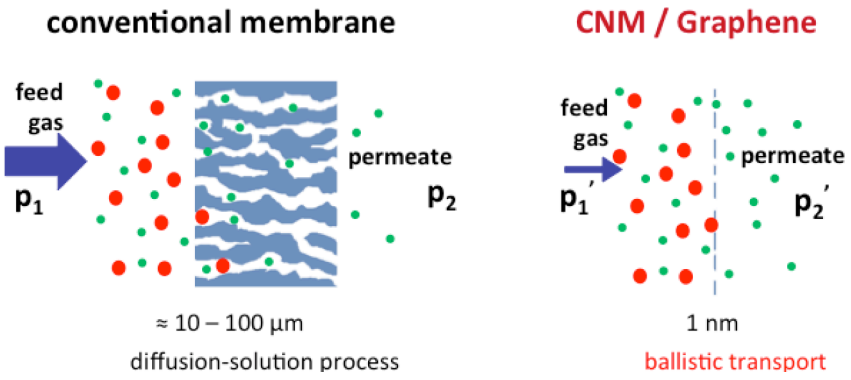

Fig. 2: Schematics of gar permeation through conventional (left) and ultrathin membranes (right). To transport molecules through a thick membrane, a pressure difference is required. When the membrane thickness lies in the range of the molecular size, an energy efficient ballistic transport with a low-pressure difference becomes possible.

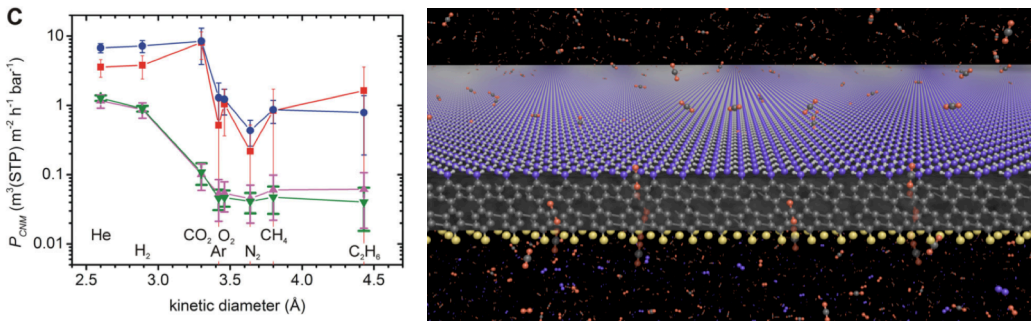

Fig. 3: Permeation of different molecules through ultrathin CNMs (left), schematics of CO_2 permeation through an ultrathin CNM CNMs made from of cross-linked 4'-nitro-1,1'-biphenyl-4-thiol (from ref. 7).

References

[1] D. Anselmetti, A. Gölzhäuser: *Converting Molecular Monolayers into Functional Membranes,* Ang. Chem. Int. Ed., **53**, 12300 (2014).

[2] A. Turchanin, A. Gölzhäuser*: Carbon Nanomembranes from Self-Assembled Monolayers: Functional surfaces without bulk*, Progress in Surface Science, **87**, 108 (2012).

[3] P. Angelova, H. Vieker, N. Weber, D. Matei, O. Reimer, I. Meier, S. Kurasch, J. Biskupek, D. Lorbach, K. Wunderlich, L. Chen, A. Terfort, M. Klapper, K. Müllen, U. Kaiser, A. Gölzhäuser, A. Turchanin: *A Universal Scheme to Convert Aromatic Molecular Monolayers into Functional Carbon Nanomembranes*, ACS Nano **7**, 6489 (2013)

[4] Z. Zheng, C. T. Nottbohm, A. Turchanin, H. Muzik, A. Beyer, M. Heilemann, M. Sauer, A. Gölzhäuser: *Janus nanomembranes: A generic platform for chemistry in two dimensions*, Angew. Chem. Int. Ed. 49, 8493 (2010).

[5] A. Turchanin, D. Weber, M. Büenfeld, C. Kisielowski, M. Fistul, K. Efetov, T. Weimann, R. Stosch, J. Mayer and A. Gölzhäuser: *Conversion of Self-Assembled Monolayers into Nanocrystalline Graphene: Structure and Electric Transport*, ACS Nano, **5**, 3896 (2011).

[6] X. Zhang, C. Neumann, P. Angelova, A. Beyer, and A. Gölzhäuser: *Tailoring the Mechanics of Ultrathin Carbon Nanomembranes by Molecular Design,* Langmuir **30**, 8221 (2014).

[7] M. Ai, S. Shishatskiy, J. Wind, X. Zhang, C.T. Nottbohm, N. Mellech, A. Winter, H. Vieker, J. Qui, K.J. Dietz, A. Gölzhäuser, A. Beyer: *Carbon Nanomembranes (CNMs) supported by polymer: mechanics and gas permeation*, Adv. Mater. **26**, 3421 (2014).

Extreme doping levels and many-body interaction in epitaxial graphene on SiC(0001): Can we access superconductivity and plasmonic?

U. Starke, S. Link, S. Forti, H.M. Benia, A. Stöhr, M. Konuma, Y. Niu[1], A.A. Zakharov[1]

Max-Planck-Institut für Festkörperforschung, Heisenbergstr. 1, D-70569 Stuttgart, Germany
(corresponding author: U.Starke, e-mail: u.starke@fkf.mpg.de)

[1]*MAXLab, Lund University, S-22100 Lund, Sweden*

Wafer scale graphene can be grown on SiC single crystals. The resulting epitaxial graphene is regarded as a suitable candidate for carbon based electronics [1,2]. Although the presence of the SiC substrate has a strong influence on the electronic and structural properties of the graphene layers, these properties can be manipulated by functionalizing the graphene/SiC interface on an atomic scale. Intercalation under the first carbon honeycomb layer can relieve the strong covalent bonds of its atoms to the SiC(0001) substrate [3,4] and manipulate the π-band structure in a large range of aspects. We have shown in recent years that this carbon layer can be turned into quasi-free standing monolayer graphene and that designed doping levels are accessible [5-10]. Indeed, the process of intercalation drastically affects the electronic properties of the graphene layer by the interaction with the underlying substrate, and the effects can be selected by the choice of element. Here, we will show how extreme doping levels and drastic renormalization magnitudes give access to novel graphene properties that may promise applications such as plasmonics and superconductivity.

The resulting atomic and electronic properties as well as the dynamics of the corresponding intercalation and desorption processes are characterized using various surface science techniques. The atomic structure and chemical bond configuration are studied using low-energy electron diffraction (LEED) and X-ray photoelectron spectroscopy (XPS), respectively. The electronic structure is analyzed using angle-resolved photoemission spectroscopy (ARPES). The spatial formation of the graphene layers and areas of different doping is studied *in situ* by low energy electron microscopy (LEEM), μ-LEED, photoelectron microscopy (PEEM) and μ-XPS. In addition, the electronic structure can be resolved on the nanoscale using μ-ARPES in the LEEM and a nano-ARPES beamline.

We have found previously, that gold intercalation can yield two phases of different carrier type in the graphene [11]. With the improved preparation quality of our furnace grown graphene layers, we retrieve a highly ordered graphene/intercalant/substrate system with hybridization of the graphene and the Au electronic bands. Periodic replicas of the π-bands are clearly resolved. In high resolution ARPES experiments at synchrotron facilities, we show

that a severe renormalization of the graphene bands takes place. We observe a strong electron-plasmaron interaction which can be used to estimate the tunability of graphene's dielectric constant due to the intercalation [12].

By intercalation of lanthanide elements, in this case Gadolinium, extremely high doping levels can be reached. As a result, the Van-Hove singularity in the π-band structure at the M-point of pristine graphene is shifted towards the Fermi level that spectral weight is measured in ARPES along the KMK-line [13]. Thus, the intercalation's influence on the electronic structure of the graphene can be viewed as a topological transition from a situation with 2 hole pockets to one electron pocket. The doping is accompanied by a strong bending of the bands in the vicinity of the Fermi energy, possibly by hybridization with the Gd orbitals and the occurance of band replicas due to strong electron-phonon coupling. We speculate that the high density of states at the Fermi level is a situation potentially allowing to reach superconductivity in graphene.

This work was supported by the Deutsche Forschungsgemeinschaft within the framework of the Priority Programme 1459 Graphene (Sta315/8-1,2). This research was partially funded by the European Community's Seventh Framework Programme: Research Infrastructures (FP7/2007-2013) under grant agreement no 226716. We are indebted to the staff at MAX-Lab (Lund, Sweden), BESSY II (Berlin, Germany) and SOLEIL (Gif-sur-Yvette, France) for their advice and support.

[1] C. Berger et al., J.Phys. Chem. B **108**, 19912 (2004).
[2] K.V. Emtsev, et al., Nature Materials **8**, 203-207 (2009).
[3] K.V. Emtsev, F. Speck, Th. Seyller, L. Ley, and J.D. Riley, Phys. Rev. B **77**, 155303 (2008).
[4] C. Riedl, C. Coletti, and U. Starke, J. Phys. D **43**, 374009 (2010).
[5] C. Riedl, C. Coletti, T. Iwasaki, A.A. Zakharov, and U. Starke, Phys. Rev. Lett. **103**, 246804 (2009).
[6] S. Forti, et al., Phys. Rev. B **84**, 125449 (2011).
[7] K.V. Emtsev, A.A. Zakharov, C. Coletti, S. Forti, and U. Starke, Phys. Rev. B **84**, 125423 (2011).
[8] J. Baringhaus, et al., Appl. Phys. Lett., **104**, 261602 (2014).
[9] J. Baringhaus, A. Stöhr, S. Forti, U. Starke, and C. Tegenkamp, Sci. Rep. **5**, 9955 (2015).
[10] C. Coletti, et al., Appl. Phys. Lett. **99**, 081904 (2011).
[11] I. Gierz et al., Phys. Rev. B **81**, 235408 (2010).
[12] S. Link, S. Forti, H.M. Benia, A. Stöhr, M. Konuma, A.A. Zakharov and U. Starke, to be published.
[13] S. Forti, S. Link, A. Stöhr, Y. Niu, A.A. Zakharov and U. Starke, to be published.

Generation of Stainless Steel Nanoparticles with Carefully Tuned Composition

C. Preger, L. Ludvigsson, B. O. Meuller and M. E. Messing

Solid State Physics, Lund University, Box 118, 221 00 Lund, Sweden
(corresponding author: M. E. Messing, e-mail: maria.messing@ftf.lth.se)

The number of nanoparticle-based products on the market is expected to increase considerably during the coming decades. This forces industry to have highly meticulous manufacturing of large amounts of nanoparticles using cheap and environmentally friendly methods. In the case of metal oxide particle generation methods that meet these demands are relatively well established. However, for pure metal particles no recognized method is used today but physical production via spark discharge is considered highly promising [1, 2].

Nanoparticle generation by spark discharge where the formation of a plasma channel between two conducting electrodes leads to a spark discharge that evaporate material [3] is reasonably energy efficient. Other advantages with this method includes a continuous generation process, high cleanliness of the nanoparticles, avoidance of chemical precursors and the possibility to easily manufacture alloy and mixed metal particles including particles of materials that are immiscible in bulk form [4].

A complex alloy produced on industrial scale in the form of micro powders is stainless steel. Its interesting magnetic properties, corrosion resistance and strength make stainless steel highly useful for a variety of applications including production of metallic gears. An important part in such production is sintering of the powders. Due to higher surface energies nanoparticles can be sintered at lower temperatures than micron sized particles and hence the addition of nanoparticles to micron sized powders carry the potential to reduce energy consumption and cost during sintering. In the present work we present the first successful generation of stainless steel nanoparticles produced by aerosol methods.

The spark discharge generator consists of a chamber housing two opposing electrodes that are separated by a small gap. Nanoparticles are formed when material ablated from the electrodes via the spark, are transported away from the heated gap region by means of a carrier gas. To create a spark discharge between the electrodes a self-pulsed circuit is used, consisting of a capacitor bank driven by a high voltage DC power supply connected in parallel to the electrode gap. Several parameters can be adjusted to affect and control the particle production including the capacitance, the discharge frequency (by the out-put current), the electrode distance, the electrode material, the carrier gas flow rate, the type of carrier gas and the geometry of the spark discharge generator.

To generate stainless steel particles pre-alloyed electrodes with different chromium content was used. We will report on the influence on different generation parameters on particle production focusing on the clear effect of carrier gas type. We will show that the chromium content in the particles can be tuned and report the results of our careful studies of the nanoparticle surface layer.

This work was performed within NanoLund at Lund University. The research leading to these results received funding from the Swedish Research Council and the European Union Seventh Framework Programme (FP7/2007–2013) under Grant Agreement n° 280765 (BUONAPART-E). This publication reflects only the author's/ authors' view(s), and the community is not liable for any use made of the information contained therein.

[1] www.buonapart-e.eu

[2] L. Ludvigsson, B. O. Meuller and M. E. Messing, J. Phys. D: Appl. Phys. 48, 314012 (2015)

[3] S. Schwyn, E. Garwin and A. Schmidt-Ott, J. Aerosol Sci. 19, 639 (1988)

[4] N. S. Tabrizi, Q. Xu, N. M. van der Pers and A. Schmidt-Ott, J. Nanopart. Res. 12, 247 (2010)

Composition and local atomic arrangement of decagonal Al-Co-Ni and Al-Co-Cu quasicrystal surfaces

J. Yuhara[1], K. Horiba[1], R. Zenkyu[1], M. Sato[1], M. Schmid[2], P. Varga[2]

[1]*School of Engineering, Nagoya University, Nagoya, Japan.*

[2]*Institut für Angewandte Physik, Technische Universität Wien, Vienna, Austria.*

(corresponding author: J. Yuhara, e-mail: j-yuhara@nagoya-u.jp)

The surface structures of decagonal quasicrystals have been studied by scanning tunneling microscopy (STM), showing several types of clusters with fivefold symmetry. However, a structural model has not been determined because of the difficulty to determine the surface composition quantitatively. So far, the surface composition of the Co-rich d-Al-Co-Ni quasicrystal has been investigated by Auger electron spectroscopy (AES) and low energy ion scattering (LEIS), indicating that Al atoms segregate to the surface on annealing [1], but others have suggested a bulk terminated structure without any surface reconstruction [2]. In the present study, we examine the surface composition of decagonal Al-Co-Ni and Al-Co-Cu surfaces by AES and LEIS and propose the surface structure for characteristic local clusters observed in STM images [1,3-5].

The three types of the characteristic clusters for the d-Al-Co-Ni surface are observed in the STM images, as shown in Fig.1. The clusters marked in yellow and red circles are frequently observed while the clusters marked in green circle are rarely observed. From the estimated surface composition by LEIS and AES, the two types of the characteristic clusters are determined by comparison of the STM image and the simulated image of the structure optimized models obtained by DFT (Fig.2), performed on several compositional models which are based on the W-(AlCoNi) bulk model [6]. The topmost layer is composed of Al atoms, and the compositional ratio for 2 and 4 atomic layers of the surface is consistent with the LEIS and AES results. Similarly, the characteristic clusters for the d-Al-Co-Cu surface are determined. The characteristic clusters for these two surfaces are discussed.

References:

[1] J. Yuhara *et al.*, Phys. Rev. B **70** (2004) 024203.

[2] N. Ferralis *et al.*, Phys. Rev. B **69** (2004) 153404.

[3] R. Zenkyu *et al.*, Phil. Mag. **91** (2011) 2854.

[4] R. Zenkyu *et al.*, Phys. Rev. B **86** (2012) 115422.

[5] J. Yuhara *et al.*, Phil. Mag. **91** (2011) 2846.

[6] M. Mihalkovič and M. Widom, alloy database at http://alloy.phys.cmu.edu/

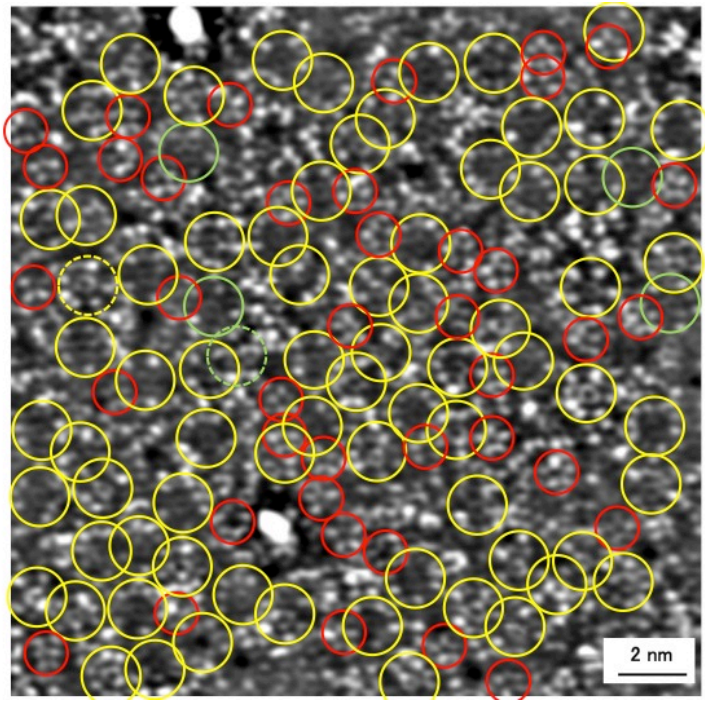

Fig.1 Experimental STM image of the d-Al-Co-Ni surface. Three types of local clusters are shown in yellow, red, and green circles.

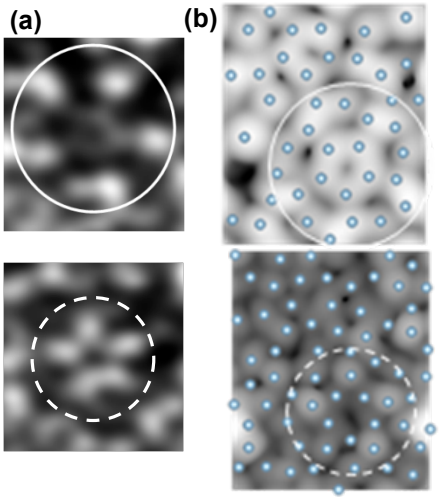

Fig.2 (a) Experimental STM image of the d-Al-Co-Ni surface. (b) Simulated STM image with the atomic arrangement of the topmost layer of Al atoms shown as overlay.

Topologically-ordered states on the surface of 3D Dirac materials

Alexander P. Protogenov[1,2] and Evgueni V. Chulkov[3,4,5,6,7]

[1] *Institute of Applied Physics of the RAS, Nizhny Novgorod 603950, Russia; alprot@appl.sci-nnov.ru*
[2] *Donostia International Physics Center (DIPC), 20018 San Sebastián/Donostia, Spain*
[3] *Departamento de Física de Materiales, Facultad de Ciencias Químicas, Uviversidad del País Vasco, Apartado 1072, 20080 San Sebastián/Donostia, Spain*
[4] *Donostia International Physics Center (DIPC), 20018 San Sebastián/Donostia, Spain*
[5] *Centro de Física de Materiales CFM-Materials Physics Center MPC, Centro Mixto CSIC-UPV/EHU, 20018 San Sebastián/Donostia, Spain*
[6] *Saint Petersburg State University, St. Petersburg, 198504, Russia*
[7] *Tomsk State University, Tomsk, 634050, Russia*

It is well known that a hallmark of two- or three-dimensional topological insulators is the existence of stable edge or surface electron modes. These Fermi excitations are characterized by the linear Dirac dispersion and helical distribution of spins locked to momentum. The time reversal symmetry of topological insulators results in suppression of backscattering in materials with a moderate structural disorder. Topological insulators can be considered as an example of symmetry-protected topological phases. It should be noted that symmetry-protected phases are gapped phases in matter possessing certain global symmetry. If this symmetry is broken, the ground state of the system can be continuously transformed to a trivial gapped phase. This implies that the time-reversal invariant protected phase of a topological insulator has no intrinsic topological order, i.e., no ground state degeneracy and no braiding statistics of topological quasi-particles. Such a topological order with a nontrivial value of the $\mathbb{Z}_2$ topological invariant belongs to the so-called short-range entangled states [1]. A feature of the long-range entangled topological order in $(2+1)D$ systems is that the total many-particle quantum state cannot be transformed to direct product states via local unitary transformations. As a result, the quantum state of a subsystem "knows" about the existence of quantum states of all other subsystems. In this case, the surface phase has a degenerate ground state and anyon excitations with fractional quantum numbers and nontrivial statistics [2].

We did not consider the relationship between surface anyon modes and bulk electron states. Taking into account strong interaction between electrons, the key question is as follows: is there any relation between anyon excitation on the surface and bulk electron states in $(3+1)D$ systems, which is similar to the bulk-boundary correspondence in topological insulators for free electrons? What constraint is imposed on quantum numbers of surface and bulk excitations and on surface phase states by the existence of such correspondence in systems of interacting electrons with long-range entangled surface topological order? A partial answer to these questions in different models [3] and different approaches [4] has been recently obtained. In particular, it has been found in Refs. [5, 6] that all those nontrivial surface states with their global symmetry properties cannot be implemented in strictly two-dimensional systems without reference to the bulk topological order. It is shown in Refs. [7–11] that excitations on the surface of topological insulators can be gapped under strong interaction while preserving all significant symmetries. The condition for implementing this surface phase is the introduction of the intrinsic long-range entangled topological order on the surface. We briefly review recent developments in physics of strongly interacting surface electron states in topologically-ordered three-dimensional systems. We also discuss the possibility of physical implementation and manifestation of the new surface topological order.

We acknowledge the support by the Basque Departamento de Educacion, UPV/EHU (Grant No. IT-756-13), Spanish Ministerio de Economia y Competitividad (MINECO Grant No. FIS2013-48286-C2-2-P), and Tomsk State University Academic D.I. Mendeleev Fund Program in 2015 (ResearchGrant No. 8.1.05.2015). Partial support by the Saint Petersburg State University Project No. 11.50.202.2015 is also acknowledged. This work was also supported in part by the Russian Foundation for Basic Research (Grant No. 14-02-00174).

[1] X.-G. Wen, "Symmetry-protected topological invariants of symmetry-protected topological phases of interacting bosons and fermions", Phys. Rev. B **89**, 035147 (2014); arXiv:1301.7675.
[2] C. Nayak, S.H. Simon, A. Stern, M. Freedman, and S. Das Sarma, "Non-Abelian Anyons and Topological Quantum Computation", Rev. Mod. Phys. **80**, 1083 (2008).
[3] A.P. Protogenov, E.V. Chulkov, and J.C.Y. Teo, "Topological phase states of the $SU(3)$ QCD", J. Phys. Conf. Ser. **482**, 012035 (2014).
[4] C.-K. Chiu, J.C.Y. Teo, A.P. Schnyder, and S. Ryu, "Classification of topological quantum matter with symmetries", arXiv:1505.03535.

[5] M.A. Metlitski and Ashvin Vishwanath, "Particle-vortex duality of $2D$ Dirac fermion from electric-magnetic duality of $3D$ topological insulators", arXiv: 1505.05142.
[6] C. Wang and T. Senthil, "Dual Dirac liquid on the surface of the electron topological insulator", arXiv: 1505.05141.
[7] C. Wang, A.C. Potter, and T. Senthil, "Gapped symmetry preserving surface state for the electron topological insulator", Phys. Rev. B **88**, 115137 (2013).
[8] M.A. Metlitski, C.L. Kane, and M.P.A. Fisher, "A symmetry-respecting topologically-ordered surface phase of 3d electron topological insulators", Phys. Rev. B **92**, 125111 (2015).
[9] X. Chen, L. Fidkowski, and A. Vishwanath, "Symmetry enforced non-Abelian topological order at the surface of a topological insulators", Phys. Rev. B **89**, 165132 (2014).
[10] P. Bondersson, C. Nayak, and X.-L. Qi, "A time-reversal invariant topological phase at the surface of a 3D topological insulator", J. Stat. Mech. (2013) P09016; arXiv: 1306.3230.
[11] D.F. Mross, A. Essin, and J. Alicea, "Composite Dirac Liquids: Parent States for Symmetric Surface Topological Order", Phys. Rev. X **5**, 011011 (2015).

Electronic and spin structure of Sn-based ternary topological insulators

M.G. Vergniory[1], T.V. Menshchikova[2], I.V. Silkin[2], S.V. Eremeev[2,3], and E.V. Chulkov[1,2,4],

Departamento de Fisica de Materiales, Facultad de Ciencias Quimicas, UPV/EHU and Centro de Fisica de Materiales, Centro Mixto CSIC-UPV/EHU, Apartado 1072, 20080 San Sebastian/Donostia, Basque Country, Spain
(corresponding author: E.V. Chulkov, e-mail: evguenivladimirovich.tchoulkov@ehu.eus)

[1] *Donostia International Physics Center, P. Manuel de Lardizabal 4, San Sebastian, 20018 Basque Country, Spain*

[2] *Tomsk State University, pr. Lenina 36, 634050 Tomsk, Russian Federation*

[3] *Institute of Strength Physics and Materials Science, Siberian Branch, Russian Academy of Sciences, Akademicheskii pr. 2/4, Tomsk, 634021 Russian Federation*

[4] *St. Petersburg State University, 198504 St. Petersburg, Russian Federation*

Various families of 3D TIs that hold spin-polarized surface states (SSs) have been recently studied, such as the binary Bi2Te3, Bi2Se3, and Sb2Te3 [1-3]. These compounds are strong TIs with the topological SS (TSS) mostly located in the first atomic layers adjacent to the vacuum side. However, as was shown by first-principles calculations, the strong spin-orbit entanglement in these materials reduces the spin polarization of the surface states [4]. For instance, Bi2Se3 possessing a rather wide bulk energy gap supporting the Dirac state was predicted to have only 50% of spin polarization in the TSS, which turned in good agreement with recent experiment [4].

Here we present and discuss ab initio calculation results for the electronic and spin structure of two compounds SnSb4Te7 and SnBi6 Te10, which are strong three-dimensional TIs. They belong to a wider family of TIs, SnX2Te4 or SnX4Te7 (X = Sb and Bi) [6]. We demonstrate that SnSb4 Te7 and SnBi6 Te10 present ordered stable phases and a band gap around 100 meV. We also show that the electronic structure of these compounds can be tuned by considering different cleaved surfaces, and in particular some of the surface terminations can reach a spin polarization of almost 80%.

[1] M. Z. Hasan and C. L. Kane, Rev. Mod. Phys. 82, 3045 (2010)

[2] S. V. Eremeev, Yu. M. Koroteev and E. V. Chulkov, JETP Lett. 91, 387 (2010)

[3] S. V. Eremeev, G. Landolt, T. V. Menshchikova, B. Slomski, Y. M. Koroteev, Z. S. Aliev, M. B. Babanly, J. Henk, A. Ernst, L. Pattheya, A. Eich, A. A. Khajetoorians, J. Hagemeister, O. Pietzsch, J. Wiebe, R. Wiesendanger, P. M. Echenique, S. S. Tsirkin, I. R. Amiraslanov, J. H. Dil, and E. V. Chulkov, Nat. Commun. 3, 635 (2012).

[4] O. V. Yazyev, J. E. Moore, and S. G. Louie, Phys. Rev. Lett. 105, 266806 (2010)

[5] J. S´anchez-Barriga, A. Varykhalov, J. Braun, S.-Y. Xu, N. Alidoust, O. Kornilov, J. Min´ar, K. Hummer, G. Springholz, G. Bauer, R. Schumann, L. V. Yashina, H. Ebert, M. Z. Hasan, and O. Rader, Phys. Rev. X 4, 011046 (2014)

[6] L. E. Shelimova, O. G. Karpinskii, M. A. Kretova, I. V. Kosyakov,V.A. Shestakov,V. S. Zemskov, and F. A. Kuznetsov, Inorgan. Mater. 36, 768 (2000).

Friday

Local investigation of laser induced damage below the melting threshold

Ch. Zaum[1], K. Morgenstern[2]

[1]*Leibniz Universität Hannover, Institut für Festkörperphysik, Abteilung für atomare und molekulare Strukturen (ATMOS), Appelstr. 2, D-30167 Hannover, Germany*

[2]*Ruhr-Universität Bochum, Lehrstuhl für physikalische Chemie I, D-44780 Bochum, Germany*

Because of the ultra-high peak power and ultrashort duration time, femtosecond laser were used extensively to study ultrafast melting of different materials in an attempt to unravel the microscopic mechanisms of homogeneous and heterogeneous melting [1]. Despite of the large effort, the microscopic mechanism of melting are still debated [2].

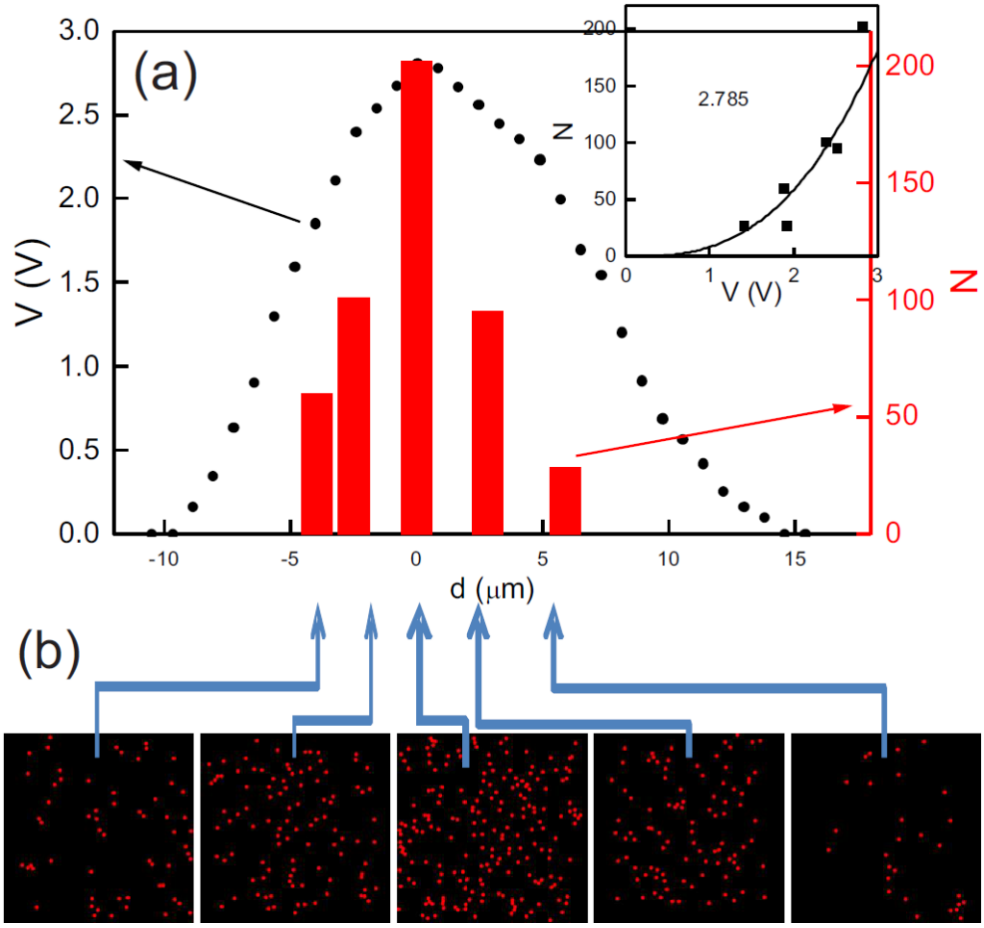

Figure 1: Spatial dependence of defect creation: (a) Dependence of the number of laser-induced defects N (right axis) and photo electron signal V (left axis) on position within the focus d; fluence of 30.3 J/m^2 and absorbed fluence of 6.9 J/m^2; inset: N vs. V with fit yielding an exponent of 2.79 (b) difference of defects as extracted from STM images before and after illumination at the indicated position within the focus.

At much lower fluence than used in laser ablation, short pulse laser were used to induce reactions, called femtochemistry, to resolve molecule dynamics at surfaces [3]. Above a threshold, the non-adiabicity of a reaction is deduced from a non-linear fluence dependence of the molecule's dynamics, often desorption. These non-linear dependencies are observed above fluences of a few ten J/m^2, i.e. a few mJ/cm^2. They show surprisingly diverse exponents ranging from 2 to 15 (c.f. [3]), which are theoretically not understood.

We illuminated Ag(100) sample by femtosecond laser light. Ag was chosen for these experiments, due to its weak electron-phonon coupling and strong electron thermal conductivity, which will show more evident traces of melting in comparison to transition metals, which strong electron-phonon coupling and weak electron thermal conductivity. The commercial laser (REGA 9050 from Coherent) provides 50 fs laser pulses at 800 nm with a repetition rate of 250 kHz. In this experiment, we use the frequency doubled wave length of 400 nm, which has a pulse length of (72 ± 2) fs. After laser illumination we investigated the induced adatoms and vacancies locally by low temperature scanning tunneling microscopy at 5 K. The images reveal that the laser induces defects in the surface above an adsorbed fluence of a few ten J/m^2. The dependence on laser pulse length confirms an electron induced origin of the surface defect creation. The short-pulse illumination leads to the creation of adatoms starting at an adsorbed fluence of ≈ 2.7 J/m^2 and of vacancies starting at ≈ 4.5 J/m^2. The spatial dependence of the number of defects depends non-linearly on the local fluence (Fig 1a). Our results suggest that non-adiabatic dynamics might involve a considerable change in surface structure. The principle aim of the work is to precisely characterize how an ultra-short pulse modifies the surface below the threshold of laser ablation.

Support by the German Research Foundation through grant MO960/ 19-1.

[1] C.V. Shank, R. Yen, C. Hirlimann, Phys. Rev. Lett. 50, 454 (1983); A. Assion, T. Baumert, M. Bergt, T. Brixner, B. Kiefer, V. Sefried, M. Strehle, G. Gerber, Science 282, 010 (1998); C.W. Siders, A. Cavalleri, K. Sokolowski-Tinten, Cs. Toth, T. Guo, M. Kammler, H. Horn von Hoegen, K.R: Wilson, D. von der Linde, C.P.J. Barty, Science 286, 1340 (1999); C. Guo, G. Rodriguez, A. Lobad, A.J. Taylor, Phys. Rev. Lett. 84,4493 (2000); A. Rousse, C. Rischel, S. Fourmaux, I. Uschmann, S. Sebban, G. Grillon, Ph. Balcou, E. Forster, J.P. Geindre, P. Audebert, J.C. Gauthier, D. Hulin, Nature (London) 410, 65 (2001); K. Sokolowski-Tinten, C. Blome, C. Dietrich, A. Tarasevitch, M. horn von Hoegen, D. von der Linde, A. Cavalleri, J. Squier, M. Kammler, Phys. Rev. Lett. 87, 225701 (2001); F. Vidal, T.W. Johnston, S. Laville, O. Barthelemy, M. Chaker, B. Le Dorgoff, J. Margot, M. Sabsabi, Phys. Rev. Lett. 86, 2573 (2001); R. Stoian, A. Rosenfeld, D. Shkenasi, I.V. Hertel, N.M. Bulgakova, E.E.B. Campbell, Phys. Rev. Lett. 88 (2002) 097603; Y. Shimotsuma, P. Kazansky, J. Qiu, K. Hirao, Phys. Rev. Lett. 91, 247405 (2003); B.J. Siwick, J.R. Dwyer, R.E. Jordan, R.J. Dwayne Miller, Science 302, 1382 (2003); K.J. Gaffney et al., , Phys. Rev. Lett. 95, 125701 (2005); C.D. Stasnciu, F. Hansteen, A.V. Kimel, A. Kirilyuk, A. Tsukamoto, A. Itoh, Th. Rasing, Phys. Rev. Lett. 99, 047601 (2007); M. Harb, R. Ernstorfer, C.T. Hebeisen, G. Sciani, W. Peng, T. Dartigalongue, M.A. Eriksson; M.G. Lagally, S.G. Kruglik, R.J. Dwayne Miller, Phys. Rev. Lett. 100, 155504 (2008).

[2] K. Lu, Y. Li, Phys. Rev. Lett. 80, 4474 (1998); Z.H. Jin, P. Gambsch, K. Lu, E. Ma, Phys. Rev. Lett. 87, 055703 (2001); R.W. Cahn, Nature (London) 413, 582 (2001); D.S. Ivanov, L.V. Zhigilei, Phys. Rev. B 68, 064114 (2003).

[3] C. Frischkorn, M. Wolf, Chem. Rev. 106, 4207 (2006).

In-situ atomic-scale control of the growth of a polar perovskite oxide: $SrTiO_3$(110) homoepitaxy by pulsed laser deposition

Michele Riva,[a] Stefan Gerhold,[a] Bilge Yildiz,[a,b] Michael Schmid,[a] and Ulrike Diebold[a]

[a]*Institute of Applied Physics, TU-Wien, Wiedner Haupstraße 8-10, A-1040 Wien, Austria*
(corresponding author: M. Riva, e-mail: riva@iap.tuwien.ac.at)

[b]*Massachusetts Institute of Technology, 77 Massachusetts Avenue, Cambridge, Massachusetts 02139, United States*

By combining pulsed laser deposition (PLD), high-pressure reflection high energy electron diffraction (RHEED), *in-situ* scanning tunneling microscopy (STM), x-ray photoelectron spectroscopy (XPS), and low-energy electron diffraction (LEED), we investigate the homoepitaxial growth of $SrTiO_3$ on the (110) surface, from the first stages of sub-monolayer growth up to several nanometers-thick films.

The polar instability of the $SrTiO_3$(110) surface is compensated by the formation of a variety of reconstructions, that can be finely tuned by adjusting the Sr and Ti content of the near-surface region [1]. The most stable surface structure, *i.e.*, the $SrTiO_3$(110)-(4 × 1) reconstruction, is part of a homologous series of (n × 1) (n = 4, 5, 6) reconstructions, and consists of a porous network of added TiO_4 tetrahedra [2, 3]. The Ti-richer (2 × 4) reconstruction, that exhibits a different symmetry and morphology, can co-exist with the (4 × 1) structure on the surface, upon appropriate sample preparation.

Islands grown by PLD on either (4 × 1) or (2 × 4) patches show a reconstruction, which is coherent with the one of the surrounding terrace, *i.e.*, the substrate reconstruction segregates to the topmost layer. Analysis of STM images reveals that adspecies diffuse anisotropically on the $SrTiO_3$(110) surface [4], with the preferential direction uniquely determined by the surface structure. The rotation in the high-mobility direction, combined with a reduced interlayer mass transport, result in the preferential accumulation of the deposited material at the 1D interface between (4 × 1) and (2 × 4) regions.

Deviations from the ideal Sr/Ti composition in the PLD flux are found to be detrimental for the morphological and structural quality of thick films: Sr-rich fluxes result in poor structural ordering at the surface of the grown films, while the preferential accumulation of the deposited material at (4 × 1)/(2 × 4) boundaries results in the development of deep pits with elevated rims for Ti-rich incoming fluxes. Reduction of these off-stoichimetries by optimization of the PLD parameters allows growing atomically-flat films with several nanometers thickness.
The dependence of the surface structure on the near-surface composition, combined with the segregation of off-stoichiometries to the surface [5], allows the determination of the stoichiometry of the incoming flux with exquisite precision: by quantitative STM analysis of the change of the film structure upon growth, we obtain a resolution better than 0.2% in the Sr/Ti stoichiometric ratio.

Support by the Austrian Science Fund FWF (SFB 'Functional Oxide Surfaces and Interfaces FOXSI' Project F45) and by the ERC Advanced Grant 'OxideSurfaces' (Project ERC-2011-ADG_20110209) is kindly acknowledged. SG acknowledges partial support by the FWF Doctoral College Solids4Fun, project number W1243.

References

1. Z. Wang, F. Yang, Z. Zhang, Y. Tang, J. Feng, K. Wu, Q. Guo, and J. Guo, Phys. Rev. B **83** 155453 (2011).
2. J. A. Enterkin, A. K. Subramanian, B. C. Russell, M. R. Castell, K. R. Poeppelmeier, and L. D. Marks, Nature Materials **9**, 245 (2010).
3. F. Li, Z. Wang, S. Meng, Y. Sun, J. Yang, Q. Guo, and J. Guo, Phys. Rev. Lett. **107**, 036103 (2011).
4. S. Gerhold, M. Riva, B. Yildiz, M. Schmid, and U. Diebold, submitted to Surf. Sci.
5. J. Feng, F. Yang, Z. Wang, Y. Yang, L. Gu, J. Zhang, and J. Guo, AIP Advances **2**, 041407 (2012).

The Role of Entropic Forces in the Dynamics of a molecular Rotor

M. Penedo, J. C. Gehrig, M. Parschau, J. Schwenk, M. A. Marioni, E. W. Hudson, and H. J. Hug[1]

EMPA, Swiss Federal Laboratories for Materials Science and Technology, CH-8600 Dübendorf, Switzerland

(corresponding author: M. Penedo, e-mail: marcos.penedo-garcia@empa.ch)

[1] *Department of Physics, University of Basel, CH-4056 Basel, Switzerland*

The tendency of systems with many degrees of freedom to increase their entropy manifests as so called „entropic" forces associated with changes of a system attribute. Particularly in biochemical and biological processes [1], and in heterogeneous catalysis [2] entropic forces play an important role. Studying them at the level of individual molecules would improve our understanding of chemical reaction and transformation kinetics, and this possibility can be addressed with scanning probe microscopy (SPM). To-date the conservative forces of an AFM or STM tip on molecules have been studied in some detail [3,4], but the possibility that it also affects the stochastic forces on molecules has not been addressed.

Here we demonstrate that the proximity of an STM tip to a dibutyl-sulfide (DBS) molecular rotator [5] adsorbed on Au(111) results in both conservative and entropic forces that substantially change its rotation dynamics. The fact has been disregarded to-date and becomes fully apparent when transition rates are measured as a function of relative tip-molecule position. The STM tip alters the energy-barrier to hopping but also the apparent attempt frequency, even though the topography of a stationary molecule is not substantially modified in the process. Apparent attempt frequency and energy barrier compensate (the higher the energy barrier, the higher the attempt frequency), and can be observed as a function of relative tip-molecule position in the hopping rate.

The apparent attempt frequency is a measure of the entropy changes upon moving from ground to transition state. Thus, the tip not only exerts conservative forces on the molecules (Figure b), but gives rise to entropic forces (Figure c) of comparable size that can partially compensate them. The tip geometry could be engineered and the apex functionalized to make explicit use of entropic forces. They will likely constitute a new tool to study catalysis and molecular conformational changes.

Support by the Swiss National Science Foundation, EU FP7 program (MDSPM project) and Empa is hereby gratefully acknowledged.

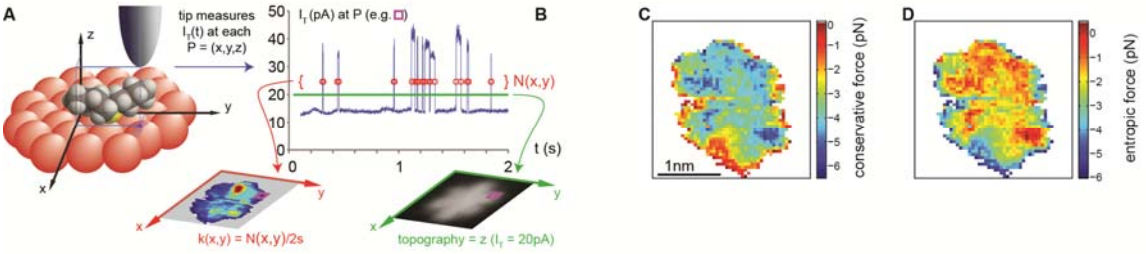

(a) Measurement principle: The DBS molecule adsorbed on the Au(111) surface is scanned at a rate of 602 s/line. z-feedback keeps the average tunnelling current constant at 20 pA, and telegraph noise recorded at a high measurement bandwidth allows measurement of the molecular hopping rate at various temperatures. From these data site-specific energy barriers and attempt rates were obtained. Maps of entropic **(b)** and conservative forces **(c)** were calculated. Locations with a stronger restoring conservative force (high energy barrier) show a correspondingly increased entropic force facilitating a transition of the molecule over the energy barrier (compensation effect).

[1] J H. Dong, R. Lund, and T. Xu, Biomacromolecules 16, 743 (2015)

[2] G. C. Bond, M. A. Keane, H. Kral, and J. A. Lercher, Catalysis Reviews 42, 323 (2000)

[3] Y J. A. Stroscio, F. Tavazza, J. N. Crain, R. J. Celotta, and A. M. Chaka, Science 313, 948 (2006)

[4] M. Ternes, C. P. Lutz, C. F. Hirjibehedin, F. J. Giessibl, and A. J. Heinrich, Science 319, 1066 (2008)

[5] A. E. Baber, H. L. Tierney, and E. C. H. Sykes, ACS Nano 2, 2385 (2008)

Bipolar conductance switching of single anthradithiophene molecules

R. Pétuya[1], B. Borca[2], V. Schendel[2], I. Pentegov[2], T. Michnowicz[2], U. Kraft[2], H. Klauk[2], P. Wahl[2,3], U. Schlickum[2], K. Kern[2,4] and A. Arnau [1,5]

[1] *Donostia International Physics Center, E-20018 Donostia-San Sebastián, Spain (corresponding author: R. Pétuya , e-mail: remipetuya@gmail.com)*

[2] *Max-Planck-Institute for Solid State Research, 70569 Stuttgart, Germany*

[3] *SUPA, School of Physics and Astronomy, University of St Andrews, North Haugh, St Andrews, KY16 9SS, United Kingdom*

[4] *Institut de Physique de la Matière Condensée, École Polytechnique Fédérale de Lausanne (EPFL), CH-1015 Lausanne, Switzerland*

[5] *Departamento de Fisica de Materiales UPV/EHU and Material Physics Center (MPC), Centro Mixto CSIC-UPV/EHU, E-20018 Donostia - San Sebastián, Spain*

Molecular electronics appears to be one of the great challenges in the nanoscience field of investigation [1]. Functional molecules, with ability to switch between two or more stable states, may have a promising future as logical component or for data storage purpose. Scanning Tunneling Microscope (STM) measurements have evidenced bipolar conductance switching process of anthradithiophene (ADT) molecules (pentacene analogue) corresponding to bistable molecular adsorption conformations on Cu(111). First principle calculations using a vdW-DF-cx [2,3] approach are performed to investigate the switching mechanism locally activated by the STM tip apex. In agreement with a recently proposed model [4] of switching between different adsorption conformations of molecules on a metallic surface, we found that the two conductance states correspond to two different adsorption geometries [5]. In the “off” state, obtained upon evaporation, the molecules adsorb at short distance and adopt a bent geometry whereas in the “on” state, the molecule adsorb at larger distance from the surface with a flat geometry. In addition, the competing effects of the sulfur groups and the acene rings position with the substrate atoms in the adsorption geometry is scrutinized for the *cis* and *trans*-ADT isomers.

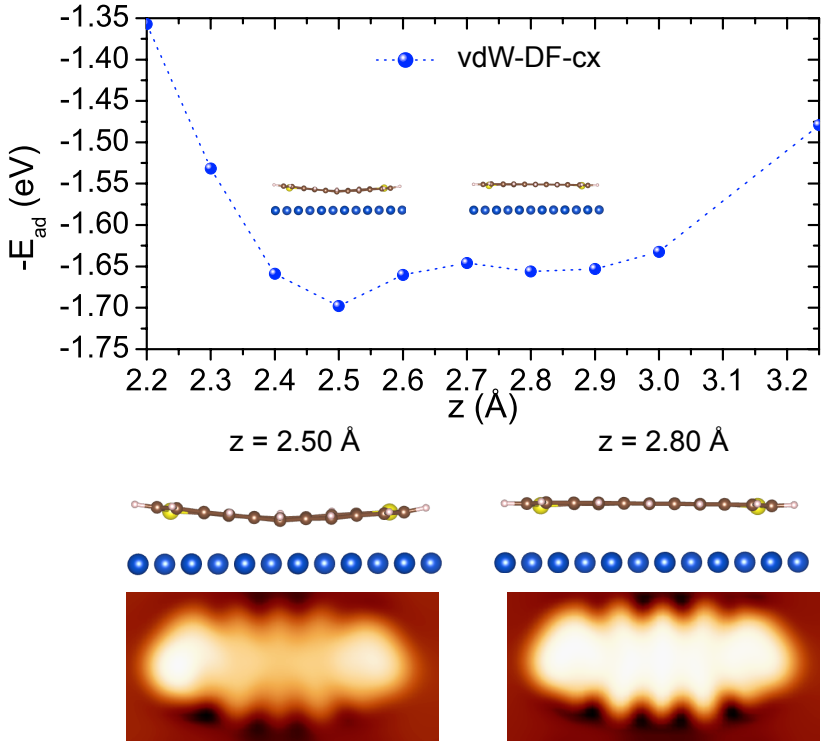

[1] Van der Molen,S. J. et al. *Nature Nanotechnology*, 8, 385-389 (2013)
[2] Berland, K. et al. *Physical Review B*, 89, 035412 (2014)
[3] Björkman, T. *Journal of Chemical Physics*, 141, 074708 (2014)
[4] Liu, W. et al. *Nature Communications*, 4, 3569 (2013)
[5] Borca, B. et al. *ACS Nano*, DOI: 10.1021/acsnano.5b06000 (2015)

Comparing adsorption and reactivity of pentacene and biphenyl-dicarboxylic acid on thin CoO(111) films

M.A. Schneider, P. Ferstl, T. Schmitt, M. Schuler, and L. Hammer

Solid State Physics, FAU Erlangen-Nürnberg, Germany
(corresponding author: M.A. Schneider, e-mail:alexander.schneider@fau.de)

The investigation of the adsorption properties of organic molecules on oxide surfaces is of great interest due to a variety of aspects. Since organic chemistry allows tailoring molecules and their properties almost at will the question arises if oxide surfaces can be similarly functionalized as metal surfaces by adsorption of suitably functionalized molecules. While a large amount of atomic scale data of different molecular systems and their self-assembly on metal surfaces has been compiled during the last two decades [1], comparable data available on oxide surfaces remains scarce by comparison [2]. This is partially due to the difficulties encountered in preparing well characterized oxide surfaces and in accessing them by standard surface science tools including scanning probe methods. Further, when annealing a molecular layer on an oxide surface (e.g. to improve its self-assembly) one might easily trigger chemical reactions (notably the oxidation of the organic compounds) that destroy the properties of the molecules. This leads to another area of interest, namely the oxidation of volatile organic compounds (VOCs) at suitably chosen catalytically active (oxide) surfaces [3]. Here besides triggering the oxidation at low temperatures, catalyst selectivity (e.g. CO_2 vs. CO production) is of great interest.

In our contribution we compare the adsorption properties of two organic molecules – pentacene and 4,4'-biphenyl dicarboxylic acid (BDA) – on CoO(111) thin films. Pentacene does not provide any specific functionality for self-assembly or chemical reactions, whereas one might expect self-assembly via self-complementary hydrogen bonding of the carboxyl groups or deprotonation and subsequent bonding to the cations of the oxide surface in the case of BDA. As a substrate we use thin CoO(111) films grown on Ir(100). The structural properties of these films are well characterized [4] and the films are accessible to STM.

The thinnest 2D oxide that can be grown on Ir(100) is the CoO(111) bilayer (1BL). This film is a highly corrugated (O-O buckling ~1Å), quasi-hexagonal layer and its lattice constant varies ~1% in response to departure from ideal stoichiometry [5]. Due to the corrugation one might expect that the adsorbed molecules adapt their adsorption site to the corrugated substrate. This is not the case. Neither pentacene nor BDA are predominantly found in adsorption configurations along high-symmetry directions of the substrate. In the case of BDA this is due to carboxylate formation and bonding to Co atoms of the substrate while for

pentacene the reason must lie within the overall interaction of the aromatic rings with the oxide surface (Fig1 a+b).

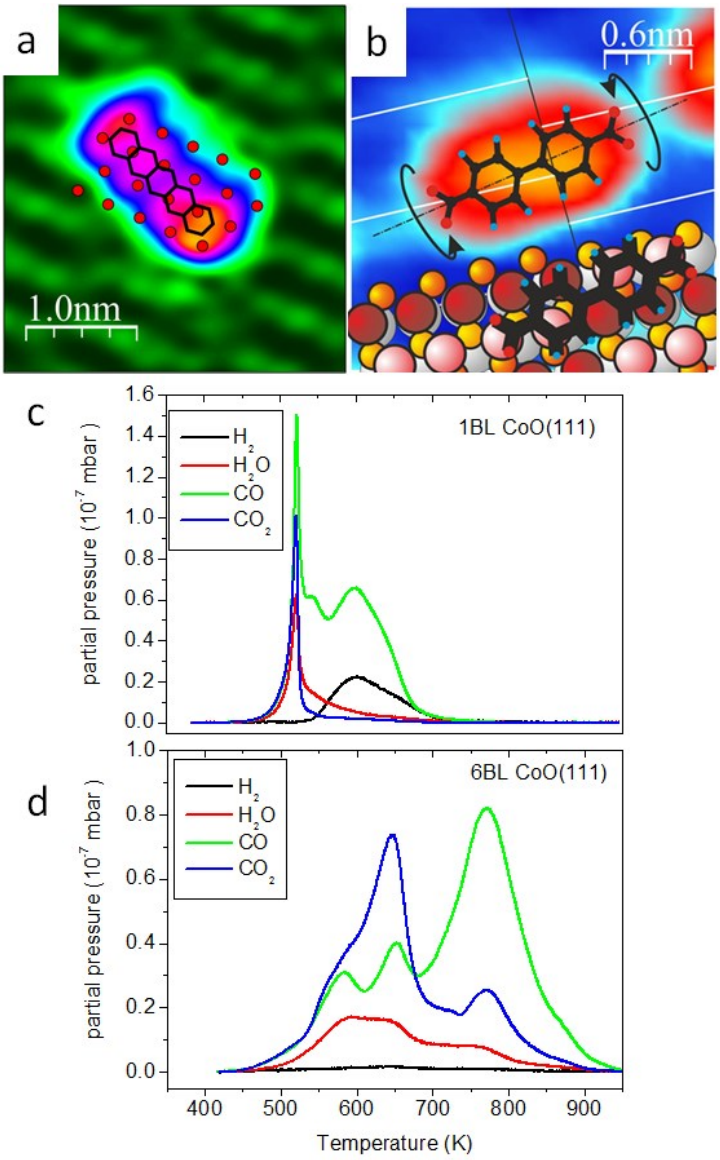

Figure 1: Adsorption geometry for a) pentacene and b) BDA on a 1BL CoO(111) film on Ir(100). Models show O-atoms in reddish colors. c) and d) TDS of the oxidation reaction of a pentacene monolayer on 1BL (c) and on 6BL (d) CoO(111) on Ir(100) in UHV.

With increasing CoO(111) film thickness the corrugation of the molecule-substrate potential diminishes. Further the reactivity with respect to the deprotonation of the BDA reduces as now even for deposition at room temperature hydrogen-bonded molecular structures are observed. The oxidation of pentacene follows a similar trend. The thicker the oxide layer the higher the temperature at which oxidation takes place in UHV. Interestingly the oxide thickness also influences the relative abundance of the reaction products (Fig.1 c+d). This is monitored and analyzed by thermal desorption spectroscopy (TDS). An interpretation using the structural information from STM and LEED is attempted.

Support by the Deutsche Forschungsgesellschaft (DFG) via the research unit FOR1878 “funCOS: Functional Molecular Structures on Complex Oxide Surfaces” is gratefully acknowledged.

References

[1] J. V. Barth, Annu. Rev. Phys. Chem. 58, 375–407 (2007); A. Kühnle, Current Opinion in Colloid & Interface Science 14, 157–168 (2009); L: Bartles, Nature Chemistry 2, 87–95 (2010)

[2] F. Zasada, J. Phys. Chem. C 115, 4134 (2011); S.-C. Li, L.-N. Chu, X.-Q. Gong, U. Diebold, Science 328, 882 (2010); Pan, Y., Nilius, N., Schneider, W.-D., Freund, H.-J. Surface Science 628, 111 (2014); J. Neff, M. Kittelmann, R. Bechstein, A. Kühnle , Phys. Chem. Chem. Phys. 16, 15437 (2014)

[3] E. Ntainjua N., H. T. Stuart, Top. Catal. 52, 528 (2009)

[4] W. Meyer, et al., Phys. Rev. Lett. 101, 016103 (2008)

[5] C. Tröppner, et al., Phys. Rev. B 86, 235407 (2012)

A multi-technique approach in studies of Ni-TPP self-assembly on the Cu (100) surface.

G. Zamborlini

Peter Grünberg Institute (PGI-6), Research Center Jülich, 52425 Jülich, Germany
(Corresponding author: g.zamborlini@fz-juelich.de)

Porphyrins are archetypal metallorganic complexes present in many biochemical molecules like chlorophyll, haemoglobin and cytochrome. They exhibit great structural flexibility because of the wide variation of their functionalization, which gives rise to promising technological applications (gas sensors, field-effect transistors light emitting diodes etc.). Supramolecular multiporphyrin arrays are considered ideal model systems for the study of energy transfer mechanisms and for the natural photosynthetic system [1][2].

Intensive experimental and theoretical efforts in the past decade made significant progress in the understanding of porphyrin assembly on metal surfaces. Adsorption, is often accompanied by charge transfer to or from the substrate with the consequent redistribution of charge within the molecule[3][4].

In this work we present a comprehensive characterization of the geometrical and electronic structure of self-assembled nickel-tetraphenylporphyrin (Ni-TPP) films on Cu(100). The adsorption of the Ni-TPP was studied by a multitechnique approach combining scanning tunnelling microscopy (STM), low-energy electron diffraction (LEED) and Angle-Resolved Photoemission Spectroscopy (ARPES) complemented by density functional theory (DFT).

STM image reveals the presence of two distinct domains (A and B, figure 1a, top), with lattice vectors rotated by an angle of 16°. The square unit cell has a base vector of ~17 Å and contains one molecule. An angle of ±18° between the molecular axis (of domain A and B respectively) and [110] crystal direction was deduced from high resolution STM measurement (fig 1a, bottom, 1c). The observed structure can be described well by 4,3/-3,4 and its mirror -4,3/3,4 matrices. Close to the 1 ML regime, Ni-TPP/Cu(100) shows a sharp LEED pattern, which supports long-range order of the studied molecular network (see Fig. 1b). The measured diffraction pattern is in good agreement with the simulated superstructure using matrices determined in the STM experiment (see blue and red circles on fig 1c, corresponding to the two different domains).

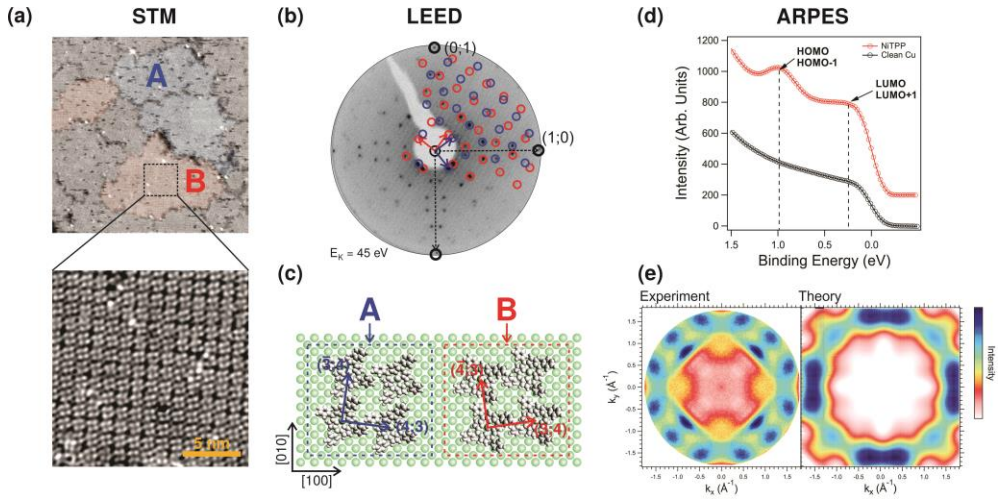

Figure 1. (a) STM (b) LEED image and (c) proposed adsorption model of Ni-TPP on Cu(100) substrate; (d) photoelectron spectra recorded at hv=26 eV; (e) measured ARPES pattern of the NiTPP monolayer on Cu(100) recorded for the LUMO corresponding hemispherical cut through the Fourier-transform of the calculated 3D models (DFT+U, gas phase).

In the next step ARPES was employed to investigate the electronic structure at the molecule/metal interface of Ni-TPP/Cu(100) system. This technique gives direct information about the density of states in the region close to the Fermi level, where low-energy molecular orbitals (MO) are involved. This is particularly useful to determine the molecule-substrate interactions and the charge transfer phenomena between adsorbed molecules and metal surfaces. The VB spectra of Ni-TPP/Cu(100) system show two features originating from the ionization of low energy MOs (see fig 1d) and they have been further analyzed by molecular tomography. The features are superimposed on the *sp* band of the copper substrate which shows a rather featureless plateau (see Fig. 1d). Comparing ARPES patterns with DFT calculations we can unambiguously assign observed spectral features to the ionization of the highest occupied and lowest unoccupied molecular orbitals (HOMO and LUMO) of adsorbed molecule[5]. In the simulated ARPES image ("Theory") in Figure 1e the symmetry of the substrate and the angle between the two molecules that belong to different domains found in the STM experiment were taken into account. The image shows a good agreement between the experimentally measured pattern (see Fig 2e) and the simulated one. The presence of LUMO in the photoemisson spectrum supports the charge transfer scenario between molecules and the metal substrate.
In conclusion, the adsorption and growth behaviour of Ni-TPP molecule on the Cu(100) surface has been studied using different spectroscopic techniques, providing information regarding their geometric and electronic structure.

[1] N. A. Rakow, K. S. Suslick, Nature, 2000, 406, 710.
[2] K. Flechtner et al. J. Am. Chem. Soc., 2007, 129, 12110.
[3] G. Di Santo et al, J. Phys. Chem. C., 2011, 115, 4155–4162
[4] C. Castellarin Cudia, Surface Science, 600 (2006) 4013–4017
[5] Puschnig. P et al, Science 2009, 326, 702.

Role of Structural and Charge-State Fluctuations on the Tunneling Spectroscopy and Imaging of Dangling-Bond Pairs and Dimers on Si(001):H and Ge(001):H

Mads Engelund,[1] Szymon Godlewski,[2] Marek Kolmer,[2] Rafal Zuzak,[2] Bartosz Such,[2] Marek Szymonski,[2] Aran García-Lekue[3, 4], Pedro B. Mendonça,[1] Thomas Frederiksen,[3, 4] and Daniel Sánchez-Portal[1, 3]

[1]*Centro de Física de Materiales CSIC-UPV/EHU, Paseo Manual de Lardizabal 5, 20018, Donostia-San Sebastián, Spain*

[2]*Centre for Nanometer-Scale Science and Advanced Materials, NANOSAM, Faculty of Physics, Astronomy and Applied Computer Science, Jagiellonian University, Krakow, Poland*

4 Donostia International Physics Center, Paseo Manual de Lardizabal 4, 20018, Donostia-San Sebastián, Spain

[5]*IKERBASQUE, Basque Foundation for Science, E-48013, Bilbao, Spain*

(corresponding author: D. Sánchez-Portal, sqbsapod@ehu.eus)

Dangling bond (DB) arrays on Si(001):H and Ge(001):H surfaces can be patterned with atomic precision and they exhibit complex and rich physics making them interesting from both technological and fundamental perspectives. However, this complex behavior often makes scanning tunneling microscopy (STM) images and spectroscopy (STS) data difficult to interpret and even harder to simulate. Recently it was shown that low-temperature imaging of unoccupied states of an unpassivated dimer on Ge(001):H results in a symmetric butterfly-like STM motiv, despite that the equilibrium dimer configuration is expected to be a bistable, buckled geometry [1]. This phenomenon was related to the to rapid fluctuations between the two dimer configurations under imaging conditions. Here we complement this analysis with additional STM experiments on both Si(001):H and Ge(001):H and novel theoretical modeling based on density functional theory. We propose a dynamical model simple (based on Tersoff-Hamann theory [2] and a two-state equation rate) that allows us to reproduce the detailed features of the observed symmetric empty-state images. Thus, we corroborate the the idea that the observed pattern are due to fast flipping events and provides new insights between the tunneling current and the flipping rates. Furthermore, based on our model, we propose a method to actively switch these two microscopic states with high selectivity. We argue that our model is general and can be applied to other systems that exhibit fast fluctuations during STM imaging.

Recently, we have also experimentally and theoretically studied the electronic properties of close-spaced DB pairs in a Si(001):H p-doped surface [3]. Two types of DB pairs we

considered, called “cross” and “line” structures. Our STS data show that, although the spectra taken over different DBs in each pair exhibit a remarkable resemblance, they appear shifted by a constant energy that depends on the DB-pair type. This spontaneous asymmetry persists after repeated STS measurements. By comparison with density functional theory (DFT) calculations, we demonstrate that the magnitude of this shift and the relative position of the STS peaks can be explained by distinct charge states for each DB in the pair. We also explain how the charge state is modified by the presence of the STM tip and the applied bias. Our results indicate that, using the STM tip, it is possible to control the charge state of individual DBs in complex structures, even if they are in close proximity. This observation might have important consequences for the design of electronic circuits and logic gates based on DBs in passivated silicon surfaces.

This work is funded by the FP7 FET-ICT “Planar Atomic and Molecular Scale devices” (PAMS) project (contract No. 610446), the Spanish Ministerio de Economía y Competitividad (MINECO) (Grant No. MAT2013-46593-C6-2-P), the Basque Dep. de Educación and the UPV/EHU (Grant No. IT-756-13), and from the Foundation for Polish Science (FNP). MK also acknowledges financial support from the Polish National Science Centre (Grant No. DEC-2013/08/T/ST3/00047).

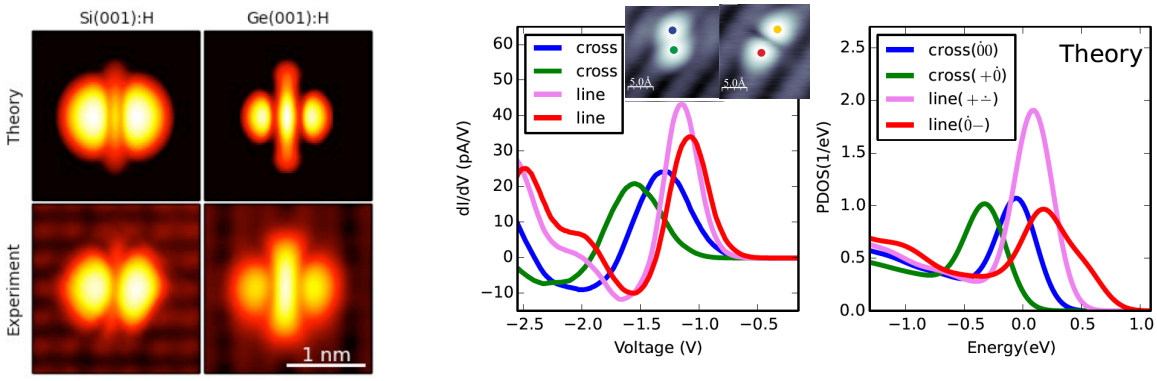

Figure 1. Left, bottom panels: Experimental constant-current empty-state images of DB dimers on Si(001):H and Ge(001):H (I = 20 pA,V_S = 1.3 V for Ge(001):H and I = 10 pA, V_S = 2.0 V for Si(001):H). Left, top panels: Corresponding simulated STM images using our two-level fluctuation model. Middle panel: STS spectra of different DBs on different types of DB-pairs (STM images in the insets). Right panel: calculated projected density of states for each type of pair assuming that transition to a neutral charge-state takes place when a positively-charged DB is imagined with a sufficiently large negative bias (energies relative to the valence-band top of the Si(001):H).

[1] S. Godlewski, M. Kolmer, J. Lis, R. Zuzak, B. Such, W. Gren, M. Szymonski, and L. Kantorovich, Phys. Rev. B 92, 115403 (2015)

[2] J. Tersoff and D.R. Hamann, Phys. Rev. Lett. 50, 1998 (1983); Phys. Rev. B 31, 805 (1985)

[3] M. Engelund, R. Zuzak, S. Godlewski2, M. Kolmer, T. Frederiksen, A. García-Lekue, D. Sánchez-Portal and M. Szymonski, Sci. Rep. 5, 14496 (2015).

Sterical and conformational aspects of metal-organic coordination in self-assembled monolayers

H. Aitchison[1], C. Benzin[2], H. Lu[3], M. Zharnikov[3], A. Grohmann[2], M. Buck[1]

[1]*EaStCHEM School of Chemistry, Univ. St Andrews, St Andrews, KY16 9ST, UK*
corresponding author: M. Buck, e-mail: mb45@st-andrews.ac.uk

[2] *Institut für Chemie, TU Berlin, Straße des 17. Juni 135, 10623 Berlin, Germany*

[3] *Angewandte Physikalische Chemie, Univ. Heidelberg, INF 253, 69120 Heidelberg, Germany*

Metal-organic coordination chemistry has been established as a versatile tool for the generation of surface confined two-dimensional networks [1,2] and the control of the third dimension in thin films with the latter encompassing amorphous or crystalline porous structures or compact layers [3-6]. The layer thickness is precisely defined by a layer by layer (LbL) growth which is accomplished by solution processing involving alternating steps of metal ion and organic ligand coordination.

While, in principle, the LbL approach enables the growth of layers with molecular precision, this might only be achieved if the dynamics and sterical requirements of the assembly process can be controlled down to the molecular level. A particularly critical point in this context is the initial stage of the LbL process and the very few experiments investigating the nucleation and growth process down to the molecular level suggest that at present these initial stages are rather different from the ideal LbL process [7,8].

Aiming for a better control of the initial stages of layer growth based on metal-organic coordination we investigate the correlation between

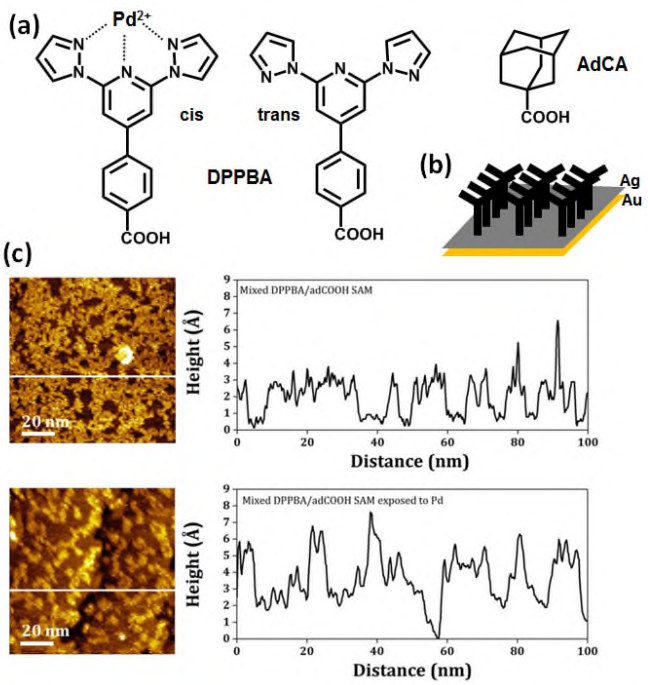

Fig. 1: (a) Structures of 4-(2,6-di(1*H*-pyrazol-1-yl)pyridine-4-yl)benzoic acid (DPPBA) in cis and trans conformation and adamantanecarboxylic acid (AdCA). For the cis conformation of DPPBA Pd coordination is shown. (b) Cartoon of the structure of a DPPBA SAM. (c) STM images and height profiles of a mixed DPPBA/AdCA before (top) and after (bottom) exposure to a Pd^{2+} solution.

the structures of self-assembled monolayers which are commonly used as seed layers and their complexation behaviour.

One example is the pyrazolyl compound DPPBA which as shown in Fig. 1a coordinates Pd-ions via the nitrogens. The molecules form a highly ordered self-assembled monolayer (SAM) on a Ag modified Au surface via coordination bonding of the carboxylic acid moiety to the substrate. Similar to a thiol analogue investigated previously [9] the monolayer exhibits a characteristic row structure with densely packed molecules as illustrated by the cartoon of Fig. 1b. However, this SAM does not coordinate Pd which is explained by the molecule being adsorbed in a trans conformation (see Fig. 1a) and unable to change to the cis conformation due to sterical hindrance. The situation is different if the molecule is coadsorbed with adamantane carboxylic acid. As seen from the change in the height profile upon exposure to Pd solution (see Fig. 1c) and the Pd signature in XPS the DPPBA molecules are now able to coordinate which demonstrates that dilution of the molecule introduces the required conformational degree of freedom.

Support by the Leverhulme Trust, EPSRC doctoral training grant scheme, DFG and EC is gratefully acknowledged.

[1] J.V. Barth, Surf. Sci. 603, 1533 (2009).

[2] D. Grumelli, B. Wurster, S. Stepanow and K. Kern, Nature Comm. 4, 2904 (2013).

[3] J. Liu, W. Zhou, J. Liu, I. Howard, G. Kilibarda, S. Schlabach, D. Coupry, M. Addicoat, S. Yoneda, Y. Tsutsui, T. Sakurai, S. Seki, Z. Wang, P. Lindemann, E. Redel, T. Heine and C. Wöll, Angew. Chem. Int. Ed. 54, 7441 (2015).

[4] C. Musumeci, G. Zappalà, N. Martsinovich, E. Orgiu, S. Schuster, S. Quici, M. Zharnikov, A. Troisi, A. Licciardello and P. Samorì, Adv. Mater. 26, 1688 (2014).

[5] S. Richter, C.H.H. Traulsen, T. Heinrich, J. Poppenberg, C. Leppich, M. Holzweber, W.E.S. Unger and C.A. Schalley, J. Phys. Chem. C 117, 18980 (2013).

[6] L. Motiei, R. Kaminker, M. Sassi and M.E. van der Boom, J. Am. Chem. Soc. 133, 14264 (2011).

[7] C. Shen, I. Cebula, C. Brown, J. Zhao, M. Zharnikov and M. Buck, Chem. Sci. 3, 1858 (2012).

[8] A. Summerfield, I. Cebula, M. Schröder and P.H. Beton, J. Phys. Chem. C 119, 23544 (2015).

[9] C. Shen, M. Haryono, A. Grohmann, M. Buck, T. Weidner, N. Ballav and M. Zharnikov, Langmuir 24, 12883 (2008).

Self-assembled bridged-triphenylamines on bulk insulator surfaces: The role of functional groups

Christian Steiner[1], Tim Sander[1], Maximilian Ammon[1], Natalie Hammer[2], Bettina Gliemann[2], Ute Meinhardt[2], Bernd Meyer[3], Milan Kivala[2], Sabine Maier[1]

[1]*Department of Physics, Friedrich-Alexander University Erlangen-Nürnberg, Germany*

[2]*Department of Chemistry and Pharmacy, Friedrich-Alexander University Erlangen-Nürnberg, Germany*

[3]*Interdisciplinary Center for Molecular Materials and Computer-Chemistry-Center, Friedrich-Alexander University Erlangen-Nürnberg, Germany*

(corresponding author: S. Maier, e-mail: sabine.maier@fau.de)

A major challenge in realizing single molecular electronic devices is to mechanically stabilize and electrically decouple molecules at and from a surface, respectively. Molecules on insulating surfaces suffer from a weak unspecific molecule-surface interaction, however, which leads to diffusion and the assembly of disordered aggregates. Controlling the order of molecular structures on bulk-insulating surfaces requires us to understand the interplay of the underlying intermolecular and molecule-surface interactions by carefully selecting the molecular functional groups.

Here, we present a systematic study on the adsorption and self-assembly of carboxylic, diaminotriazine and halogen substituted bridged-triphenylamines on KBr(001) and MgO(001) using non-contact atomic force microscopy (nc-AFM) in ultra-high vacuum in combination with density functional theory. We show that triphenylamines bridged with bulky dimethylmethylene side groups adopt a flat-lying adsorption geometry that yields extended two-dimensional molecular layers exhibiting long-range order. In contrast, the planar carbonyl-bridged triphenylamine molecules favor a nearly upright adsorption geometry stabilized by intermolecular π-π interactions. These nearly-upright standing molecules assemble in one-dimensional aggregates. Our nc-AFM measurements show that triphenylamine molecules with different functional end and side groups form a variety of 1D, 2D and 3D molecular assemblies on bulk insulators. The detailed analysis of the adsorption structures allows us to rationalize why specific structures are formed by the molecules and enables us to predict, how molecule-molecule and molecule-substrate interactions can be tuned in order to achieve 1D, 2D or 3D assembly of the molecules.

Author Index

Post Deadline Contributions

Ternary Oxides: Vibrational characterization by HREELS

Florian Schumann[1], Maik Christl[1], Klaus Meinel[1], Stefan Förster[1], and Wolf Widdra[1]

Institute of Physics, Martin-Luther-Universität Halle-Wittenberg, Halle, Germany
(corresponding author: W. Widdra, e-mail: wolf.widdra@physik.uni-halle.de)

Phonons and their softening are key elements for the basic understanding of many solid state phenomena. In ferroelectric and multiferroic oxides, phonons easily characterize different states; often phonon softening indicates imminent phase transitions in ferroelectrics and multiferroics. Here we present the vibrational characterization of ultrathin films of various perovskites together with their full complex dielectric response in the energy range from 2 to 500 meV by high-resolution electron energy loss spectroscopy (HREELS).

We report the full dielectric characterization for (001)-oriented single crystals of $BaTiO_3$, $SrRuO_3$, and $SrTiO_3$ with different intentional doping levels. The extracted surface dielectric function will be quantitatively compared with available bulk infrared data and allows the experimental determination of the surface-near doping level in oxides.

For ultrathin films of $BaTiO_3$(001), $SrRuO_3$(001), and $SrTiO_3$(001) as grown by MBE or PLD on various substrates, HREELS data allow for the first time the determination of the complex dielectric functions of ultrathin oxide films down to single unit cell thicknesses. These data are discussed with respect of possible two-dimensional electron gases (2DEG) at the surface, electron-phonon coupling, as well as strain-driven phonon softening.

Support by the Sonderforschungsbereich SFB-762 “Functional oxide interfaces” (projects A3 and B8) is gratefully acknowledged.

Analysis of motifs and electronic features in lanthanide-based coordination assemblies at surfaces

Ari P Seitsonen,[1] David Ecija, José I Urgel, Willi Willi Auwärter, Anthoula C Papageorgiou, Saranyan Vijayaraghavan, Sushobhan Joshi, Sybille Fischer, Joachim Reichert and Johannes V Barth

[1] Institut für Chemie, Universität Zürich, CH-8057 Zürich, Switzerland and
Départment de Chimie, École Normale Supérieure, F-75005 Paris, France
(corresponding author: Ari Paavo Seitsonen, e-mail: Ari.P.Seitsonen@iki.fi)

Physik Department E20, Technische Universität München, D-85748 Garching, Germany

The coordination chemistry of lanthanides and actinides has become a fashionable research topic in recent years. Their partially filled *f* electron shell can bestow unique properties to compounds and architectures. Supramolecular chemistry on surfaces has emerged as a versatile strategy to design interfacial nano-architectures. Hereby a delicate interplay between molecule–substrate and molecule–molecule interactions dictates the resulting structure. Protocols relying on metal-directed assembly provide frequently an excellent option given their advantageous performance with respect to the robustness and spatial regularity. Recently we have extended this approach to the family of lanthanides and showed the first designs based on five-fold lanthanide–carbonitrile motifs [1,2].

Here we report a detailed analysis of lanthanide atoms and organic molecules on metal surfaces using mainly scanning tunnelling microscopy (STM) and spectroscopy (STS) as the experimental tools and density functional theory (DFT) calculations to further investigate the structures found. We find a five-fold planar coordination motif for Ce or Gd atoms linked to NC-Ph_3-CN or NC-Ph_4-CN molecules on the employed Ag(111) substrate. Further we extend our study to the stacking of C_{60} fullerenes on $Ce(TPP)_2$ double decker molecules, where the orientation of the top TPP molecule can be switched using the STM tip [3].

We use the DFT to analyse properties such as density differences – visualised in Figure 1 – and projected densities of states to both compare with the experiments and trying to understand the coordination mechanism. Thereby we can obtain information both from the perspective of the lanthanide atom (Ln) and the changes occurring in the ligand molecules (L) both during the adsorption, being strong for the Ln and weak for L, and mutual interaction. The five-fold coordination of the Ln to the cyano groups on the ligand molecules is additional to the three bonds formed with the substrate.

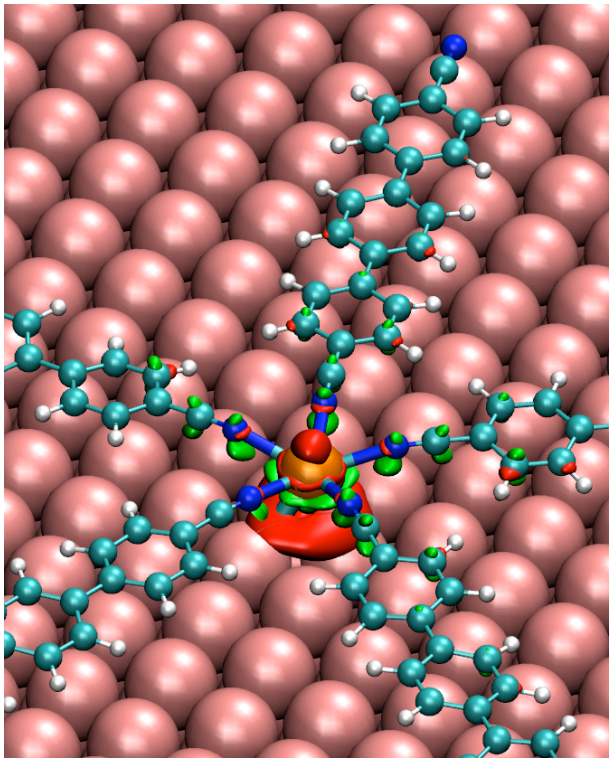

Figure 1. Density difference arising from the adsorption of the Ce-(NC-Ph_3-CN)$_5$ complex on the Ag(111) surface obtained from the DFT analysis; red and green areas denote respectively enhancement and depletion of electron density

This work was supported by the European Research Council Advanced Grant MolArt (Grant 247299) and the Technische Universität München-Institute for Advanced Study. The DFT calculations were performed at CSCS (Centro Svizzero di Calcolo Scientifico) and at the Informatikdienste der Universität Zürich.

[1] *Five-vertex Archimedean surface tessellation by lanthanide-directed molecular self-assembly*, David Écija, José I Urgel, Anthoula C Papageorgiou, Sushobhan Joshi, Willi Auwärter, Ari Paavo Seitsonen, Svetlana Klyatskaya, Mario Ruben, Sybille Fischer, Saranyan Vijayaraghavan, Joachim Reichert and Johannes V Barth, *The Proceedings of the National Academy of Sciences of the USA* 110, 6678-6681 (2013); doi:10.1073/pnas.1222713110

[2] *Five-Vertex Lanthanide Coordination on Surfaces: A Route to Sophisticated Nanoarchitectures and Tessellations*, José I Urgel, David Ecija, Willi Auwärter, Anthoula C Papageorgiou, Ari Paavo Seitsonen, Saranyan Vijayaraghavan, Sushobhan Joshi, Sybille Fischer, Joachim Reichert and Johannes V Barth, *Journal of Physical Chemistry C* 118, 12908-12915 (2014); doi:10.1021/jp502901z

[3] *Selective supramolecular fullerene-porphyrin interactions and switching in surface-confined C_{60}-Ce(TPP)$_2$ dyads*, Saranayan Vijayaraghavan, David Ecija, Willi Auwärter, Sushobhan Joshi, Knud Seufert, Ari Paavo Seitsonen, Kentaro Tashiro and Johannes V Barth, *NanoLetters* 12, 4077 (2012); doi:10.1021/nl301534p

Coulomb-blockade in two-dimensional conductive polymer monolayer

Megumi Akai-Kasaya, Y Okuaki, S Nagano[1], T. Mitani[2] and Y Kuwahara

Precision Science & Technology, Graduate School of Engineering, Osaka University, 2-1 Yamadaoka, Suita, Osaka 565-0871, Japan,
(corresponding author: M Akai-Kasaya, e-mail: kasaya@prec.eng.osaka-u.ac.jp)

[1]Nagoya University Venture Business Laboratory, Graduate School of Engineering, Nagoya University, Furo-cho, Chikusa-ku, Nagoya 464-8601, Japan

[2]Japan Advanced Institute of Sciene and Technology, 1-1 Asahidai, Nomi, Ishikawa 923-1292 Japan

Good organic conductors often have a low-dimensional configuration, e.g., quasi-one-dimensional structures or two-dimensional (2D) layers. Nevertheless, a large number of fundamental questions remain to be answered regarding the charge transport mechanism, particularly in low-dimensional structures. Recently, it has been reported that the *I-V* characteristics obey a power-law relationship in low-dimensional organic materials such as polymer nanofibers, nanotubes and polymer films [1,2]. The observed power-law relationship has been put forward as evidence for tunneling into a one-dimensional (1D) Luttinger liquid because of the quasi-1D structure of these materials[1]; however, power-law behavior was also observed for a three-dimensional (3D) polymer film [2]. The origin of such power-law behavior in organic materials is still under debate [3].

On the other hand, in inorganic granular materials, the power-law dependence of the *I-V* characteristics has commonly been attributed to dissipative tunneling processes, such as that associated with a Coulomb blockade (CB) [4,5]. The CB effect has been confirmed during charge transport through a single molecule spanning adjacent electrodes, although it has rarely been suggested as the origin of nonlinear conduction in larger condensed organic conductor systems [6]. Since the nature of the individual sites (i.e., whether they are metallic, superconducting, or semiconducting) is irrelevant, there is no reason why the CB effect should not emerge in organic materials that consist of small conducting segments.

In this study, we show experimental evidence to prove Coulomb blockade taking place on two-dimensional organic conducting polymer films [7]. The theoretical evidence through quantum calculations and the verification of conductivity models of experimental results are also demonstrated. Electronic transport was investigated in poly(3-hexylthiophene-2,5-diyl) monolayers[8]. At low temperatures, nonlinear behavior was observed in the current-voltage characteristics, and a non-zero threshold voltage appeared as shown in Fig. 1, which increased with decreasing temperature. The current-voltage characteristics could be best fitted using a power law. These results suggest that the nonlinear conductivity can be explained using a

Coulomb blockade (CB) mechanism. A model is proposed in which an isotropic extended charge state exists, as predicted by quantum calculations, and percolative charge transport occurs within an array of small conductive islands. Using quantitatively evaluated capacitance values for the islands, this model was found to be capable of explaining the observed experimental data.

The importance of the results is that percolative charge transport may well explain experimentally observed charge transport in low-dimensional organic materials. The significance of the blockade effect, i.e., the difficulty of charge injection from one conducting segment into another, should also be stressed, since this has not hitherto been taken into account when considering the charge transport mechanism in organic materials. Conductive segments in poorly conductive organic materials are expected to have a smaller electrical capacity, leading to a higher T^* for the blockade effect. The presence of structural disorder in organic materials will obscure the emergence of a distinguishable conduction threshold, although ironically, such disorder is a requirement for percolative transport. By considering both the charge blockade effect and the influence of structural disorder, it is hoped that a clear understanding of charge transport in organic materials can be achieved.

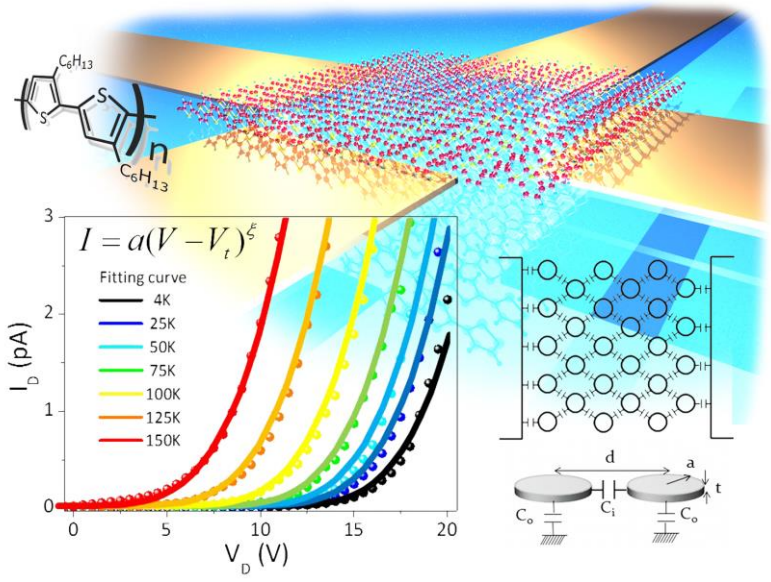

Fig1: Coulomb blockade currents measured in a conducting polymer monolayer and a 2D charge transport model. Background is schematic of the monolayer on electrodes.

a Grant-in-Aid for Scientific Research (S) (#24221009) and Grant-in-Aid for Scientific Research on Innovative Areas “Molecular Architectonics: Orchestration of Single Molecules for Novel Functions” from the Ministry of Education, Culture, Sports, Science and Technology, Japan.

[1] J. D. Yuen, R. Menon, N. E. Coates, E. B. Namdas, S. Cho, S.T. Hannahs, D. Moses, and A. J. Heeger, Nature Mater. 8, 572 (2009).

[2] A. J. Kronemeijer, E. H. Huisman, I. Katsouras, P. A. van Hal, T. C. T. Geuns, P. W. M. Blom, S. J. van der Molen, and D. M. de Leeuw, Phys. Rev. Lett. 105, 156604 (2010).

[3] A. S. Rodin and M. M. Fogler, Phys. Rev. Lett. 105, 106801 (2010).

[4] A. A. Middleton and N. S. Wingreen, Phys. Rev. Lett. 71, 3198 (1993).

[5] K. Xu, L. Qin, J. R. Heath, Nat. Nanotechnol. 4, 368 (2009).

[6] A. N. Aleshin, H. J. Lee, S. H. Jhang, H. S. Kim, K. Akagi and Y.W. Park, Phys. Rev. B 72, 153202 (2005).

[7] M. Akai-Kasaya, Y. Okuaki, S. Nagano, T. Mitani and Y. Kuwahara, *Phys. Rev. Lett.*, 115, 196801 (2015).

[8] M. Akai-Kasaya, Y. Okuaki, S. Nagano and Y. Kuwahara, J. Phys. D: Appl. Phys. 46, 425303 (2013).

The Fe_3O_4(001) Surface as a Model for Single-Atom Catalysis

Ulrike Diebold[1], Roland Bliem[1], Jiri Pavelec[1], Oscar Gamba[1], Peter Blaha[2], Michael Schmid[1], and Gareth Parkinson[1]

[1]*Institute of Applied Physics, TU Wien, Wiedner Hauptstrasse 8-10/134, A-1040 Vienna, Austria,*
[2]*Institute of Materials Chemistry, TU Wien, Getreidemarkt 9, A-1060 Vienna, Austria*

diebold@iap.tuwien.ac.at

The magnetite Fe_3O_4(001) surface exhibits a ($\sqrt{2}$x$\sqrt{2}$)R45° reconstruction over a wide range of preparation parameters. Using a combination of STM, LEED-IV, and DFT, the structure was determined as being due to ordered subsurface cation vacancies [1]. This surface renders preferred adsorption sites for metal adatoms up to a temperature where the surface reconstruction is lifted by an order-disorder transition, i.e., around 700 K [2]. Vapor-deposition of metals results in ordered arrays of isolated adatoms that can serve as ideal model systems for single-atom catalysis. Originally observed for Au [3], Pd [4], and Ag [5], adatom arrays that are stable up to 700 K were recently confirmed for a wide range of other elements. Metals that form a stable ferrite structure such as Zr, Ni, Co, Mn, or Ti [6] also adsorb at the special sites within the reconstruction, but diffuse into the selvedge upon annealing. The chemical reactivity of the clean surface [7], and of the surface modified with small clusters and adatoms [8] will be discussed.

[1] R. Bliem, E. McDermott, P. Ferstl, M. Setvin, O. Gamba, J. Pavelec, et al., Subsurface cation vacancy stabilization of the magnetite (001) surface, Science. 346 (2014) 1215–1218. doi:10.1126/science.1260556.

[2] N.C. Bartelt, S. Nie, E. Starodub, I. Bernal-Villamil, S. Gallego, L. Vergara, et al., Order-disorder phase transition on the (100) surface of magnetite, Phys. Rev. B. 88 (2013) 235436. doi:10.1103/PhysRevB.88.235436.

[3] Z. Novotný, G. Argentero, Z. Wang, M. Schmid, U. Diebold, G. Parkinson, Ordered Array of Single Adatoms with Remarkable Thermal Stability: Au/Fe_3O_4(001), Phys Rev Lett. 108 (2012) 216103. doi:10.1103/PhysRevLett.108.216103.

[4] G.S. Parkinson, Z. Novotný, G. Argentero, M. Schmid, J. Pavelec, R. Kosak, et al., Carbon monoxide-induced adatom sintering in a Pd-Fe_3O_4 model catalyst, Nat Mater. 12 (2013) 724–728. doi:10.1038/nmat3667.

[5] R. Bliem, R. Kosak, L. Perneczky, Z. Novotný, O. Gamba, D. Fobes, et al., Cluster Nucleation and Growth from a Highly Supersaturated Adatom Phase: Silver on Magnetite, ACS Nano. 8 (2014) 7531–7537. doi:10.1021/nn502895s.

[6] R. Bliem, J. Pavelec, O. Gamba, E. McDermott, Z. Wang, S. Gerhold, et al., Adsorption and incorporation of transition metals at the magnetite Fe_3O_4(001) surface, Phys. Rev. B. 92 (2015) 075440. doi:10.1103/PhysRevB.92.075440.

[7] O. Gamba, H. Noei, J. Pavelec, R. Bliem, M. Schmid, U. Diebold, et al., Adsorption of Formic Acid on the Fe_3O_4(001) Surface, J Phys Chem C. 119 (2015) 20459–20465. doi:10.1021/acs.jpcc.5b05560.

[8] R. Bliem, J. van der Hoeven, A. Zavodny, O. Gamba, J. Pavelec, P.E. De Jongh, et al., An Atomic-Scale View of CO and H_2 Oxidation on a Pt/Fe_3O_4 Model Catalyst, Angew. Chem. (2015) doi:10.1002/ange.201507368.

EnviroESCA™

THE BEGINNING OF A NEW ERA

Environmental

- Controllable atmosphere from sample loading to analysis
- Adaptable process gas dosing systems
- Specialized Sample Environments
- Compatible with all kind of samples of sizes up to Ø 60 x 40 mm

Networking

- SampleExplorer
- SmartDock
- AutoLoader
- GloveBox

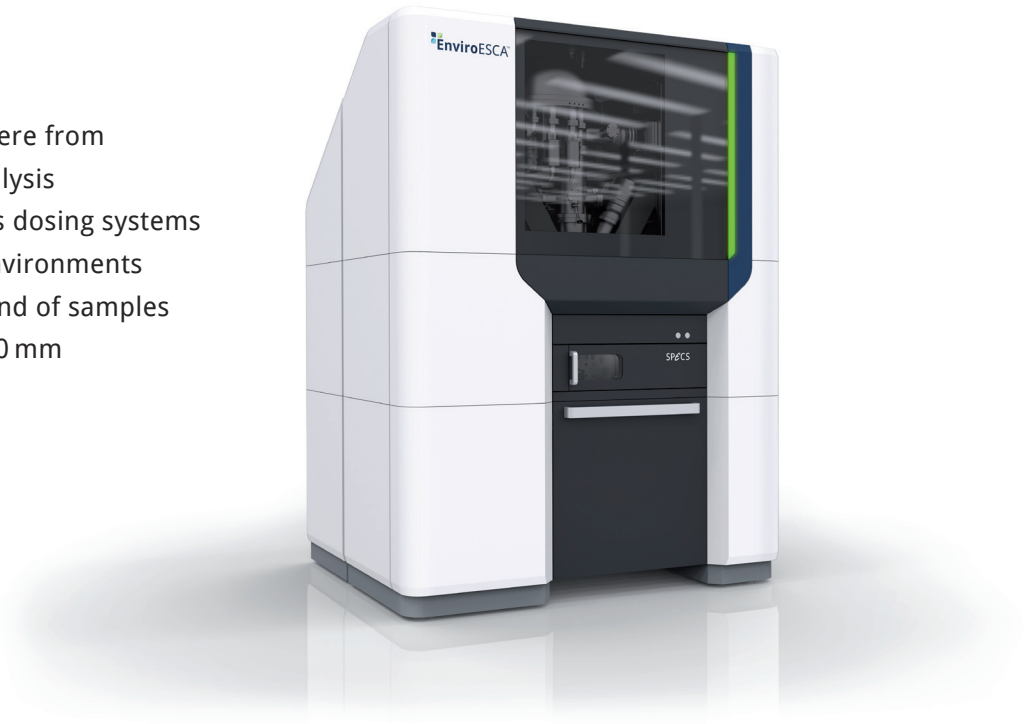

Versatile

- Revolutionary analyzer technology
- µ-Focus X-ray source
- High resolution XPS
- Automated charge compensation
- Sputter depth profiling

Reliable

- Sample journal for complete documentation
- Reproducable analysis receipes
- Comprehensive system parameter logging
- Uptime focused user support

Integral

- Ergonomic all-in-one design
- Quick installation and setup
- Minimized downtime
- Cost and time efficent servicing
- Easy consumable replacement

Optimized

- Application oriented software package
- Complete remote operation
- Fully automated vacuum system
- Simple sample loading
- Optical 3D sample navigation

SPECS Surface Nano Analysis GmbH
Voltastrasse 5
13355 Berlin / Germany
www.EnviroESCA.com
T +49 30 46 78 24-0
F +49 30 46 42 083
E info@specs.com

SPECS™

SYMPOSIUM ON SURFACE SCIENCE 2016
St. Christoph am Arlberg, Austria
Feb. 21 - 27, 2016

Friedrich Aumayr, Ulrike Diebold and Peter Varga, organizers
Institute of Applied Physics, TU Wien (Vienna University of Technology)

Sunday, 21 Feb. 2016

16:00 - 18:30	REGISTRATION
18:30 - 19:30	DINNER
20:00 - 20:20	OPENING

chair: VARGA

20:25 - 20:45	BRUNE
20:45 - 21:05	HUG
21:05 - 21:25	IBACH

Monday, 22 Feb. 2016

07:15 - 08:00	BREAKFAST

chair: VARGA

08:00 - 08:20	WÖLL
08:20 - 08:40	JELÍNEK
09:15 - 12:00	SKIING INSTRUCTIONS
12:00 - 13:00	LUNCH
13:30 - 15:30	SKIING INSTRUCTIONS

chair: TAGLAUER

16:40 - 17:00	KOSHIKAWA
17:00 - 17:20	MAIER M.
17:20 - 17:40	KAMPEN
17:40 - 18:00	HU
18:00 - 18:20	TAKEI
18:30 - 19:30	DINNER

chair: LEMELL

19:30 - 19:50	HEINZMANN
19:50 - 20:10	EBERHARDT
20:10 - 20:30	DIL
20:30 - 20:50	CHEYNIS

Tuesday, 23 Feb. 2016

07:15 - 08:00	BREAKFAST

chair: SEITSONEN

08:00 - 08:20	RUPPRECHTER
08:20 - 08:40	THORNTON
09:15 - 12:00	SKIING INSTRUCTIONS
12:00 - 13:00	LUNCH
13:30 - 15:30	SKIING INSTRUCTIONS

chair: DIEBOLD

16:40 - 17:00	SCHNEIDER W.D.
17:00 - 17:20	ORTEGA
17:20 - 17:40	SEIFERT
17:40 - 18:00	LIBUDA
18:00 - 18:20	SUCHORSKI
18:30 - 19:30	DINNER

chair: SETVIN

19:30 - 19:50	ÅHLUND
19:50 - 20:10	HOSTER
20:10 - 20:30	FERSTL
20:30 - 20:50	ŠIKOLA

Wednesday, 24 Feb. 2016

07:15 - 08:00	BREAKFAST

chair: WIDDRA

08:00 - 08:20	DRAXL
08:20 - 08:40	REUTER
09:15 - 12:00	SKIING INSTRUCTIONS
12:00 - 13:00	LUNCH
13:30 - 15:30	SKIING INSTRUCTIONS

chair: AUMAYR

16:40 - 17:00	LINSMEIER
17:00 - 17:20	BAUER

chair: LINSMEIER

17:25 - 18:20	POSTER INTRODUCTION
18:30 - 19:30	DINNER
19:30 - 21:30	POSTERSESSION

Thursday, 25 Feb. 2016

07:15 - 08:00	BREAKFAST

chair: BERGHAUS

08:00 - 08:20	GIESSIBL
08:20 - 08:40	KUNZE-LIEBHÄUSER
09:15 - 12:00	SKIING INSTRUCTIONS
12:00 - 13:00	LUNCH
13:30 - 15:30	SKIING INSTRUCTIONS

chair: HAMMER

16:40 - 17:00	FASEL
17:00 - 17:20	BARTH
17:20 - 17:40	ALTMAN
17:40 - 18:00	GÖLZHÄUSER
18:00 - 18:20	STARKE
18:30 - 19:30	DINNER

chair: ARNAU

19:30 - 19:50	MESSING
19:50 - 20:10	YUHARA
20:10 - 20:30	PROTOGENOV
20:30 - 20:50	CHULKOV

Friday, 26 Feb. 2016

07:15 - 08:00	BREAKFAST

chair: HEINZMANN

08:00 - 08:20	MORGENSTERN
08:20 - 08:40	RIVA
09:15 - 12:00	GIANT SLALOM RACE
12:00 - 13:00	LUNCH
13:30 - 15:30	SKIING INSTRUCTIONS

chair: MARBACH

16:30 - 16:50	PENEDO
16:50 - 17:10	PÉTUYA
17:10 - 17:30	SCHNEIDER M.A.
17:30 - 17:50	ZAMBORLINI
17:50 - 18:10	SÁNCHEZ-PORTAL

chair: FASEL

18:30 - 18:50	BUCK
18:50 - 19:10	MAIER S.
19:10 - 19:40	GIANT SLALOM RACE AWARD CEREMONY
20:00	CONFERENCE DINNER